Study of the impact of heterogeneity on the modeling of fluid-flow, based on a turbidite reservoir analogue

Ainsa-1 quarry outcrop, Spain

Master of Sciences thesis

Submitted by:

Erica Garrido Magaz

In collaboration with:

Rueil-Malmaison, June 2012

Abstract

Geological heterogeneity includes variations in porosity, lithology, mechanical properties, structure, etc. (Eaton, 2006) and in the case of sedimentary bodies, facies distribution acts as a constraint of them. It is proven that heterogeneity plays an important role on the control of reservoir production with regard to the fluid flow patterns.

The objective of this master's thesis was to study the possible impact of reservoir heterogeneities on the flow paths applying an analogue outcrop of deep marine depositional environment, (Ainsa-1 quarry outcrop, northeast Spain).

For that purpose it was created (1) a structural model with data loading, cell network and surface boundaries modeling, followed by a (2) facies distribution. The resulting reservoir model was checked by (3) numerical simulations of fluid flows, applying a petrophysical property model (permeability and porosity) using underdevelopment software called OpenFlow Suite 2012.

For testing the influence of large scale heterogeneities we run two-phases fluid flow simulations using a quarter five-spots injection production, which were defined for being affected mainly by permeability heterogeneities without confounding effects. Thanks to this, we provide an intuitive visualization of flow patterns, which are likely similar to the flow paths in oil-recovery processes.

Contents

List of Figures

List of Tables

Chapter 1 Introduction

Reservoir characterization is a process in which the geological current knowledge is translated into parameters in a 3D grid.

The target of the reservoir modeling is understanding and predicting reservoir's key geological, geophysical and engineering components; identification of new prospects; estimation of original oil place; quantification of reservoir potential; economic potential evaluation; development and field management.

The usual reservoir management workflow consists in:

1. Structural model construction of a structural model with data loading, horizons modeling and fault network, this means an accurate and precise description of subsurface heterogeneities.
2. The definition o a geological model with geological grid and properties modeling (facies and petrophysical).
3. The definition of a reservoir model with reservoir grid and upscaling.
4. The numerical simulations to estimate fluids displacements and improve the understanding of spatial distribution of heterogeneities.

Production decisions are made using the results of this modeling and simulation cycle. Therefore, it is important to build realistic facies models, with realism being judged by the ability of the model to predict the flow-related responses of the reservoir (Falivene et al., 2006)

Deep-water clastic reservoirs account for approximately 15% of the world's total oil reserves (Bakke et al., 2008) and these reservoirs are highly variable in geometry, size and internal character and with the added problem that the key differences are, usually, below seismic resolution. For this reason, to create reservoir models based in similar well-known outcrops, it is a powerful and useful tool for better understanding, evaluation and success prediction of

reservoir potential, impact reservoir heterogeneities on dynamic behavior and relative impact of uncertainties.

1.1 Aims and Workflow

This master's thesis is focused in the study of the impact of reservoir heterogeneity on injection/production strategies in a turbiditic multi-channel system. For that purpose, we chose the deep marine Ainsa quarry outcrop (sandstone-filled turbidite channel) to guide our comparison, due to the increase importance of these kind or reservoirs in the petroleum industry and because it is well-known and has been widely used as an analog in different reservoirs characterizations as for example in West Africa (offshore), Brazil, Gulf of Mexico and the North sea (Falivene et al. 2006).

Most common facies in this outcrop are the thick-bedded sandstones, although other facies as conglomerates, muddy and heterolithics facies (alternation of muddy-sandy lamination) also occur. The presence of these non-reservoir facies generates important effects on the dynamic behaviors and flow patterns in these bodies.

Therefore, it is really important to reproduce and construct realistic facies and petrophysical models with stochastic algorithms and perform several numerical simulations once the model is built to improve oil recovery predictions. For that purpose we used a software under-development at IFPEN called OpenFlow Suite. The results presented in this thesis will be applicable to similar facies architectures elsewhere.

The workflow we used involved the following steps:

1. Checkout and study of previous work. We decided to use the grid created in the work, *"Quantitative interpretation of multi-dimensional seismic models turbidite channels from the Ainsa-1 Quarry analogue (Spain)"* (Zadeh, 2009) because it fits with our necessities in terms of grid size, structure and average height for cells for posterior fluid flow analysis.
2. Extraction of soft data from the outcrop and the gridded outcrop
3. Extraction of hard data from the gridded outcrop by selection of 4 vertical logs across the front part of the outcrop, understanding hard data as the one that is intended for estimation over the entire grid, guided by the soft data (Scheevel et al, 2001).

4. Extraction of hard data from the previous-work model by selection of 4 vertical logs across the back part of the model.
5. Geostatistical simulation of facies distribution.
6. Modeling of petrophysical properties. Because the outcrop is not in reservoir conditions, normal reservoir values have been used to simulate the petrophysics properties.
7. Computations of several fluid-flow simulations in a simple two-wells model, injector and producer (static connectivity, effective permeability, and recovery efficiency using waterflood simulations, with different rates and time).

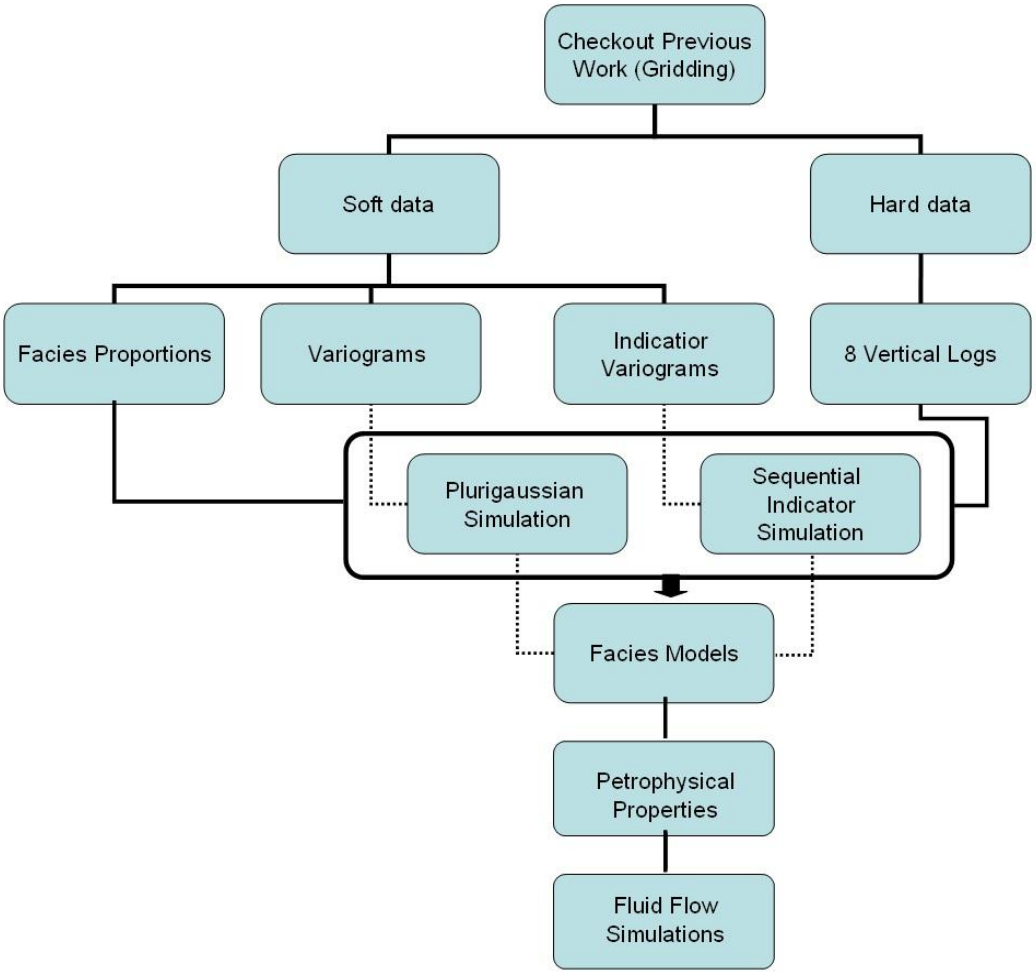

Figure 1.1 Flowchart showing the steps undertaken in this study. See text for detailed description.

Chapter 2 Geology

2.1 Geographic setting

The Ainsa quarry outcrop is situated in the Ainsa Basin, which is located in the Sobrarbe region in the Southern Pyrenees, in Northern Spain (Figure 2.1). It forms part of the central subbasin of the South Pyrenean Basin, which is divided in three subbasin by the Segre Fault (to the east of the central subbasin) and by Pamplona Fault (to the west of the central subbasin). The central subbasin is the best known of these three thanks to the work made by Mutti et al. along twenty years.

The specific outcrop of this study is located 1.4 km southeast of Ainsa town, slightly above the western bank of the Zinca River, at an altitude of 540 m above sea level.

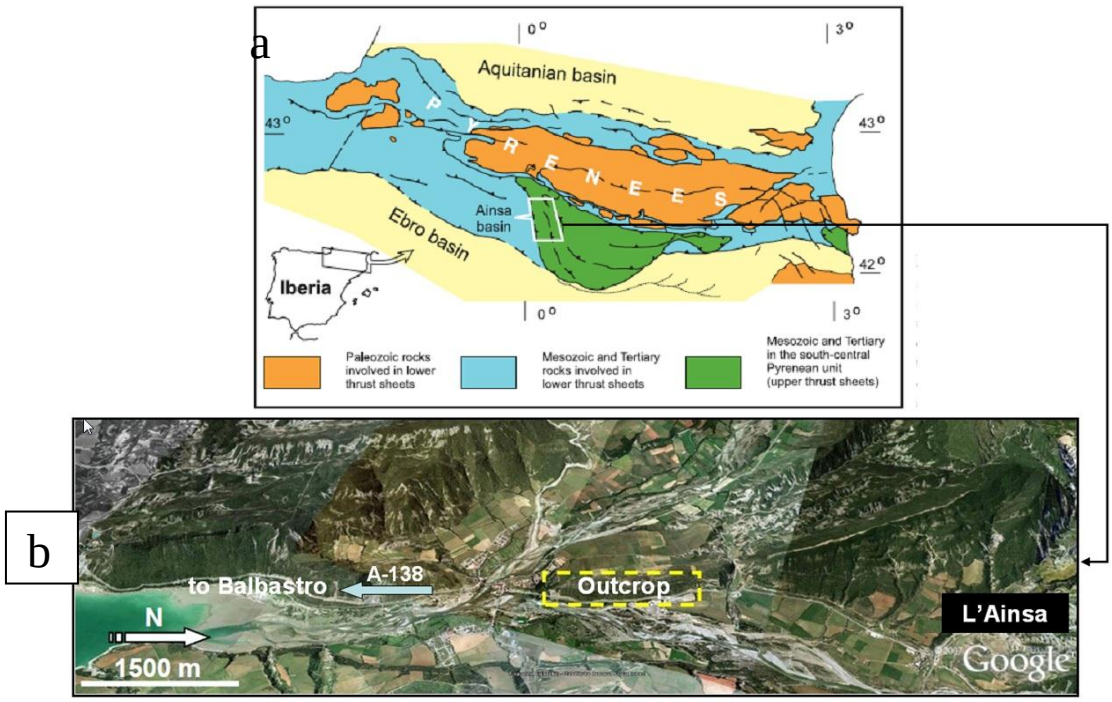

Figure 2.1 General geologic map of the Pyrenees. The Ainsa basin is at present thrust and folded in a zone of oblique ramps that separates two of the major southward displaced thrust sheets in the southern Pyrenees (Arbués et al., 2007). (b) Location of the Quarry outcrop and surrounding areas (Google maps).

2.2 Geological setting

Between the time of Eocene and mid Eocene, there is an intense geologic activity in the Pyrenees area marked by and intense sedimentation linked with the evolution of basins. This joined with the eustatic changes in Sea level are the cause of the different siliciclastic and carbonate platforms developed in the area and later eroded and redeposited resulting in turbiditic systems.

The Ainsa basin is part of the slope of the lower Eocene foredeep developed in the footwall of the Montsec thrust (Figure 2.2). Eastward the Ainsa basin was fed from a fluviodeltaic complex deposited piggyback on top of the Montes thrust sheet. Westward, it grades into the more basinal part of the foredeep (referred as the Jaca Basin) (Falivene et al., 2006).

During the early to Mid Eocene, the basin was developed as a piggyback basin on the propagating thrust front belt of the evolving Pyrenees. The filling of this basin (4000m thick) consists mainly in deep water deposits which were confined between two structural highs, which today are expressed as anticlines and they constitute slope complex deposits from the San Vicente Formation (Bakke et al., 2008). The filling of the Ainsa basin was completed during middle Lutetian to Bartonian time and is recorded by the northwest-prograding, shallow-marine to continental Sobrarbe Complex (Dreyer et al., 1999).

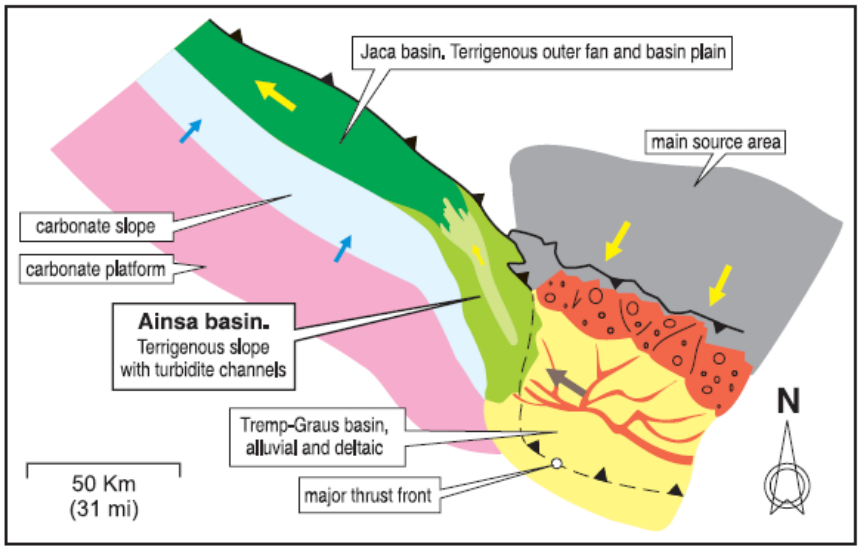

Figure 2.2 Positions of the lower to middle Eocene depositional systems in the south-central Pyrenean foreland basin. Arrows indicate provenance and dispersal (Arbués et al., 2007).

2.3 Stratigraphic framework

From largest scale to smallest scale, the basin filling has been subdivided into several allogroups (high-rank and large-scale stratigraphic units, NACSN, 1983), which had a duration of 2-5 m.y. Their boundaries are subaerial unconformities toward the hinterland and submarine angular unconformities toward the foredeep, which represent erosional submarine slopes. All allogroups have an overall regressive character and their organization respond to cycles of thrust activity.

The slope complex within the allogroups has been, also, subdivided by unconformities, which represent erosive slope conduits, as well. In the bottom part of the unconformity-bounded slope, several turbidite systems have been preserved and among them the Ainsa turbidite system, which is stratigraphically located in allogroup III (Figure 2.3). It has a width of 8 km and 9 km length with a maximum thickness of 305 m. The bottom of the system is an angular unconformity but the top is a gradual transition into a mudstone unit.

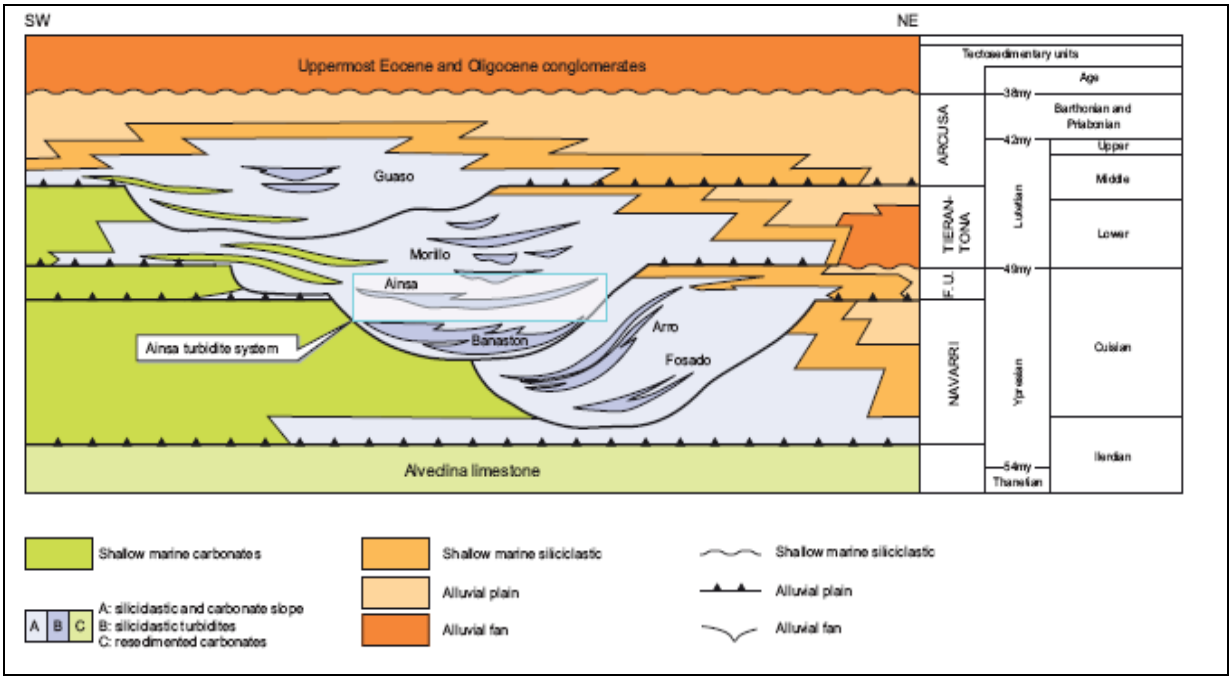

Figure 2.3 Stratigraphic cross-section of the Ainsa basin deposit. The blue box indicates the stratigraphic position of the Ainsa turbidite system (Bakke et al., 2008).

The turbidite system has been subdivided into three cycles of channel-complex development and abandonment, which are composed of stacked channel forms, and can have thickness of several tens of meters. Channel complexes can also be subdivided in sequences of channel forms (Arbués et al., 2007). Each cycle consists of:

- A lower segment characterized by the presence of one or two channel complexes.
- Upper segments (mudstone-dominated) that represent episodes of relative abandonment of the system.

2.3.1 Facies and architecture of the Quarry Outcrop

The outcrop corresponds to a partial section of one of the two-channel complex in the lowermost cycle in the Ainsa turbidite system.

The Ainsa-1 quarry outcrop characterization is performed through an accurate field study. The exposed section, along the road A-138, is up to 42 m thick and 750 m long and oriented in direction of SSE-NNW oblique to the mean paleoflow direction (290°) (Falivene et al. 2006). The base of the channel complex is not exposed, but it is interpreted to be few meters below the stratigraphically lowest bed in the outcrop. On the top of the channel complex, there is a sharp-based that corresponds roughly to the base of a 70-m-thick, muddy slump deposit that marking the separation between the Ainsa-1-quarry channel complex from the Ainsa-2 cycle (Arbués et al., 2007) (Figure 2.4b).

Based on field study carried out by Arbués et al. (2007), five facies have been distinguished:

1. ***Gravelly mudstones (gM):*** They correspond with soft-sediment deformed material with a mudstone-dominated composition, with small amounts (less than 5%) of coarser grained sediment. They have been interpreted as cohesive debris-flow deposits due to its disorganized character and mudstone-dominated composition.
2. ***Heterolithic packages and mudstone beds (H):*** this facies corresponds to packages of layered mudstones and fine-grained sandstone beds up to 10 cm thick but, thicker mudstone layers can be observed in this facies, as well. The deposition can be described in terms of the Bouma sequence, which corresponds mostly with deposits of low-density turbidity currents.
3. ***Thick-bedded sandstones (TkS):*** this facies includes sandstone beds thicker than 10 cm with grain size ranges from very fine to pebble, although up to 75% of sandstones correspond to medium to coarse grain size. The clasts include mudstone clasts and less than 5% limestone clasts gravel-size. Usually, the thicker beds are erosively based and formed by several amalgamated beds, whereas other thick-beds have sharp soles and are non-amalgamated. This facies has been interpreted as deposits of both high and low-density turbidity currents.

4. ***and 5. Mudstone-clast conglomerates (McC) and Conglomerates (C):*** both facies are up to 1m thick and have erosive bases, are clast supported (clast size ranges up to cobble) with a matrix of sand and they are very poorly to poorly sorted. Pebble and cobble-size clasts include rounded to subrounded limestone clasts and mudstone clasts.

Both facies represent the deposits left behind from hyperconcentrated flows that were experiencing a transformation into high-density turbidity currents (Arbués et al. 2007).

The Ainsa quarry outcrop division is based on erosional surfaces of turbidite channels, because their filling is multistory and includes facies associations that represent variable degrees of erosion and sediment bypass by turbidity currents (Arbués et al., 2007). Based on stacking pattern and lithology, the outcrop can be subdivided in three channel-form sets (C1–C3) (Figure 2.4b).

- ***Interval C1*** composed by five random, laterally stacked channel forms (Figure 2.4b), with gravelly mudstone and heterolithics as dominants facies, but a small percentage of thick-bedded sandstones facies is present.
- ***Interval C2*** is a 24 m thick channel form which overall characteristics are: (1) thick-bedded sandstones dominated composition, (2) coarse-grained and amalgamated toward the base and south, and (3) finer grained, thin-layered-bed, towards the top and north, where there is a major percentage of heterolithics facies. C2 is composed by two channel forms, C2.1 and C2.2, in which C2.1 can be subdivided as well in three packages: lower, middle and upper.
- ***Interval C3*** of 30 m thick is mostly composed by gravelly mudstones facies, although there are a small percentage of lenticular units of other facies (Figure 2.4b). The base of this channel-form cuts deep the top of the channel form C2, which represents an episode of cannibalistic rejuvenation.

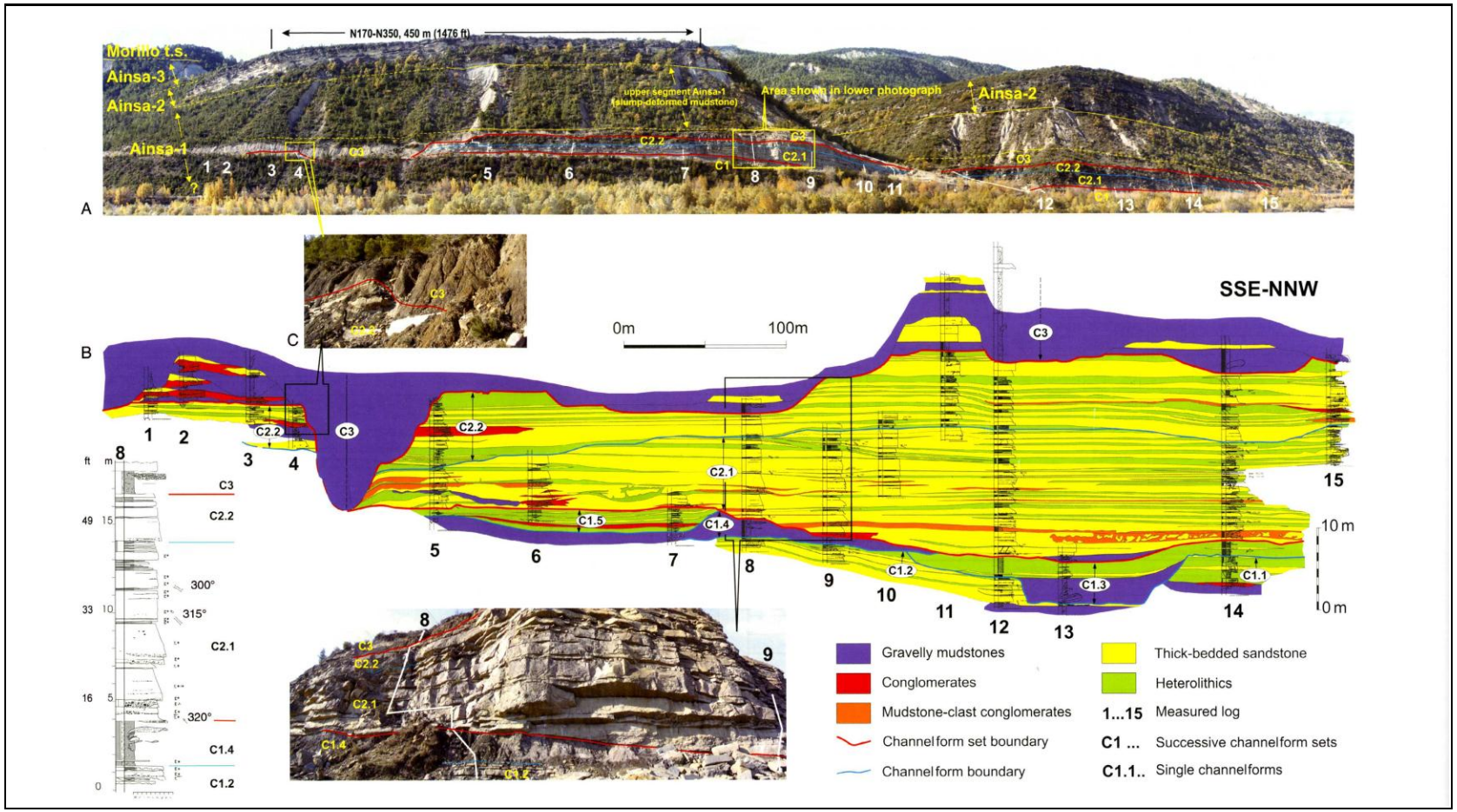

Figure 2.4 Ainsa-1 quarry channel-complex data. (A) General view of the Ainsa turbidite system, south of Ainsa. Here the Ainsa system is 210 m thick. Another turbidite system (Morillo) is visible to the south. The intervals labeled Ainsa-1, Ainsa-2 and Ainsa-3 are the three cycles of channel-complex development and abandonment that make the Ainsa turbidite system. The Ainsa-1 quarry channel-complex consists of the lower segment of the ainsa-1 cycle and is overlain by slump-deformed mudstones. (B) Characterization of the Ainsa -1 quarry channel-complex at the quarry outcrop. The scale bars are 100 m and 10 m. It resolves sandstone beds thicker than 10 cm and is base on correlation of 14 logs that also have been show in (A). Three channel form sets (C1-C3) can be distinguished based on lithological and architectural differences. (C) Local view of the deeply incised base of C3. (D) Local view of the erosional base of C2. (E) Facies details along log 8.

Chapter 3 Facies modeling

3.1 Previous work

The objective of the previous work: *"Quantitative interpretation of multi-dimensional seismic models turbidite channels from the Ainsa-1 Quarry analogue (Spain)"* (Zadeh, 2009) was to create a high resolution seismic modeling of channel complexes heterogeneities to better understand the links between seismic images and sedimentological models, to analyze the possibilities of delineating channel limits using reflectivity contrasts and to evaluate if seismic amplitude variations and estimated acoustic impedance can be used to identify the facies channel inside channels.

For this, they performed:

1. A 1D convolution model from the facies logs extracted from the outcrop (well log measurements of velocity and density provide a link between seismic data and the geology of substrata).
2. After the 1-D convolution model, a 3-D geological model was built which contained surfaces, lithology description and petroelastic parameters, which were useful for seismic modeling. In this step, they built a structural model (grid) based on geological point of view and outcrop studies and this is the grid chosen in our study.

They divided the outcrop in five sedimentary zones by six horizons zones (Figure 3.1).

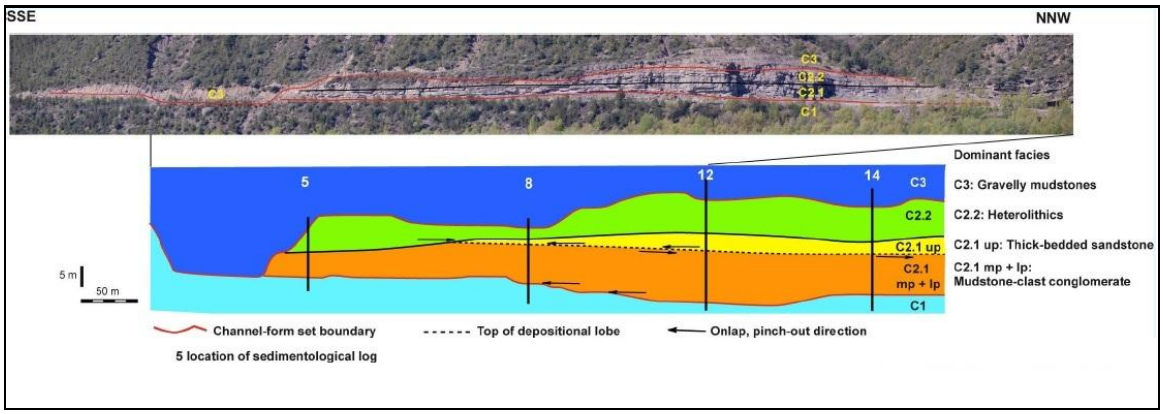

Figure 3.1 Ainsa-1 Quarry outcrop, different sedimentary zones with dominant facies in each area, explained in geology chapter (Arbués et al., 2007)

Then, they interpolate their bounding horizons using geomodeling tools and making bounding surfaces. The surfaces were limited to have an area of about 1 km^2 and made in Petrel software. A variety of algorithms are available in Petrel and they used the convergent interpolation as the default method for generating surfaces.

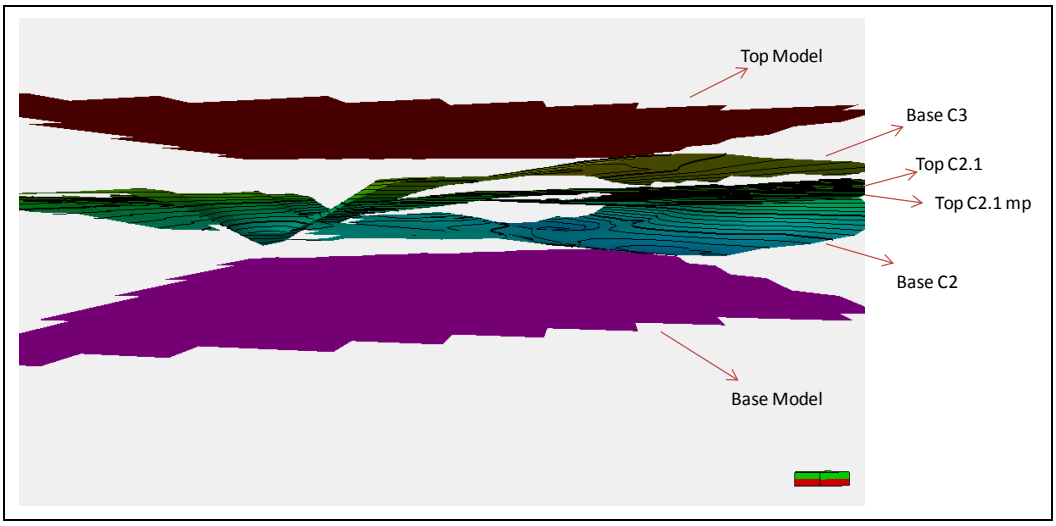

Figure 3.2 Surfaces generated for Ainsa in Petrel. Vision is from the East (Zadeh, 2009).

The first step in order to generate a model is to build a network of cells limited in a boundary at which the model is being to be constructed. Each cell has been assigned a value of the property while the value is the same all over the cell. Gridding and the size of the grids have direct effect on the quality of the model because they control the stochastic operation used for populating the property. In this case, they chose:

1. Grid size: ni × nj × nk = 64 × 70 × 145

2. Average size of cells in horizontal and vertical dimensions is: dx/dy/dz = 15/15/0.5 meters.
3. Based on geometry and architecture of the lithofacies, the space between each two horizons is divided to several zones.
4. Each zone is itself subdivided to some layers and the height of each layer corresponds to the height of the cells locating at that layer.
5. Zone division depending on the geometry of the lithofacies may be performed proportionally, following top, following base or following a reference surface.

Table 3.1 describes the zones and the layering done in this grid.

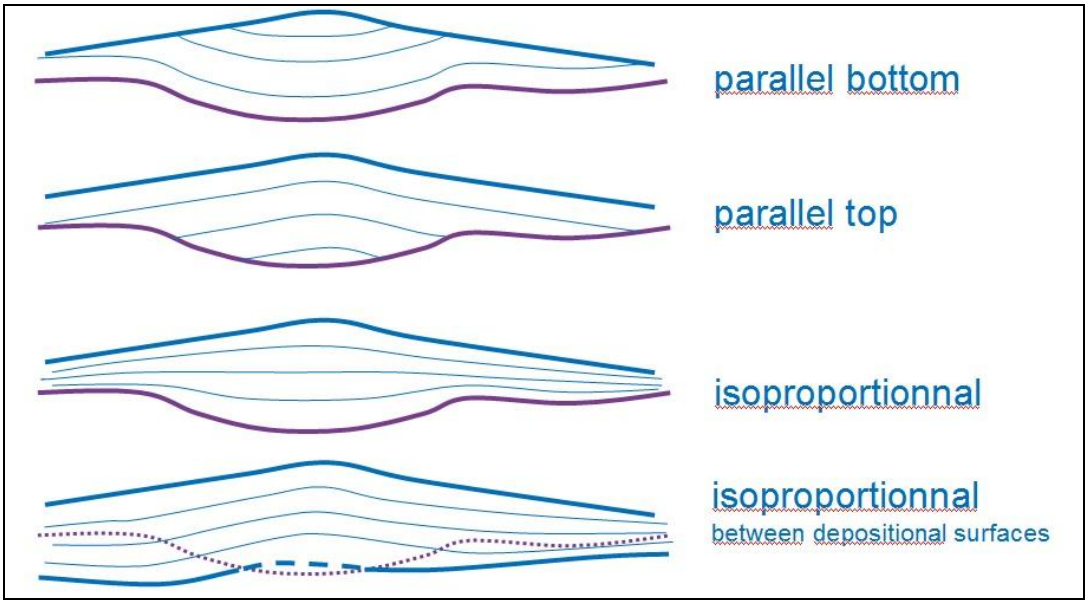

Figure 3.3 Different depositional modes for the stratigraphic model, depending on the reference level (courtesy of Brigitte Doligez, IFPEN).

Zone Name	*Bounding Horizons*	*Zone Division*	*Number of layers*
C3	Top model Base of C3	Proportional	20
C2.2	Base of C3 Top of C2.1	Follow Base	Each 50 cm=one layer
C2.2 Upper Package	Top of C2.1 Top of C2.1 mp	Follow Base	Each 50 cm=one layer
C2.1 Lower & Middle packages	Top of C2.1 mp Base C2	Follow Top	Each 50 cm=one layer
C1	Base C2 Base model	Follow Top	Each 50 cm=one layer

Table 3.1 The zones of the model and their layering

At the end, they performed the next structural model (Figure 3.4):

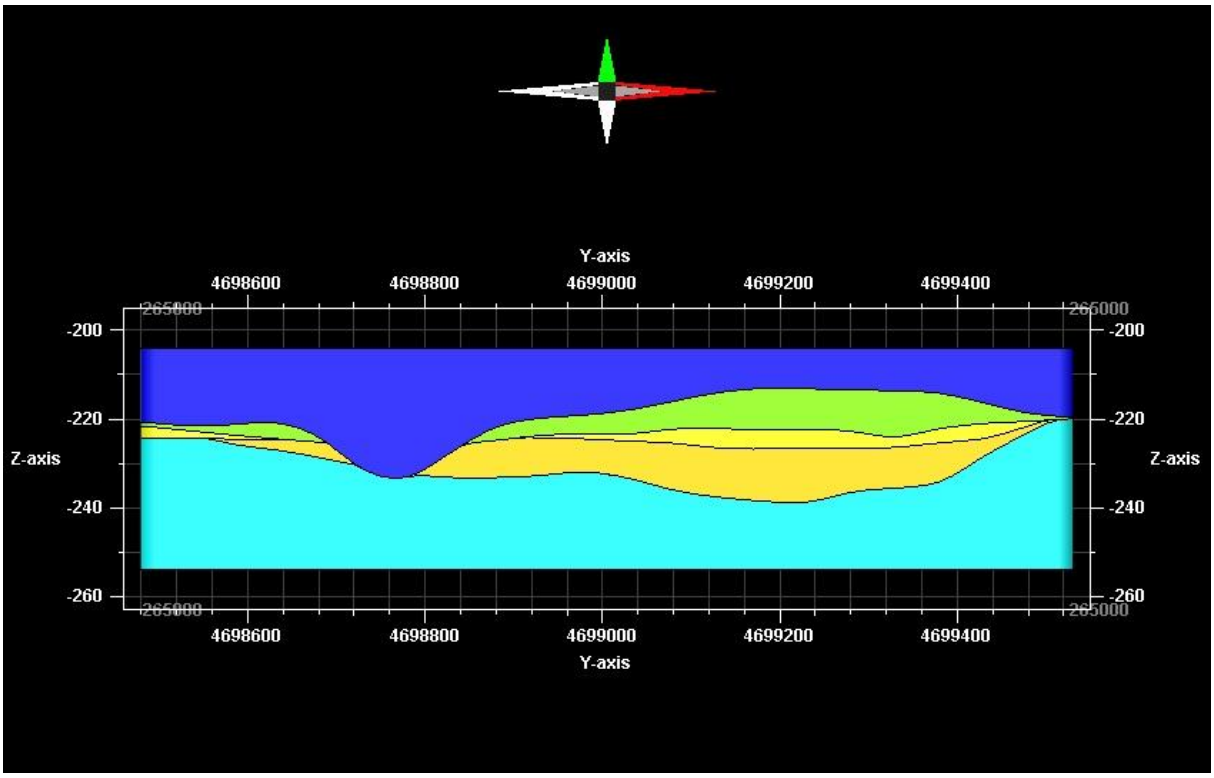

Figure 3.4 Structural model, showing the different stratigraphical zones defined in Petrel software (Zadeh, 2009).

With the structural model defined they created the facies model with extraction of soft data and hard data from the gridded outcrop by selecting four synthetic vertical logs across the outcrop; the logs and their situation in outcrop are displayed in Figure 3.5 and Figure 3.6. With this data and applying the sequential indicator simulation stochastic algorithm, they achieved to simulate the facies model. Figure 3.7 shows the 3D model in Petrel software.

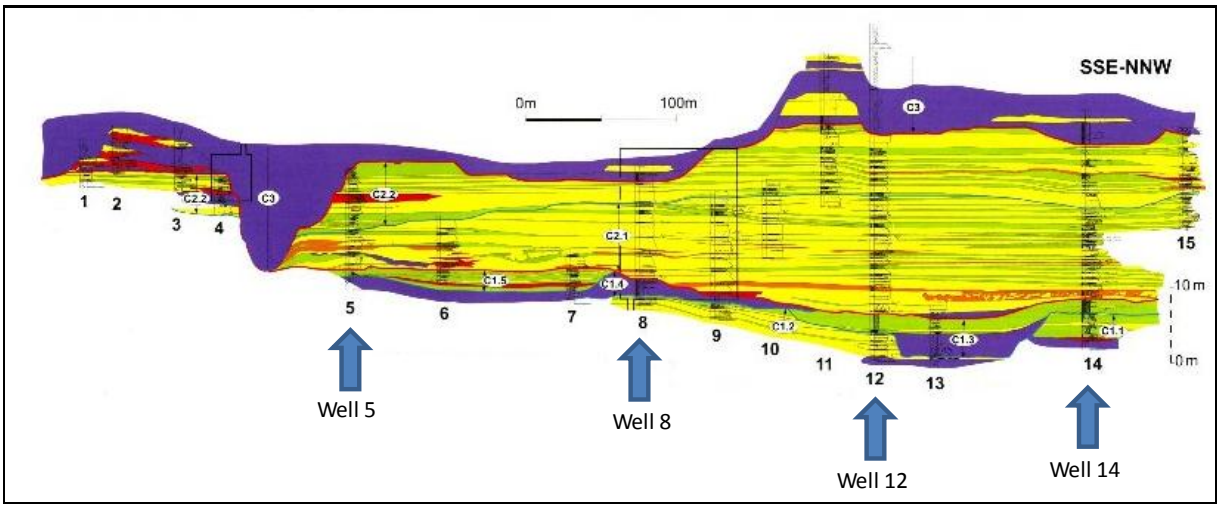

Figure 3.5 Logs and facies display in Ainsa-1 Quarry outcrop from (Zadeh, 2009).

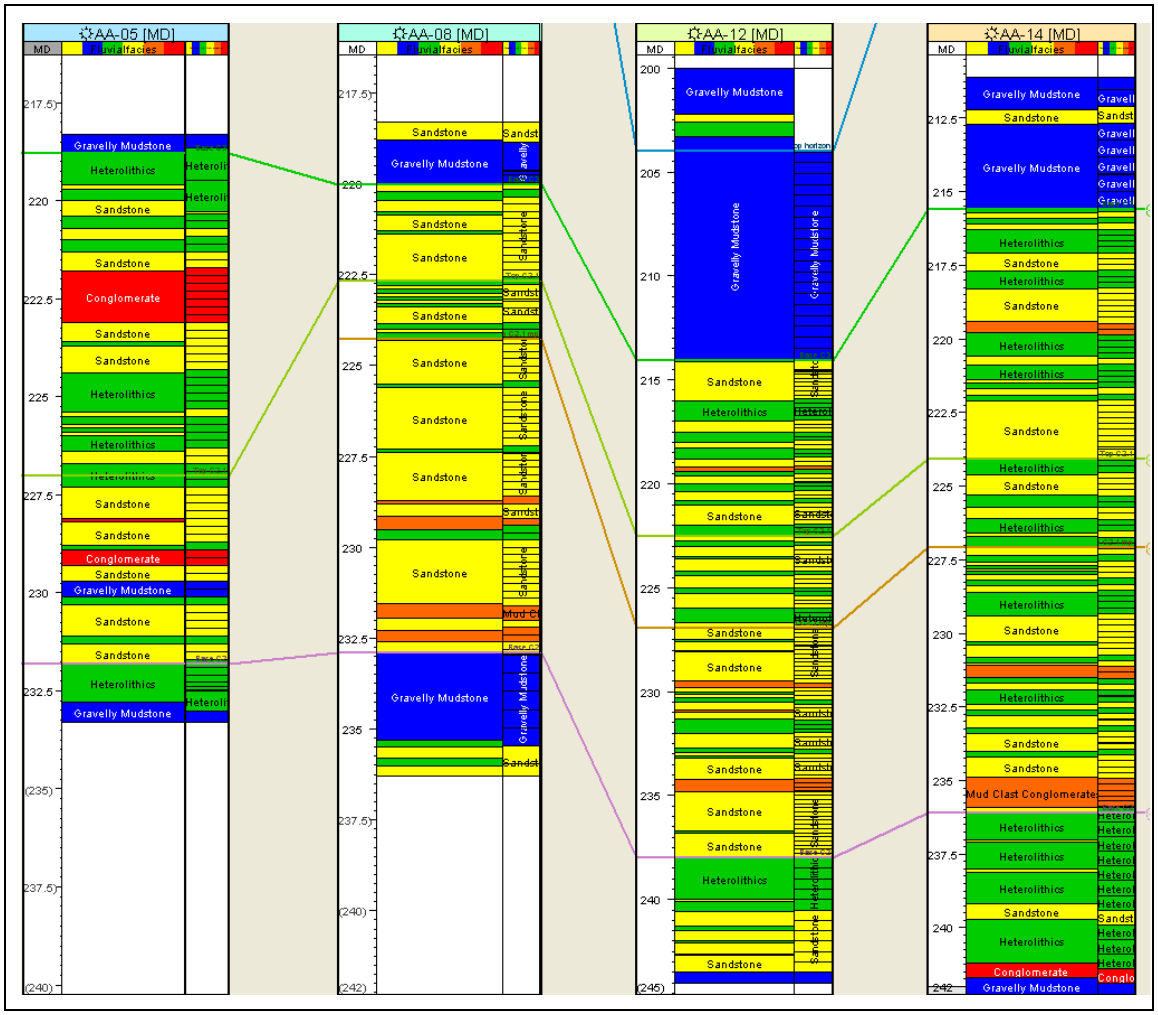

Figure 3.6 The vertical well logs considered as hard data and their corresponding upscaled facies logs (Zadeh, 2009).

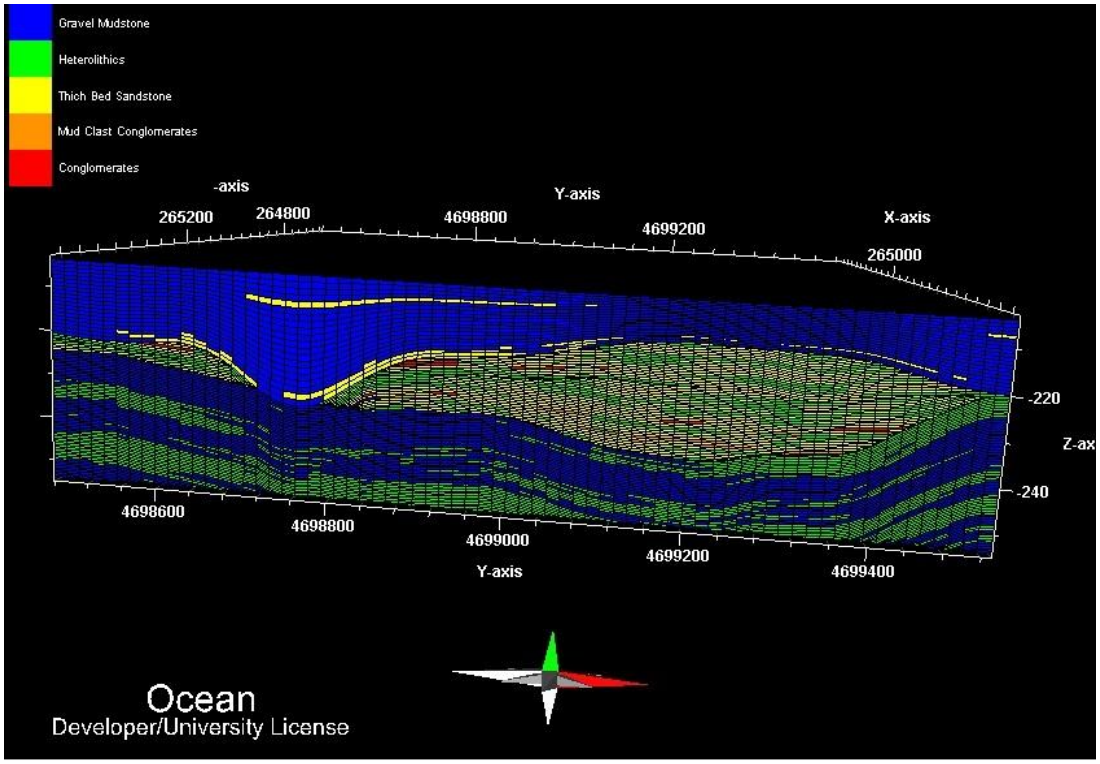

Figure 3.7 3D facies model (Zadeh, 2009). Network cells can be observed.

3.2 Stochastic facies modeling

From the grid created in the previous work: *"Quantitative interpretation of multi-dimensional seismic models turbidite channels from the Ainsa-1 Quarry analogue (Spain)"* (Zadeh, 2009), that we chose due to the grid size, structure and average height for cells which they have a good size for posterior fluid flow analysis, we simulated a 3D facies model with a software under-development called OpenFlow Suite. This means that we infilled the previous structural model (grid with zones and bounding surfaces). The 3D model is actually a 2D symmetrical model referring to the fact that it is well accurate in Y and Z direction, due to the works made in this outcrop during the last 20 years, but not well constrained in X direction.

The facies modeling involves both hard and soft data. Hard data has to remain constant during modeling without any change and the parameters modeled should get the hard data values at the locations where this kind of data exists. Hard data is discretely distributed and exist in limited number of locations. In these kinds of models, usually, well logs offer some valuable hard data for modeling geological parameters because they can reproduce an extremely well known subsurface setting, although only in the zone where they have been drilled.

For this study, the selected hard data consisted of four synthetic vertical logs were taken from the outcrop (the same vertical logs of the previous study). The four synthetic logs are from well numbers of 5, 8, 12 and 14. The logs and their situation in outcrop are displayed in Figure 3.5. Apart from this, another 4 vertical logs where extracted from the gridded characterization of the previous model (Petrel model) in the back part. In this way the filling of facies will be better constrained. In Figure 3.8 is shown the situation of these 4 new synthetic vertical logs in Petrel facies model and in Figure 3.9, the well logs.

Soft data required for conditioning the model is extracted from the outcrop characterization: facies proportions, variograms and indicator variograms. Depending on using stochastic method, some of these kinds of data may be applied.

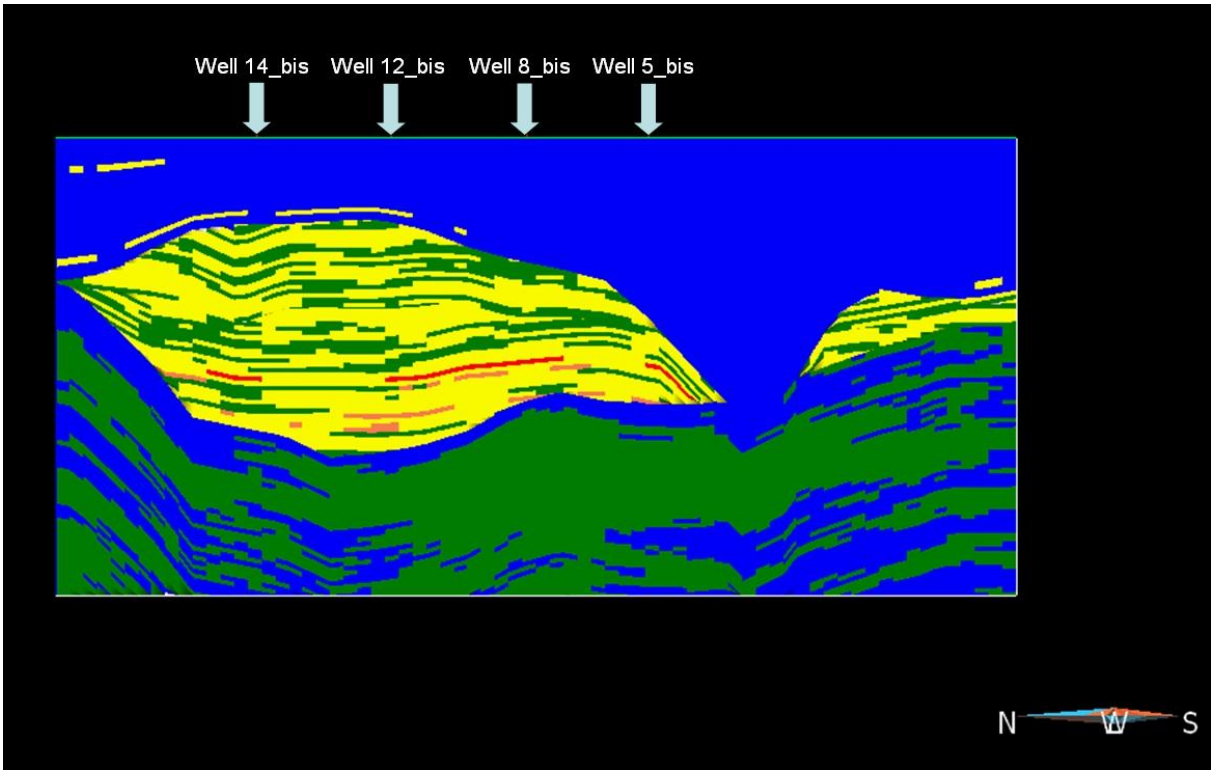

Figure 3.8 New four well logs location and facies display in the back part Ainsa-1 Quarry outcrop (Zadeh, 2009).

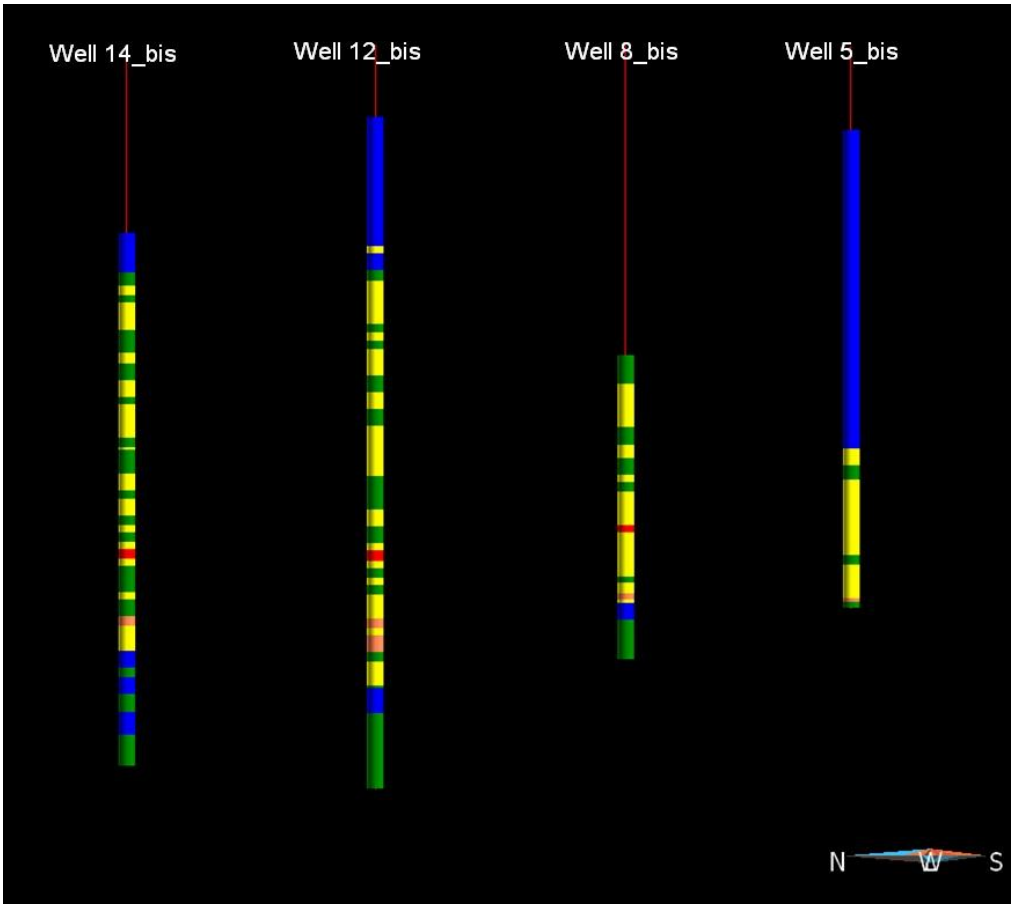

Figure 3.9 The vertical well logs, from Petrel simulation, considered as hard data situated in the back part of Ainsa-1 Quarry outcrop.

Moreover, as it can be observed in Figure 3.8 and Figure 3.9, the lithofacies scale used for demonstrating the different facies (Figure 3.10) is the same as the one used by Zadeh M.K. in 2009.

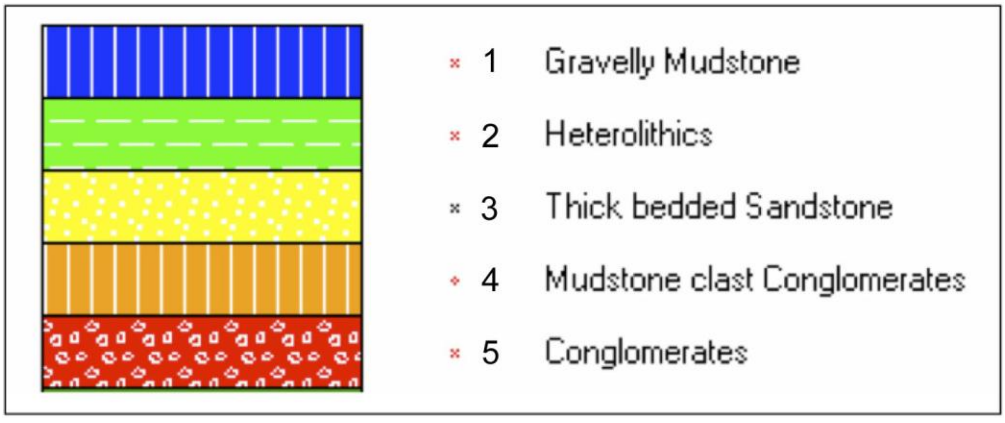

Figure 3.10 Lithofacies scale used in both studies.

After choosing the representative vertical well logs for this outcrop, the facies data of the logs is discretized to be imported into the layers created in the structural model. In other words, the

set of facies corresponding to each layer depth are being resampled by an averaging method and the output is considered to be the "upscaled facies" at the depth of the layer and the location of the log. In this study, the averaging method is *"the most represented facies"*, which takes the more frequent facies that appears at the corresponding depth of each cell and attributes it as the unique facies existing at that cell. In the Figure 3.11, Figure 3.12, Figure 3.13, Figure 3.14 and Figure 3.15, it can be observed the discretized wells logs in the different units which is divided Ainsa-1 Quarry outcrop.

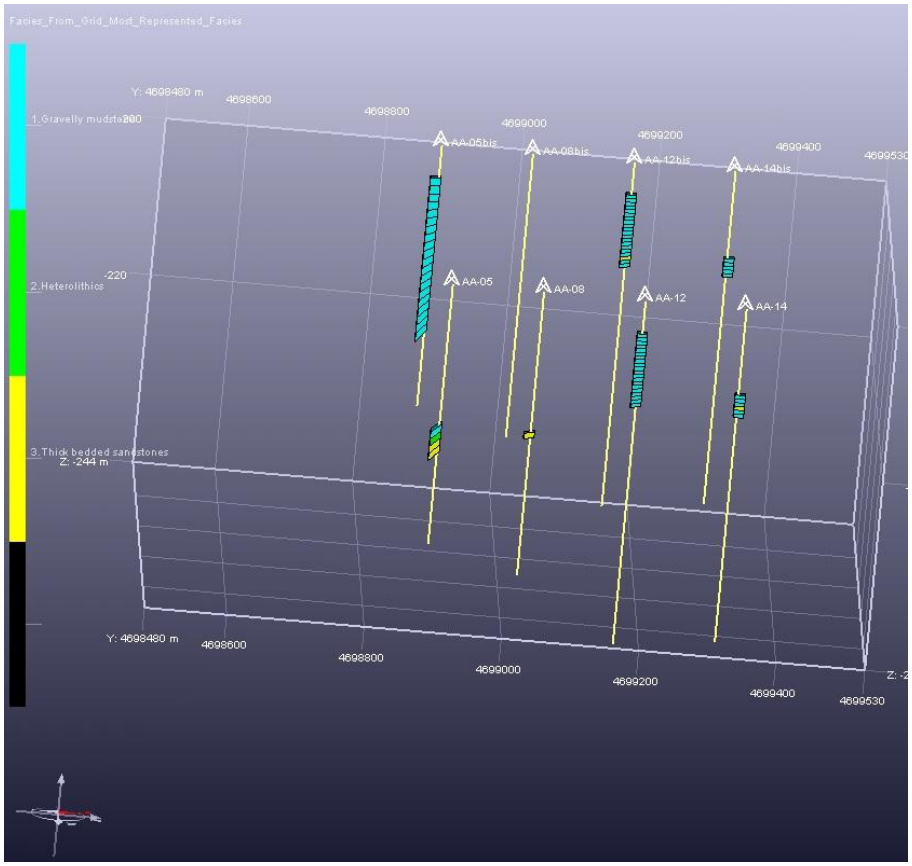

Figure 3.11 The discretized well logs in CobraFlow (OpenFlow Suite 2012) for the unit C3 of the Ainsa-1 Quarry outcrop (see Figure 3.10 for color-code).

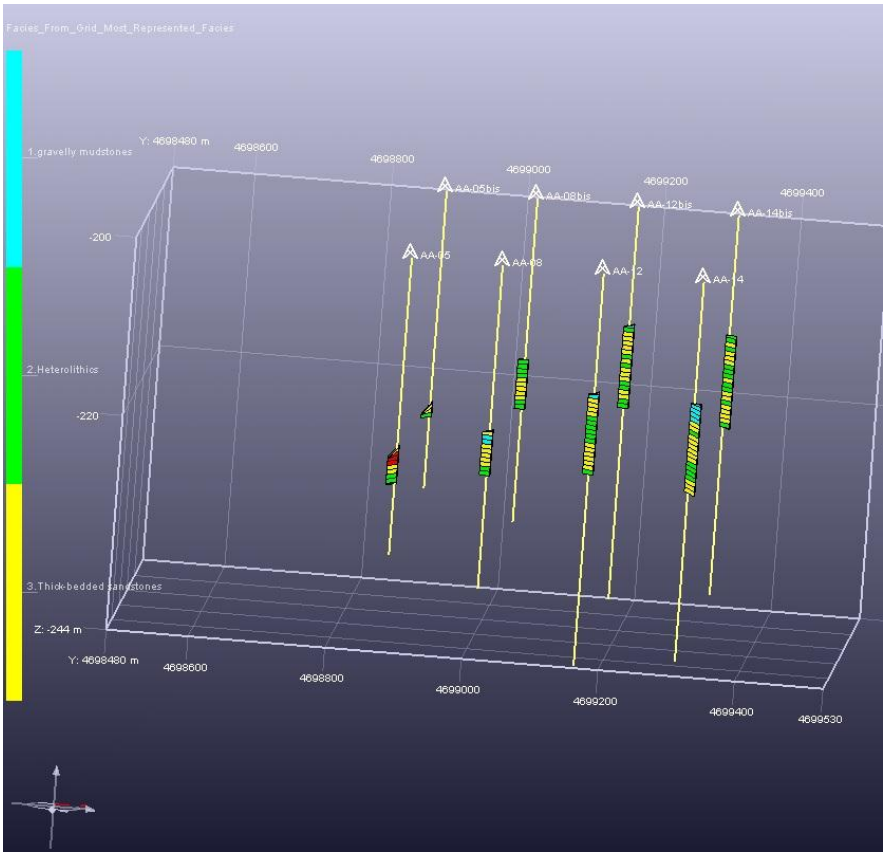

Figure 3.12 The discretized well logs in CobraFlow (OpenFlow Suite 2012) for the unit C2.2 of the Ainsa-1 Quarry outcrop (see Figure 3.10 for color-code).

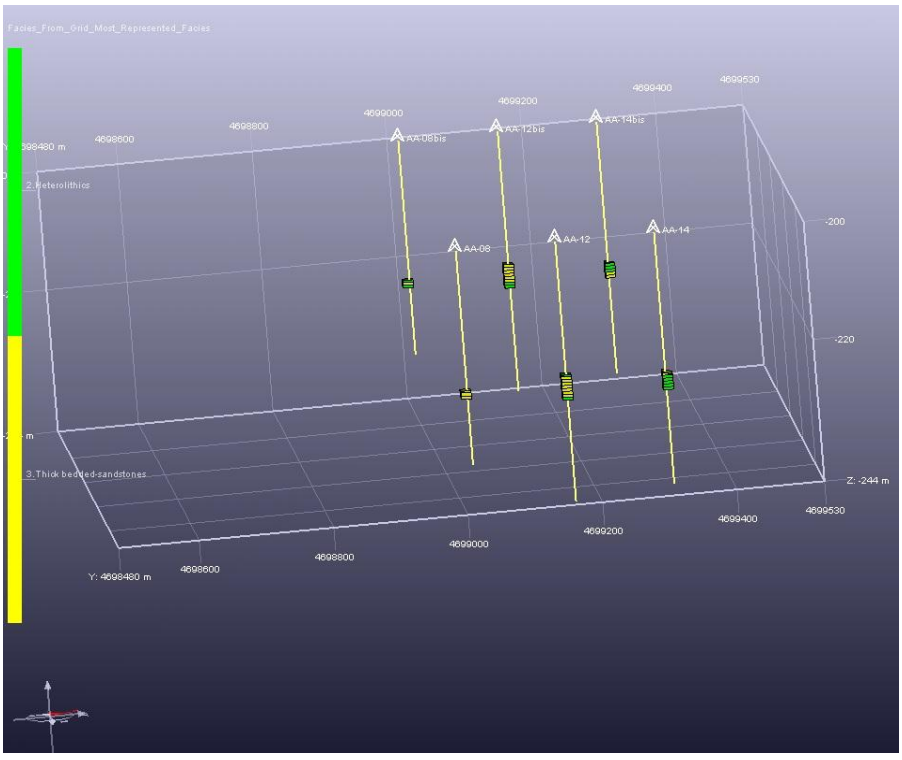

Figure 3.13 The discretized well logs in CobraFlow (OpenFlow Suite 2012) for the unit C2.1-up of the Ainsa-1 Quarry outcrop (see Figure 3.10 for color-code).

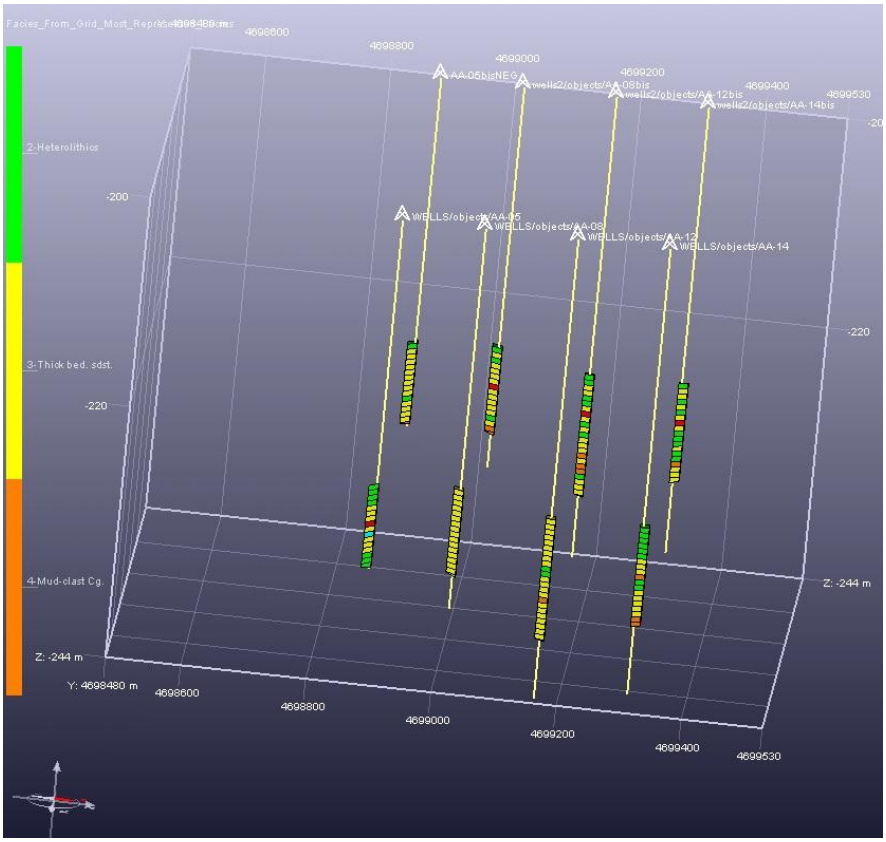

Figure 3.14 The discretized well logs in CobraFlow (OpenFlow Suite 2012) for the unit C2.1-mp-lp of the Ainsa-1 Quarry outcrop (see Figure 3.10 for color-code).

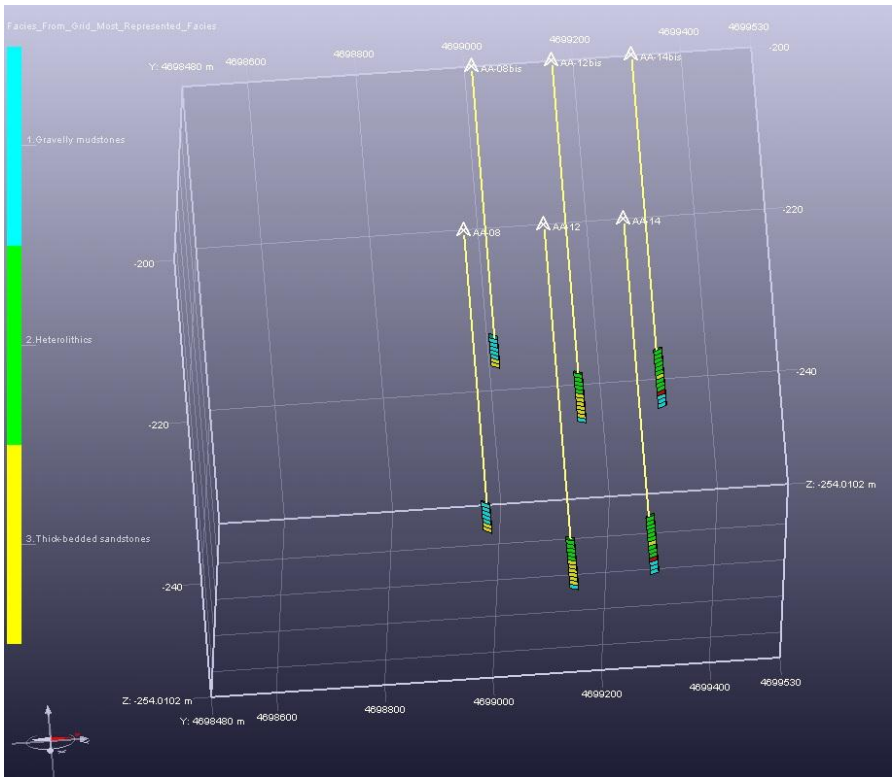

Figure 3.15 The discretized well logs in CobraFlow (OpenFlow Suite 2012) for the unit C1 of the Ainsa-1 Quarry outcrop (see Figure 3.10 for color-code).

In this step, it is crucial to check the "quality" of the discretization and that can be done by histograms. Figure 3.16 to Figure 3.20 show the different histograms for each discretized well in each unit of the Ainsa outcrop.

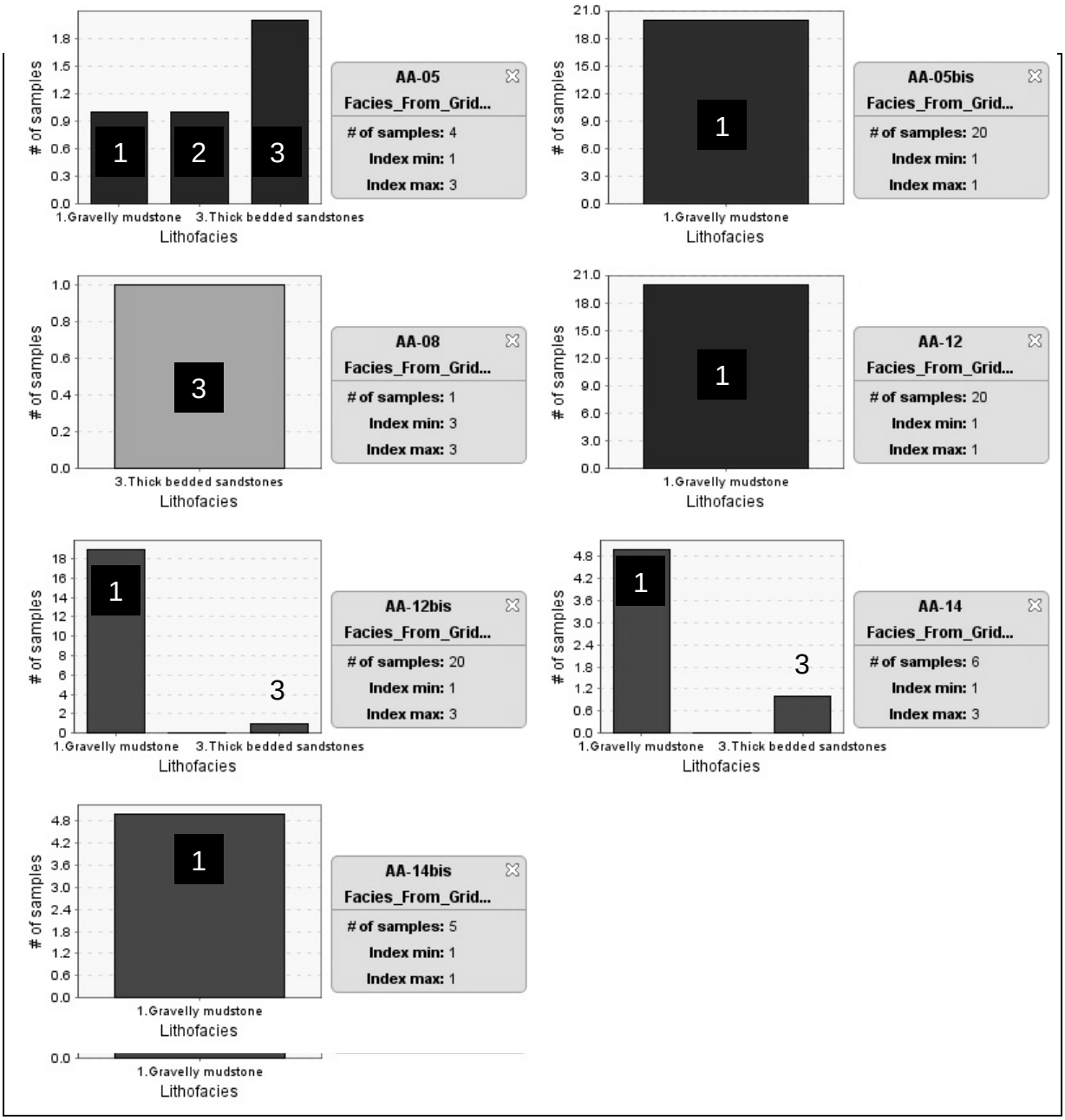

Figure 3.16 Histogram of well-log facies in the unit C3, CobraFlow (OpenFlow Suite 2012). 1: Gravelly mudstone; 2: Heterolithics ; 3: Thic-bedded sandstones.

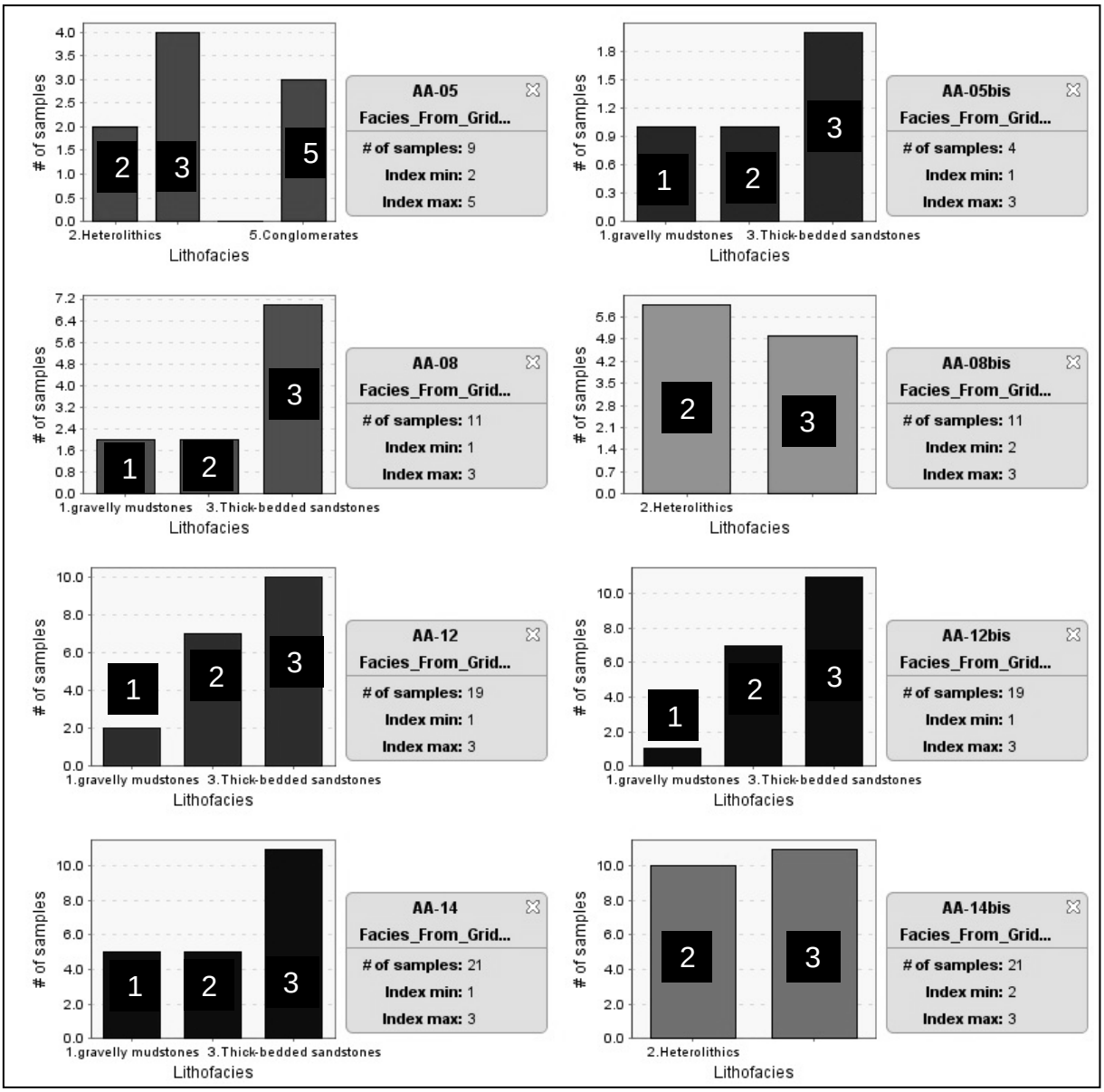

Figure 3.17 Histogram of well-log facies in the unit C2.2, CobraFlow (OpenFlow Suite 2012). 1: Gravelly mudstone; 2: Heterolithics ; 3: Thic-bedded sandstones; 5: Conglomerates.

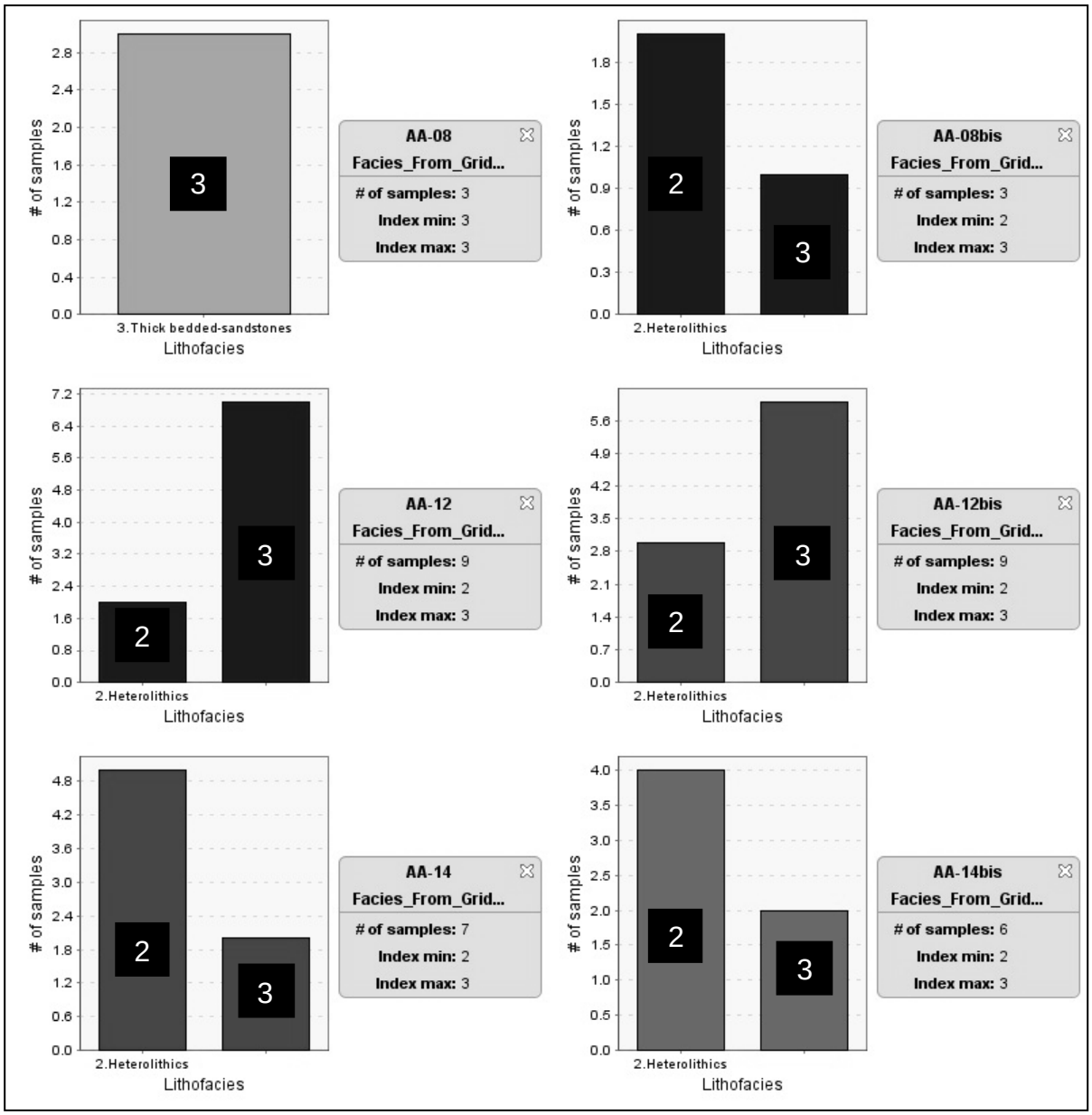

Figure 3.18 Histogram of well-log facies in the unit C2.1-up, CobraFlow (OpenFlow Suite 2012). 2: Heterolithics ; 3: Thick-bedded sandstones.

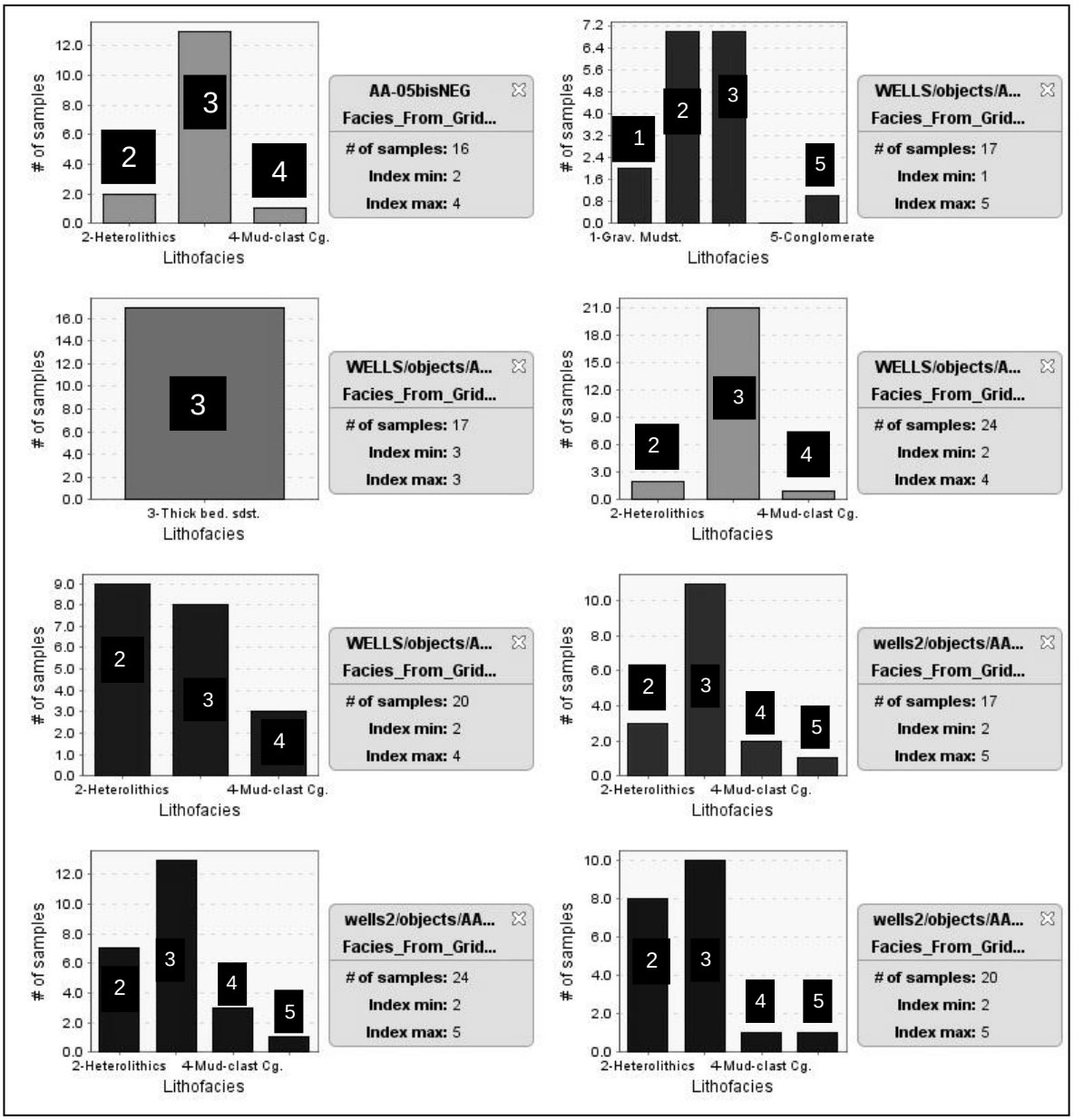

Figure 3.19 Histogram of well-log facies in the unit C2.1-mp-lp, CobraFlow (OpenFlow Suite 2012). 1: Gravelly mudstone; 2: Heterolithics ; 3: Thic-bedded sandstones; 4: Mud-clast conglomerates; 5: Conglomerates.

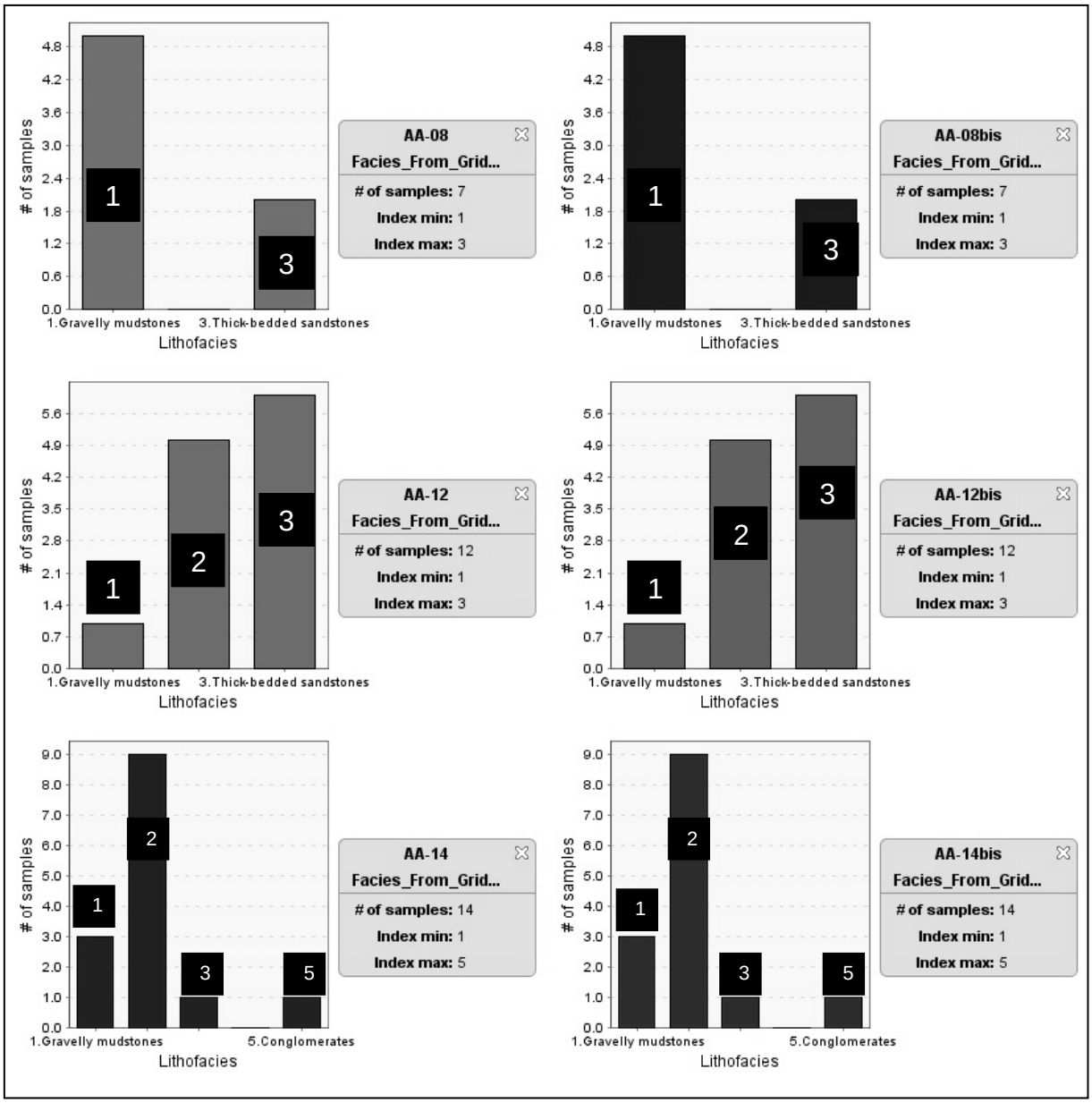

Figure 3.20 Histogram of well-log facies in the unit C1, CobraFlow (OpenFlow Suite 2012). 1: Gravelly mudstone; 2: Heterolithics ; 3: Thic-bedded sandstones; 5: Conglomerates.

3.2.1 Geostatistical approach. Stochastic Algorithms

The modeling workflow, as we have showed, consists of the following steps:

1. Interpretation of lithofacies
2. Construction of lithostratigraphic units
3. Computation of geostatistical parameters
4. Simulation of the distribution of lithofacies
5. Attribution of petrophysical properties

Therefore, after importing the existing model grid, which has the same geometry and dimensions of the outcrop and after choosing the correct hard data and discretize those logs in the different units (to have the well log information on the corresponding cells of the stratigraphic grid), stochastic algorithms are implemented to populate the discretized facies all over the gridded model.

Two categories of these algorithms exist:

1. Pixel-based methods such as Plurigaussian simulation based on Truncation Gaussian Simulation (TGS) and Sequential Indicator Simulation (SIS), which have in common that to obtain a simulated field, a value is assigned to each cell according to a probability distribution function (PDF), (Falivene et al., 2006). At each cell the PDF is calculated taking into account both hard data and soft data.
2. Object-based methods, which consist on inserting an object in the model replacing the background. Those objects can have different geometries and dimensions but they are discretized according to the grid geometry. In other words, each object spans several cells.

A channel filled with debris flow cuts deep-water sediments in Ainsa-1 outcrop. Therefore, the approach developed for the geostatistical modeling of the distribution of lithofacies in this study is based on the pixel-based methods, which correspond to stochastic, sequential, geostatistical-based facies modeling algorithms (Falivene et al., 2006), because this approach has already been applied successfully in many depositional settings, including deep offshore settings (Lerat et al., 2007). We used both plurigaussian simulation and SIS.

The Plurigaussian simulation is based in the Truncated Gaussian simulation algorithm; this means that it requires a preliminary estimation of facies proportions, in order to define the thresholds which back transform the values of the underlying Gaussian Random Function (GRF) into lithofacies.

The simulation process consists of the following steps:

1. Generation of GRF, using the variogram model fitted to the experimental variograms calculated from data, then truncation of this GRF using thresholds to divide the random space into classes: above, between and below the thresholds. In stationary configurations, heterogeneities are assumed homogeneously distributed in the

simulation volume. In this case, the thresholds are constant. Non stationary configurations correspond to cases showing lateral trends in the distribution of lithofacies proportion, for which the thresholds are variable.

2. The vertical proportion curve (VPC) represents the relative distribution of facies in the main vertical facies sequences of the geological unit (Lerat et al., 2007). It is linked to the truncation threshold of the GRF. Instead of using one single vertical proportion curve, the algorithm can deal with a 3D matrix of proportions that represents the spatial variations of facies proportions. The truncation thresholds of the GRF are variable in space and the simulated lithofacies values follow these variations. A classical method of constructing a 3D grid of proportions is to interpolate local vertical proportions curves, calculated from each well or groups of wells from similar geological environments.

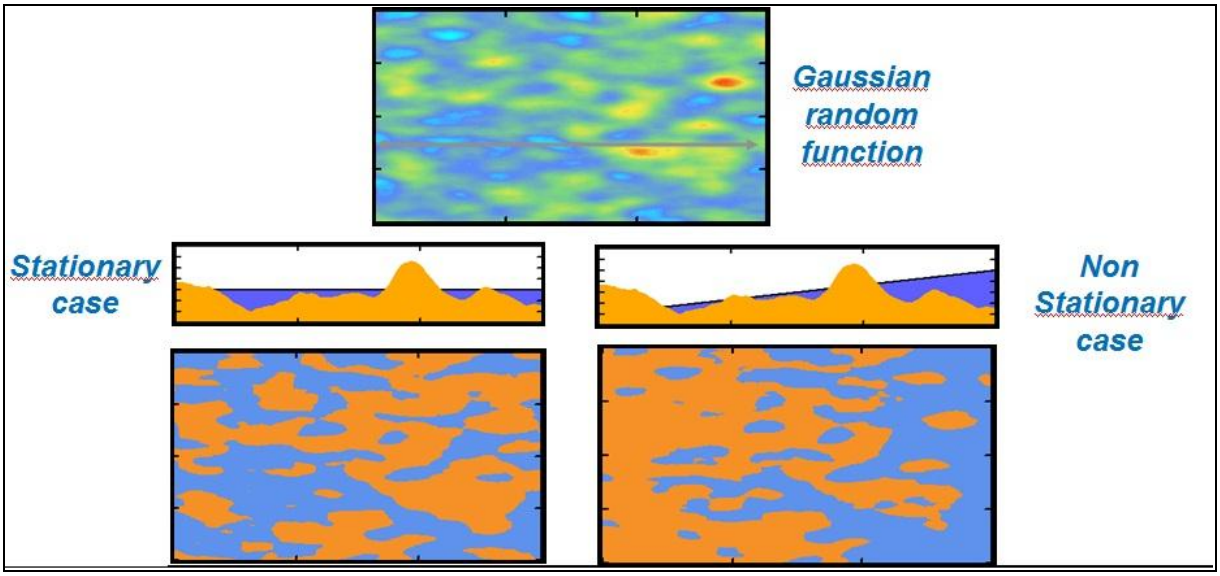

Figure 3.21 Principle of the truncated Gaussian approach for a synthetic two-facies case (courtesy of Brigitte Doligez, IFPEN).

In this study, we have used Plurigaussian simulation, non-stationary case, in the unit C2.2 and unit C1. After several runs with different methods in these units, the plurigaussian simulation created the most accurate and "realistic" facies distribution, in comparison with Ainsa-1 Quarry outcrop (Figure 2.4).

To analyze the data with this method, comparisons defined for each facies in each stratigraphical zone while trying to keep the relative proportion of each lithofacies based on the correlation panel prepared from outcrop data.

The variogram can be described as a basic tool to analyze the spatial variability of data, because it tries to capture the regional organization of data, which is not purely random. They are linked with the measure of spatial correlation between data values separated by a given distance, and reflect the intuitive idea that data values are generally more correlated for short distances than for long distances. The characteristics of a variogram are (Figure 3.22):

- Sill: plateau reached after a certain distance called the range. This plateau exists if there is no trend in the data. The sill is the data variance.
- Nugget effect: extrapolation of the variogram towards the distance origin. It is the short scale variability.
- Range: distance at which the variogram reaches the sill. Two points separated by a distance larger than the range are not correlated.

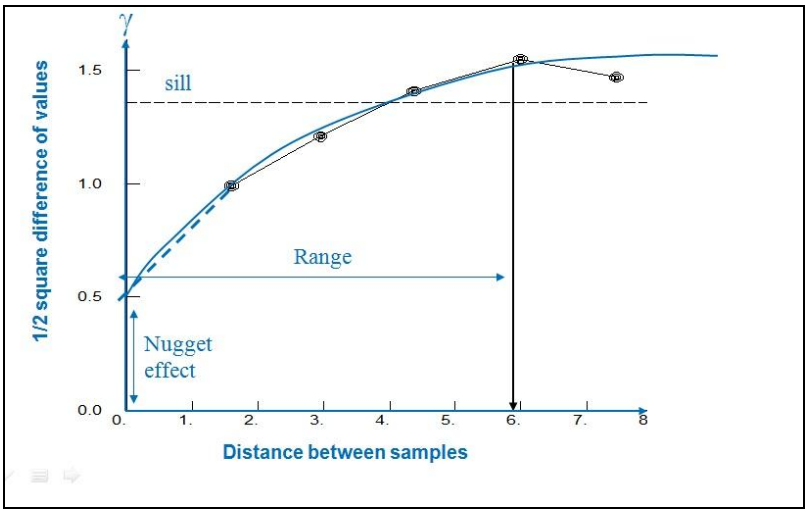

Figure 3.22 Principal variogram characteristics (courtesy of Brigitte Doligez, IFPEN).

For this reason the experimental variograms created for the units C1 and C2.2, can be described by determining values of range, sill and nugget. Since the sill and nugget has been assigned to have constant values of 1 and 0.1 respectively, the variability of the model mostly in vertical direction (2D symmetrical model) is dependent on the values attributed for the range values in major horizontal, minor horizontal and vertical directions. Referring to the study of Falivene et al. (2006), the values for major direction range, minor direction range and vertical direction range for all the facies can be considered to be the same with a good approximation and they can get the values of 500, 100 and 0.5 m respectively (vertical values should be at least the height of the cells). As mentioned before, the major direction can be oriented towards WSW-NSN and the minor direction will be towards SSE-NNW.

The SIS method which is based on indicator approach and when it deals with categorical variables like facies, the indicator approach transforms each facies into a new variable, and the value of each variable corresponds to the probability of finding the related facies at a given position (Falivene et al., 2006). The principle of the SIS method (Figure 3.23 and Figure 3.24) is that points are simulated one after another, provided that their conditional distribution given previously simulated points was known. The probability that the indicator at a target points takes the value 1 is estimated by indicator kriging (when hard data exist the value of the variable corresponding to the facies present is 1 and for the other is 0). For a better understanding, the different methods and parameters used in the different units are summarized in tables in the section 3.2.2.

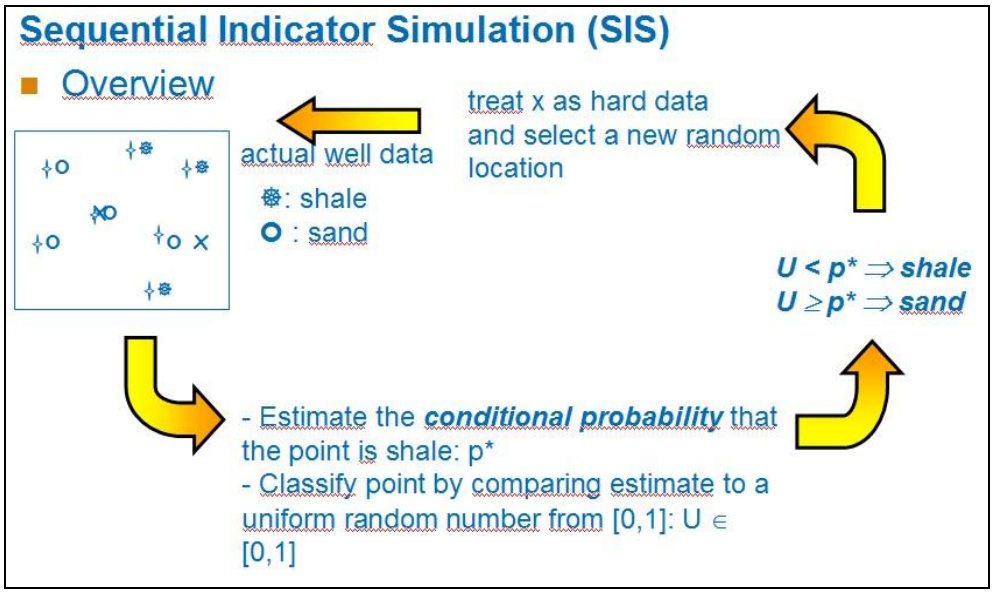

Figure 3.23 Principle of the Sequential indicator simulation (courtesy of Brigitte Doligez, IFPEN).

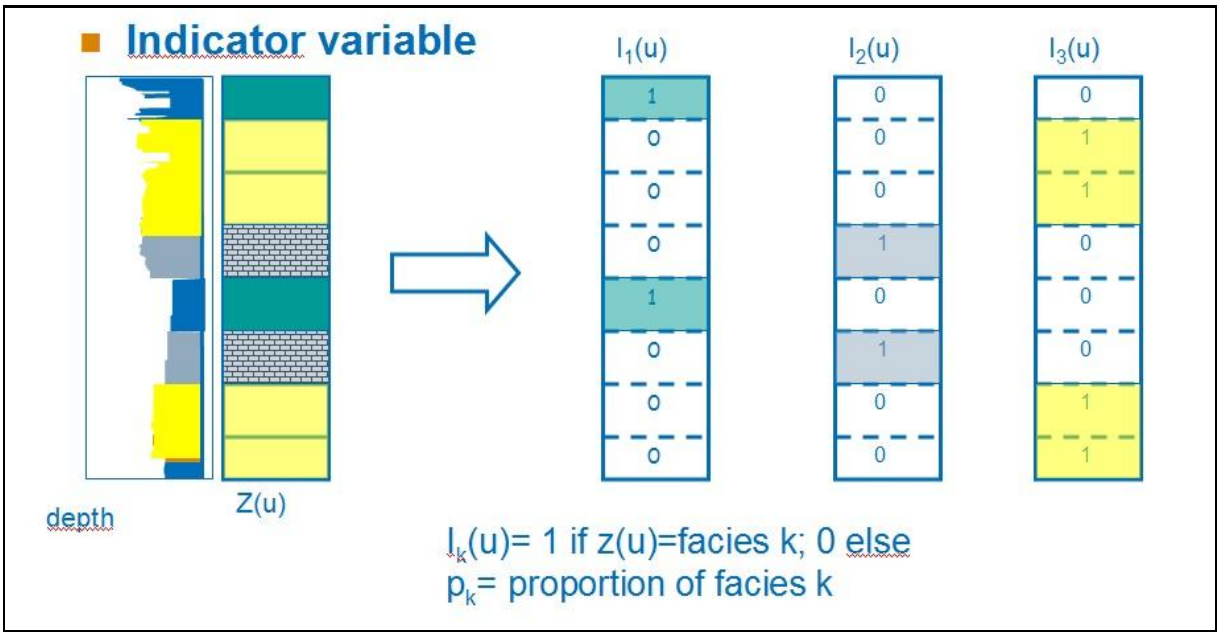

Figure 3.24 Sketch showing how SIS gives values to the hard data, (courtesy of Brigitte Doligez, IFPEN).

SIS method has been used for the units C3, C2.1-up and C2.1-mp-lp.

To analyze the data in these cases, an indicator variogram is defined for each facies in each zone, using the same values of the experimental variograms created for the Plurigaussian method. The values used for the variograms in the different methods are summarized in tables in the next section.

The next step in the stochastic facies simulation is creating the vertical proportion curves (VPC, see Figure 3.25), for each well as well as the matrix of proportion from the VPC created for both methods in each unit. The matrix of proportion in each zone is adjusted, so the facies proportions in the model come out to be identical with the real proportions in outcrop.

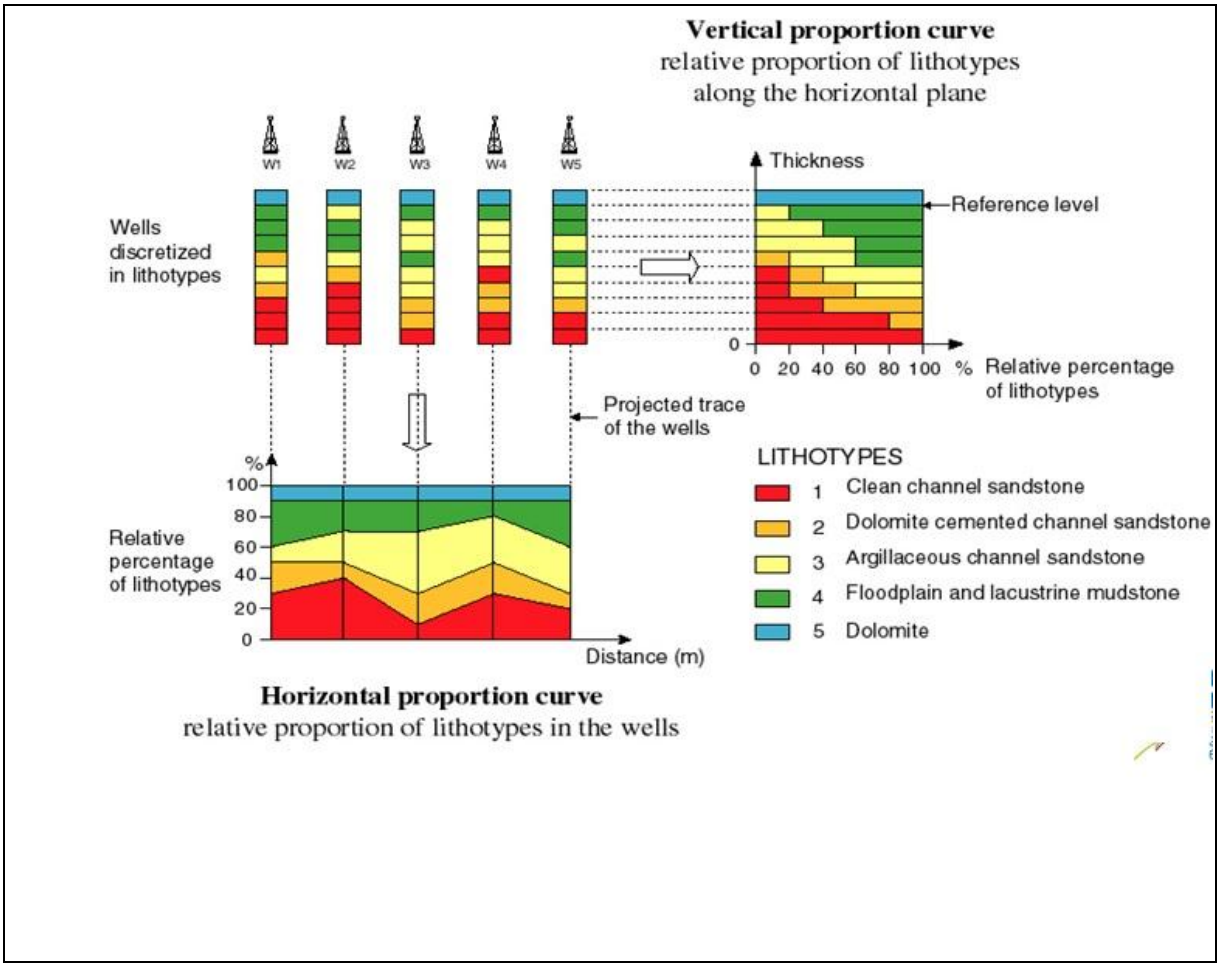

Figure 3.25 Sketch showing how a VPC is defined from well discretized logs (courtesy of Brigitte Doligez, IFPEN).

We decided to use proportion matrix (non stationary cases) because this tool allows to define realistic situations like one or two channel trend. The VPC assumes that the vertical proportion of lithotypes has no lateral trend.

For each VPC the proportion of the lithotype is calculated layer by layer. Several methods are available to assign VPC to the vertical proportion matrix macro cells:

1. Computing vertical Proportion Matrix from VPC.
2. Designing areas in which you can assign specific VPC.
3. Computing averaged VPC from wells information in a macro cell.

For this study, we chose computing vertical Proportion Matrix from both VPC and areas, depending on the geometry, sedimentation and sequence stratigraphy of each unit.

The VPC matrix construction is divided in four steps: (1) Matrix parameters (define the number of X and Y cells you want to put together to create the proportion Matrix grid), (2) computation method selection, (3) kriging parameters and (4) constraint definition (optional). In the next section, it is described how the matrix was constructed for each unit of the outcrop and why.

3.2.2 Geostatistical approach. Analysis of the simulation results

In the next pages, we display the results of the facies distribution (Figure 3.26 to Figure 3.54 and Table 3.2 to

Table 3.6). For each unit, it can be observed:

1. Matrix of proportion curve
2. Table displaying the method used in that unit and the values used for the variograms
3. View from the top of the unit
4. View from the bottom of the unit
5. View from the front part of the unit
6. View from the back part of the unit
7. Cross-sections, if necessary.

The final facies model is finally displayed in Figure 3.55.

UNIT C3

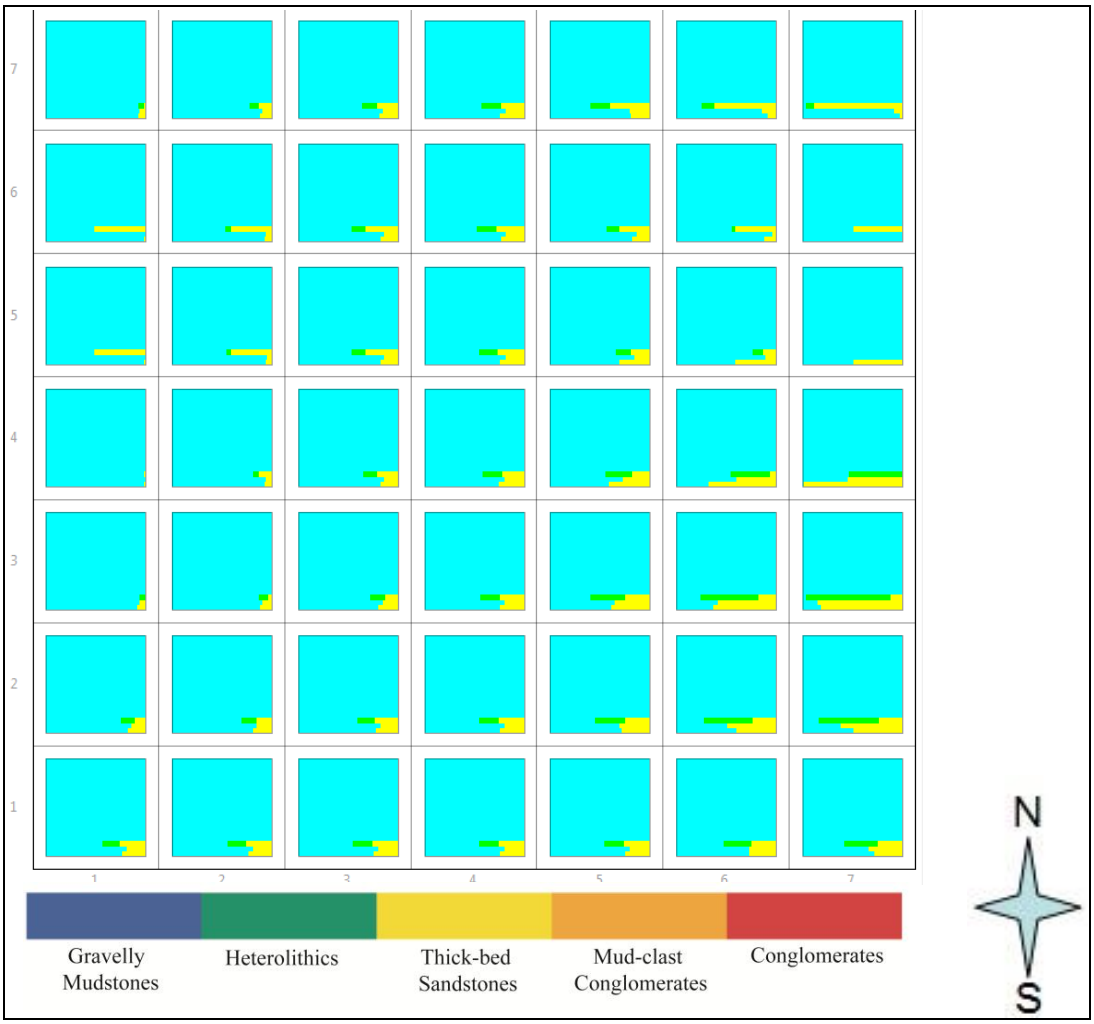

Figure 3.26 Matrix proportion curve for the unit C3 with a grid of 10X10 for X and Y and computing by the VPC created. In this unit the infill of the VPC is made with the facies gravelly mudstone because is the dominant composition and it is not used the smooth tool. It can be observed major percentage of sand composition in the SE of the outcrop. If one checks Figure 3.11, it is shown that the wells AA-05 and AA-08 have big percentage of sandstones facies and they are situated in the SE region of the outcrop.

Method	Fitting model	Range X	Range Y	Range Z	Azimuth
SIS	Non-stationary	500	100	0.5	-70

Table 3.2 Stochastic method used in unit C3 (the one chosen after comparing several runs with different methodology and parameters values) and the correspondent values of the parameter that describe the variogram. X, Y and Z in meters. The azimuth chosen is related with the orientation of the anisotropy and we used an average value parallel to the current directions (290°, i.e., WNW-ESE) cf., Chapter 2.

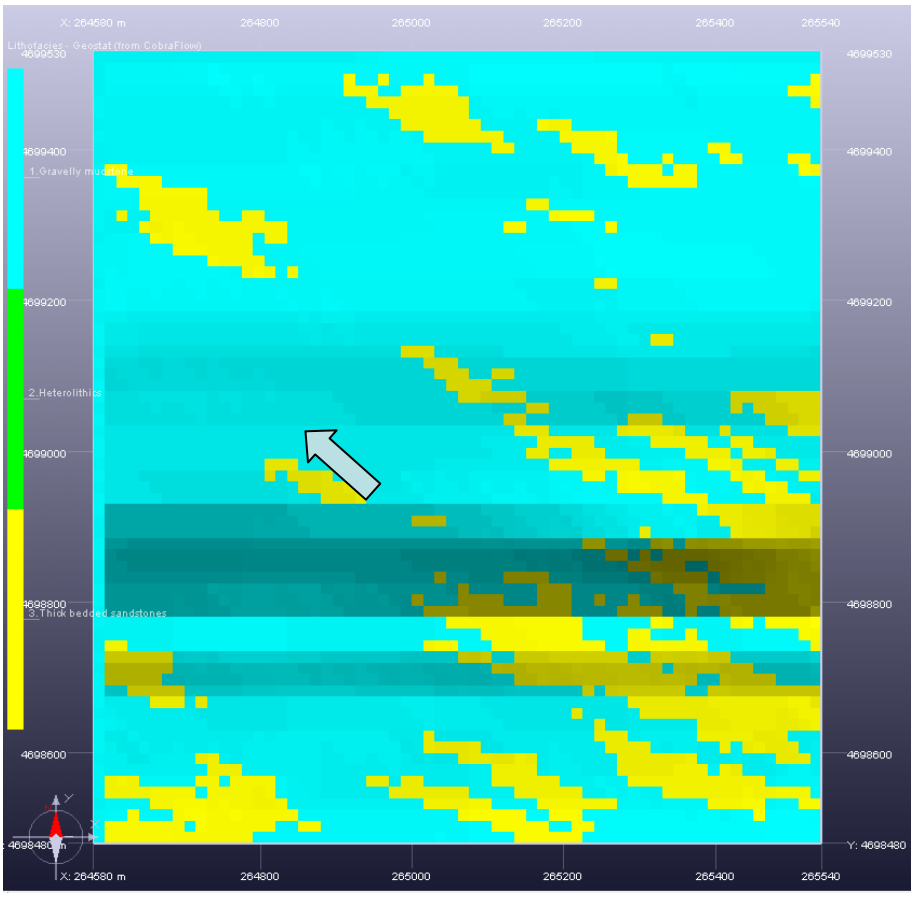

Figure 3.27 Top view of the facies distribution in unit C3 and for this reason the top of the Ainsa-1 Quarry outcrop. The blue arrow marks the orientation of the anisotropy. The dominant facies is gravelly mudstones as one expected after checking the outcrop characterization with major presence of sandstone in the SE region of this unit, cf., Figure 3.26 matrix proportion.

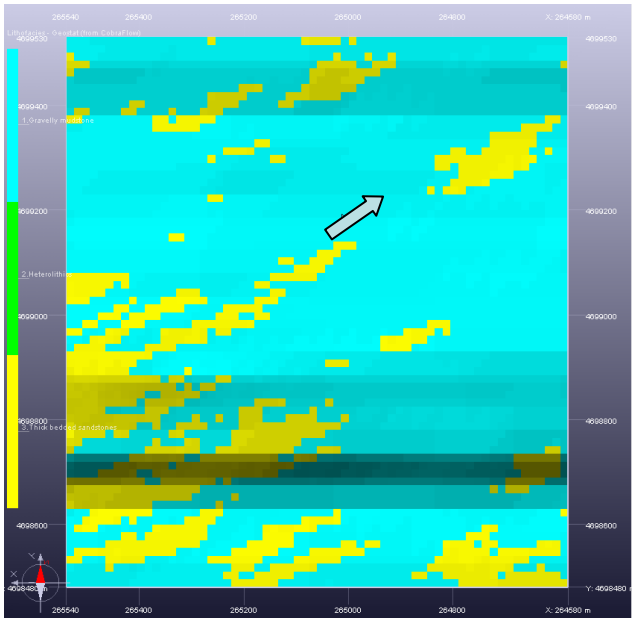

Figure 3.28 Bottom view of the facies distribution in unit C3 on Ainsa-1 Quarry outcrop. It is shown as well the anisotropy with its parallel orientation to current direction but it should take into account, that this is a mirror image of Figure 3.27.

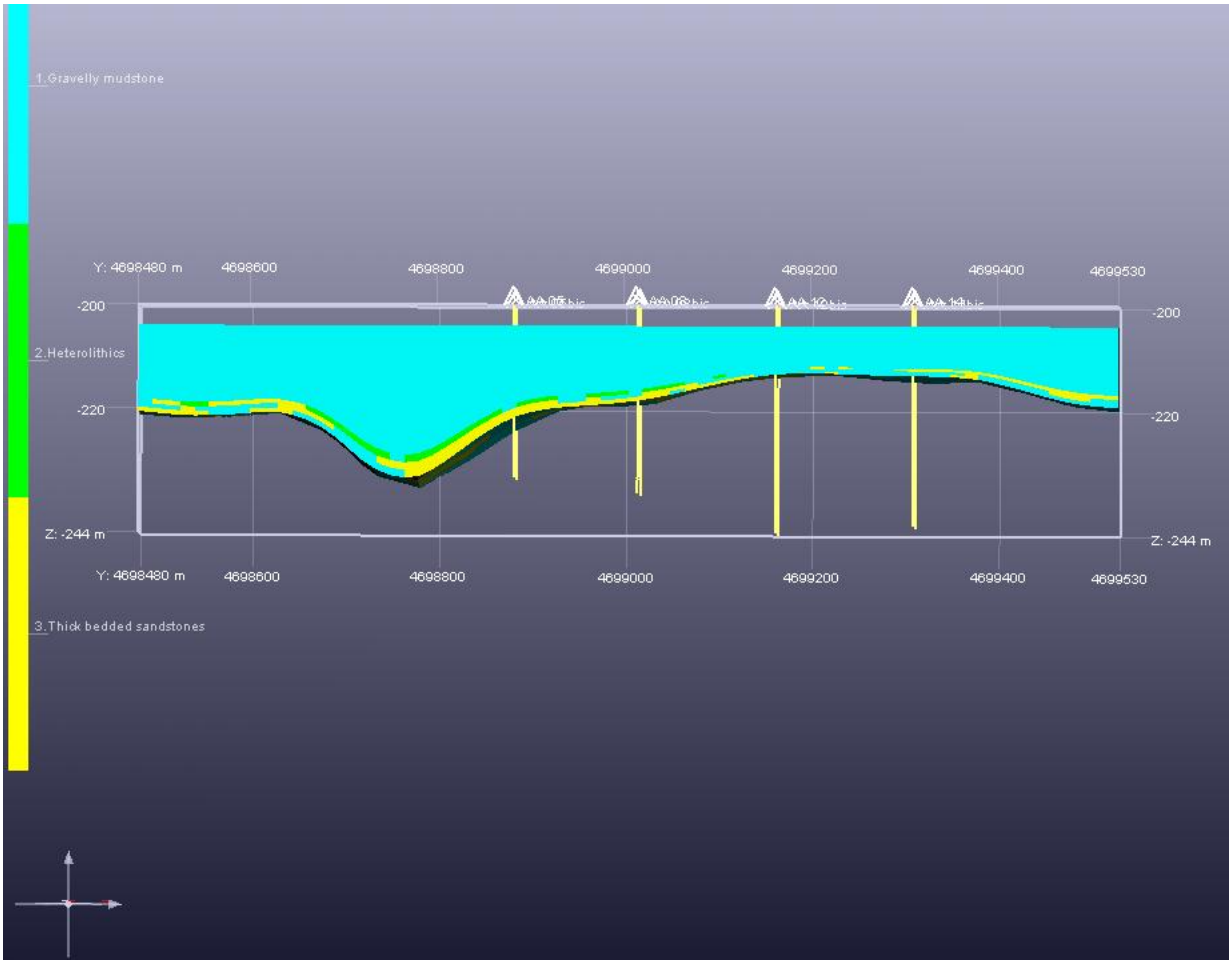

Figure 3.29 Front view of the facies distribution in unit C3 on Ainsa-1 Quarry outcrop. In the bottom part there is a layer of thick-bedded sandstones, which is continue in Y direction but not in X direction, as it can observed from the bottom view. The shape of the base of this unit is the erosive surface that cuts the top of the channel form C2, due to this unit corresponds to a muddy slump deposit, which represents an episode of cannibalistic rejuvenation.

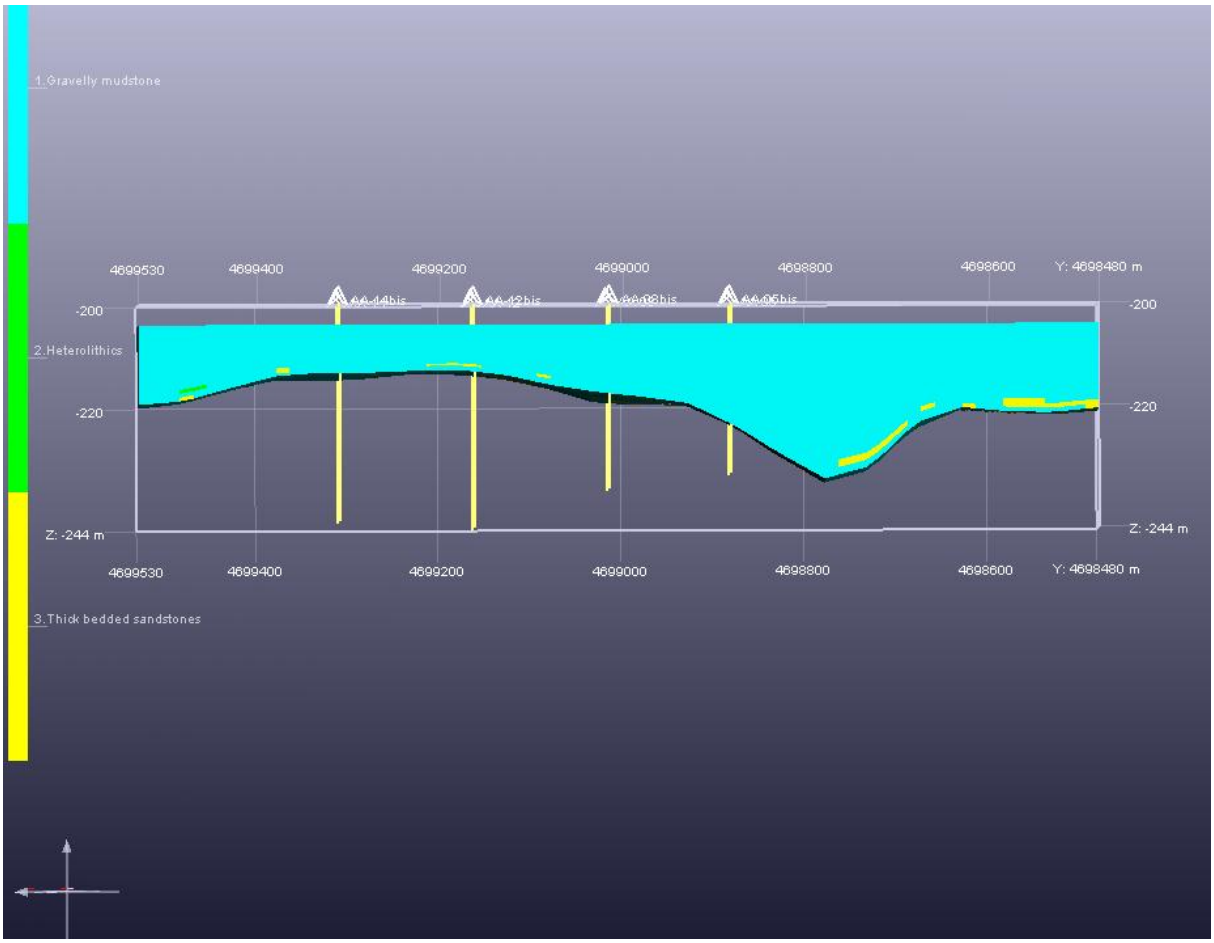

Figure 3.30 Bottom view of the facies distribution in unit C3 on Ainsa-1 Quarry outcrop. Sandstone layer remains in the South zone of the outcrop but it disappears from the North and this is related with the proportions of this facies displayed for the Proportion Matrix cf., Figure 3.26.

UNIT C2.2

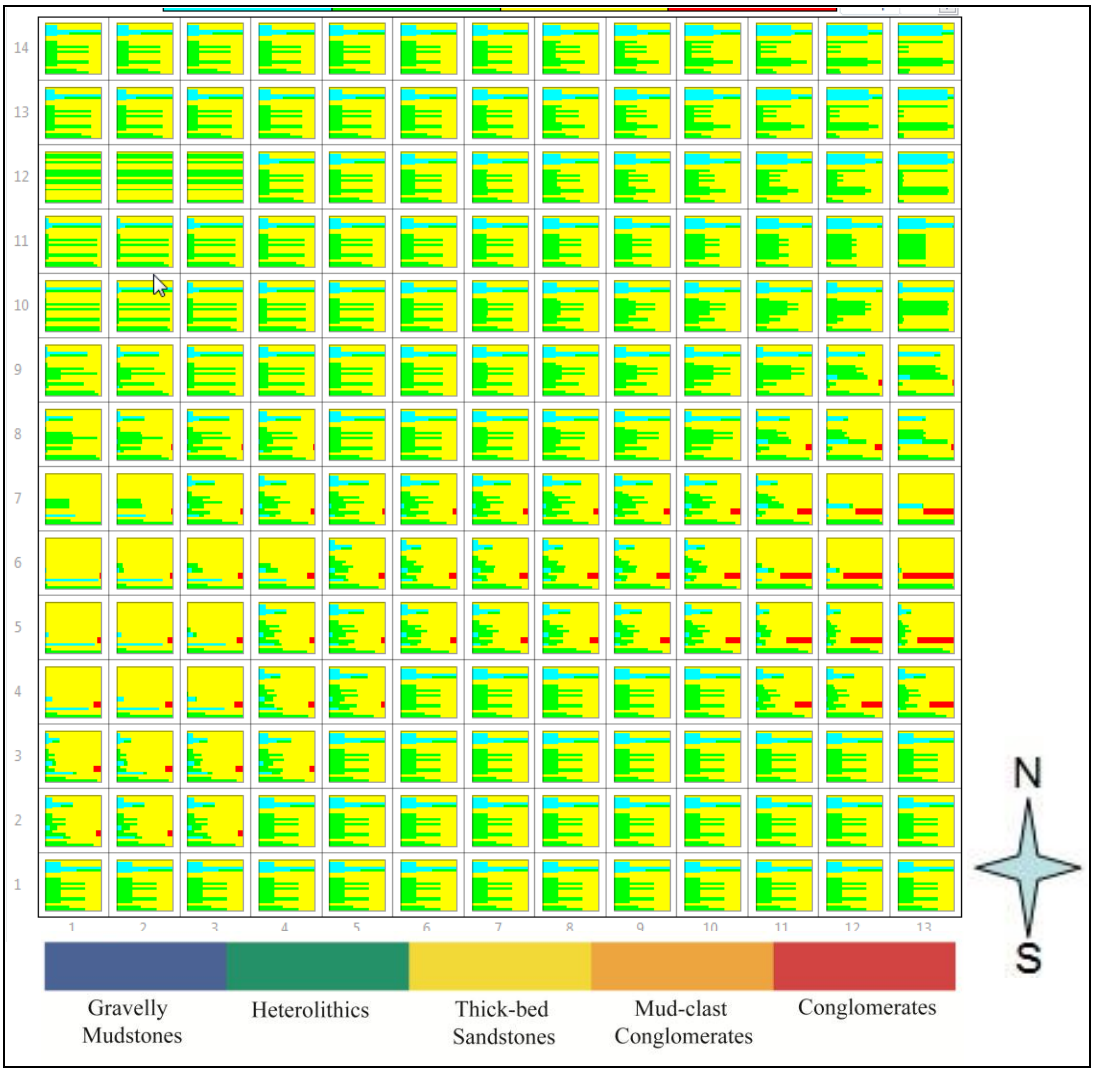

Figure 3.31 Matrix proportion curve for the unit C2.2 with a grid of 5X5 for X and Y and computing with areas. In this unit the infill of the VPC is made with the facies thick-bedded sandstones because is one of the dominant composition in this zone; although heterolythics facies appear quite often as well, it was decided to fill the VPC with sandstones on top (the layering of the grids in this zone follow the base, it is parallel to the base) because this unit is the top of the reservoir. It can be observed a channel form crossing from east the west the matrix of proportion, with high percentage of sandstone composition and less of heterolythics or non reservoir facies. This is because we divided the matrix of proportion in two areas and in the area that corresponds with the channel we assigned the VPC created from the logs AA-05 and AA-08 in the front part of the model and AA-05bis and AA-08bis in the back part of the model, which contain high percentage of sandstone facies in the discretized logs. Next picture shows the property map used to create these two areas.

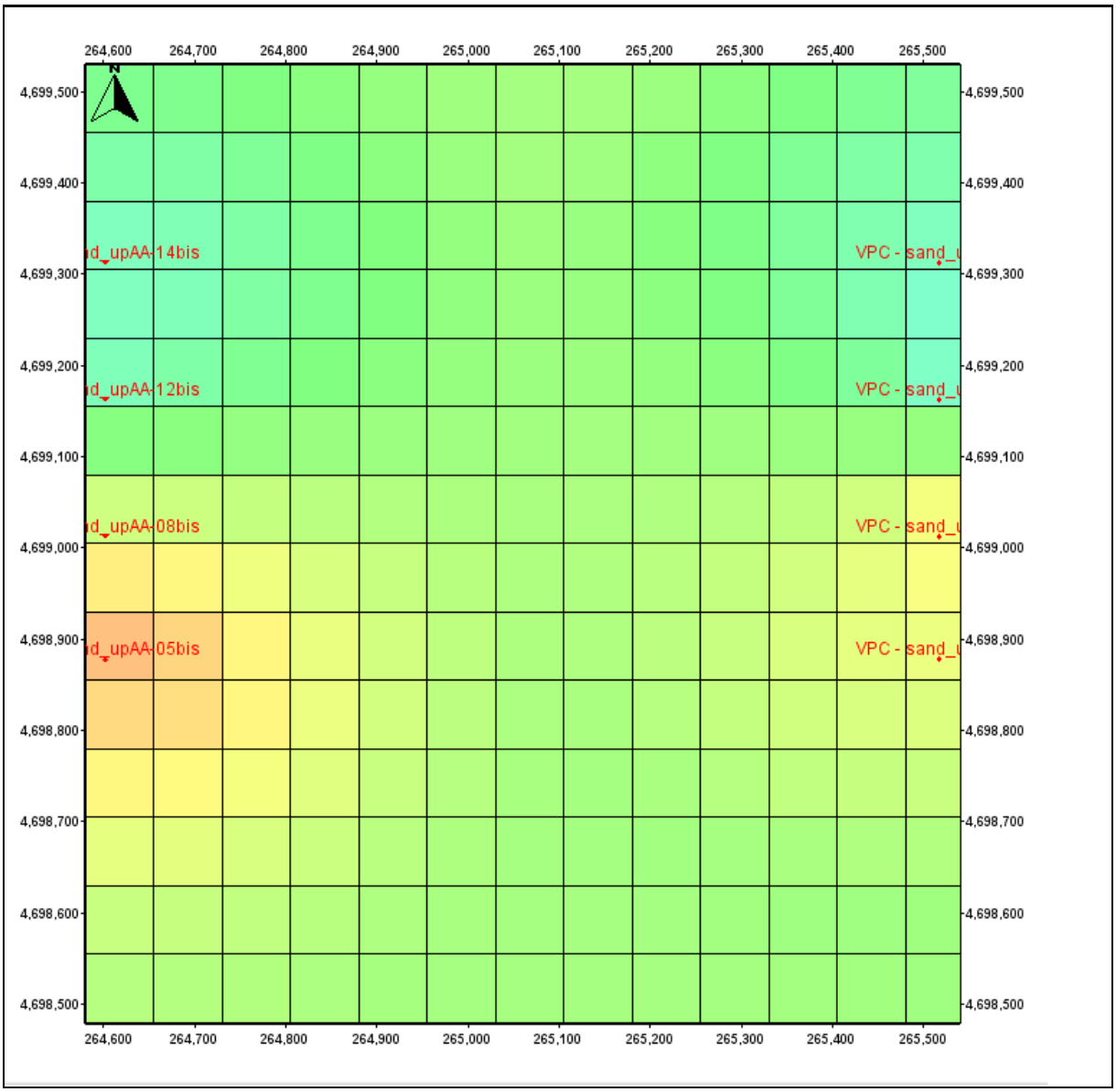

Figure 3.32 Property map used to create the matrix of proportion of the unit C2.2 showing the thickness of the lithofacies (thick-bedded sandstones), where red colors represent high thickness whereas blue represent low ones.

Method	Fitting model	Range X	Range Y	Range Z	Azimuth
Plurigaussian	Non-stationary	500	100	0.5	-73

Table 3.3 Stochastic method used in unit C2.2 (the one chosen after comparing several runs with different methodology and parameters values) and the correspondent values of the parameter that describe the variogram. X, Y and Z in meters. The azimuth chosen is related with the orientation of the anisotropy and we used an average value parallel to the current directions (290°, i.e., WNW-ESE) cf., Chapter 2.

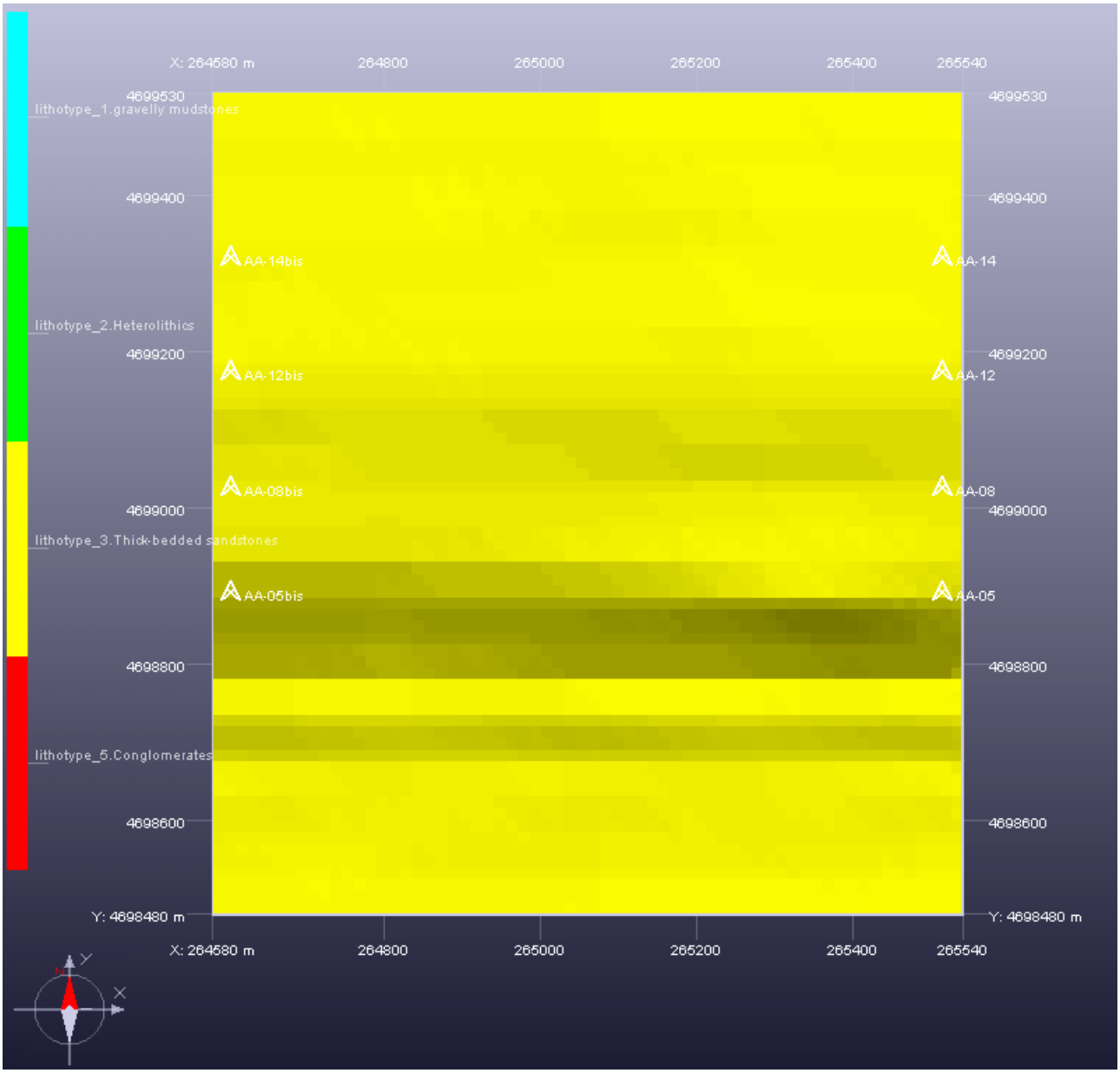

Figure 3.33 Top view of the facies distribution in unit C2.2. Only thick-bedded sandstones lithofacies appear on top of this unit because the infill of the different VPC was made with this unit, considering that forms part of the reservoir.

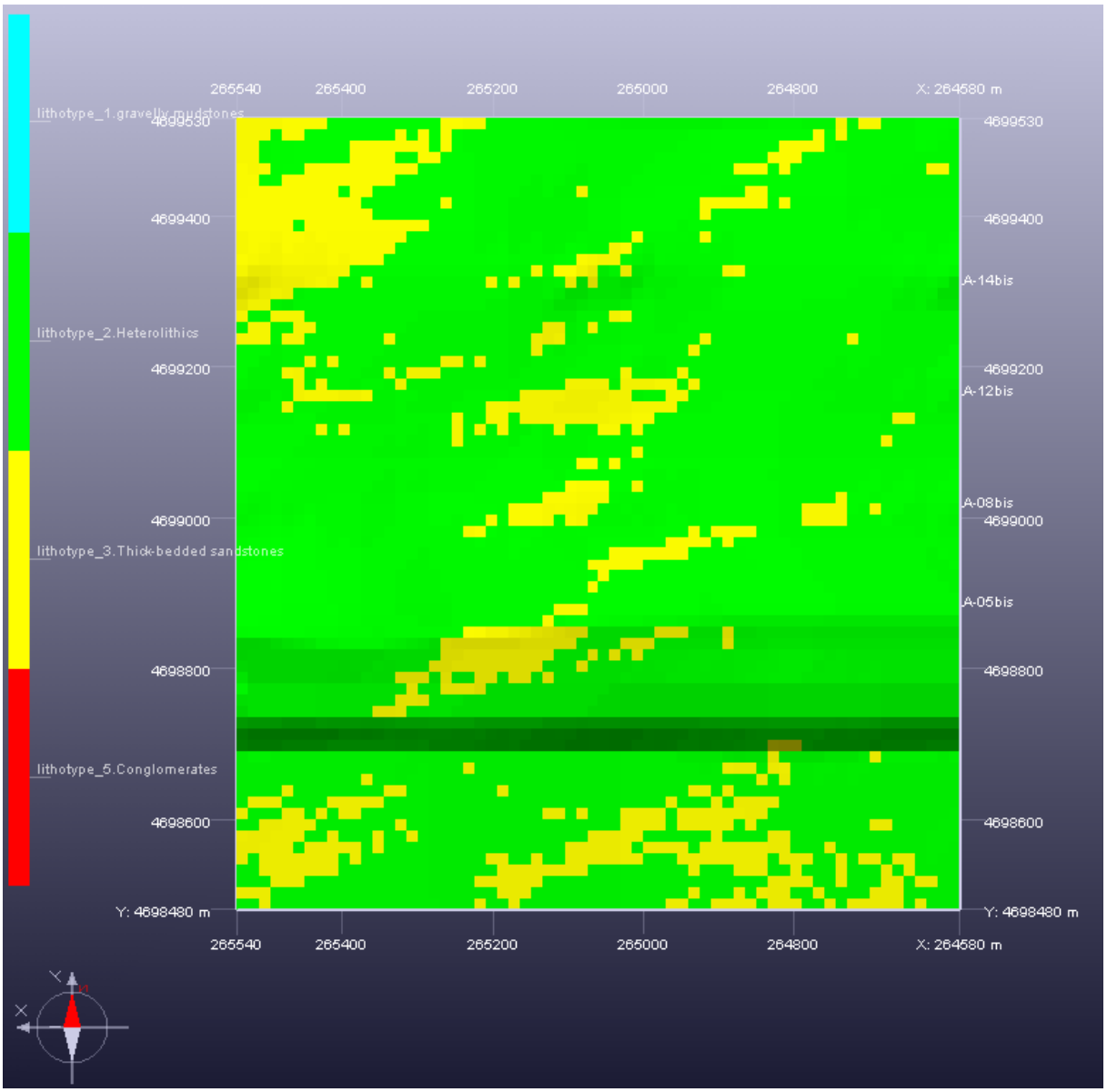

Figure 3.34 Bottom view of the facies distribution in unit C2.2 on Ainsa-1 Quarry outcrop. In here the proportion of heterolithics lithofacies is much bigger than in other areas of this unit. This is because the base of the channel form C2.2 is a package of facies heterolithics onlapping the base of the channel form northward so this run simulates in an accurate form the infill of this channel form.

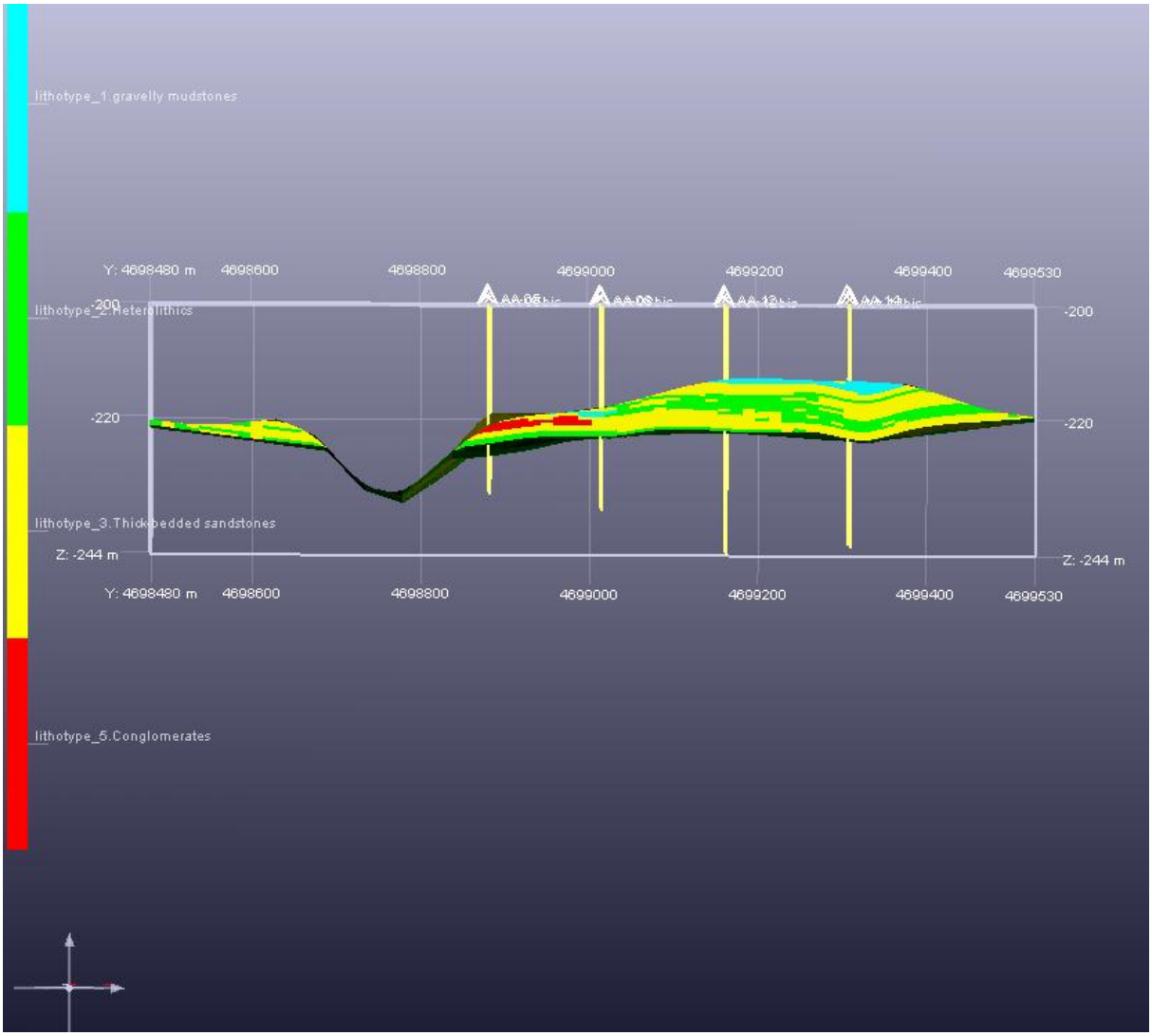

Figure 3.35 Front view of the facies distribution in unit C2.2 on Ainsa-1 Quarry outcrop. In the bottom part there is a layer of H cf., Figure 3.34, and this is overlain by vertically stacked and amalgamated beds of the thick-bedded sandstones with heterolithics layers interbedded. This layers look blocky, almost northward because not all the facies trends could be set up due to the modeling methods but all the algorithms were set up to reach the facies proportions. It appears a layer of conglomerates lithofacies southward.

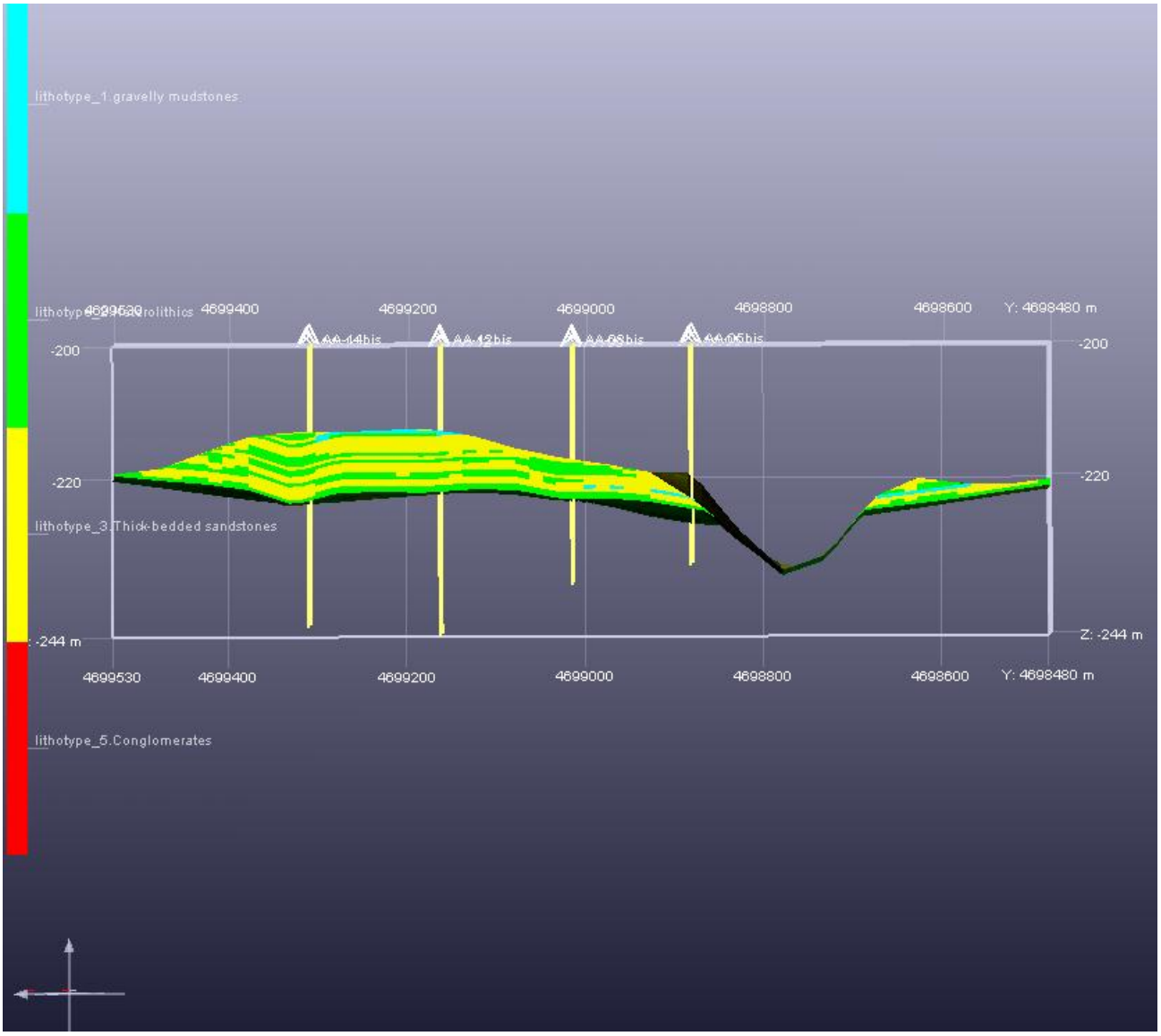

Figure 3.36 Back view of the facies distribution in unit C2.2 on Ainsa-1 Quarry outcrop. Conglomerates facies disappear towards the west and the amount of H increases and it looks more plane-parallel-bedded.

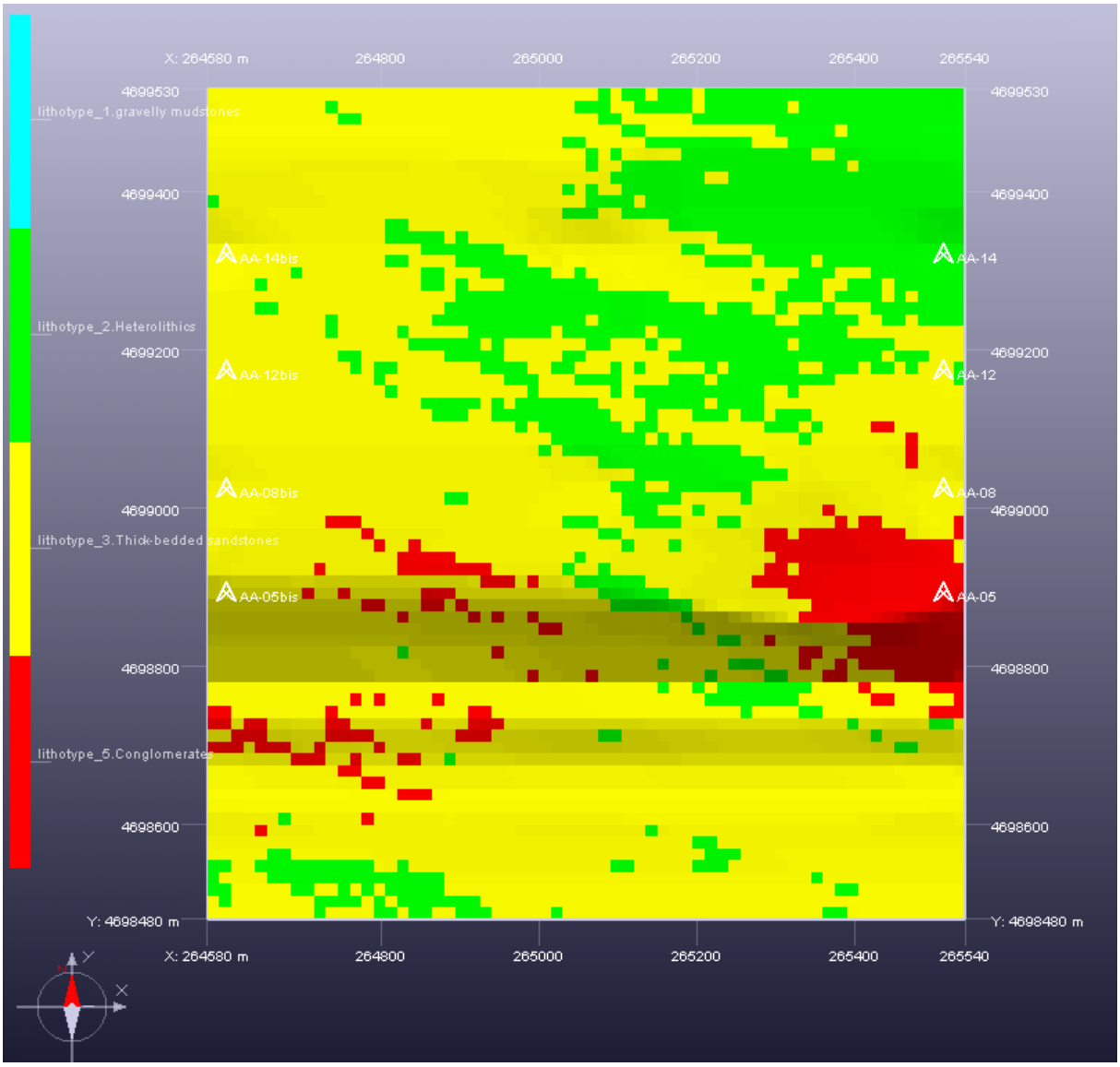

Figure 3.37 Cross section of the unit C2.2 of the Ainsa-1 quarry outcrop in K = 7. The orientation of the anisotropy is shown by the different non reservoir and reservoir lithofacies (H and C) with an angle of 287° in this unit. Conglomerates percentage decreases westwards and Northwards. If one checks the Matrix of proportion, conglomerates lithofacies are localized SE in the channel area created from the property map, where the well AA-05 is set up.

UNIT C2.1_up

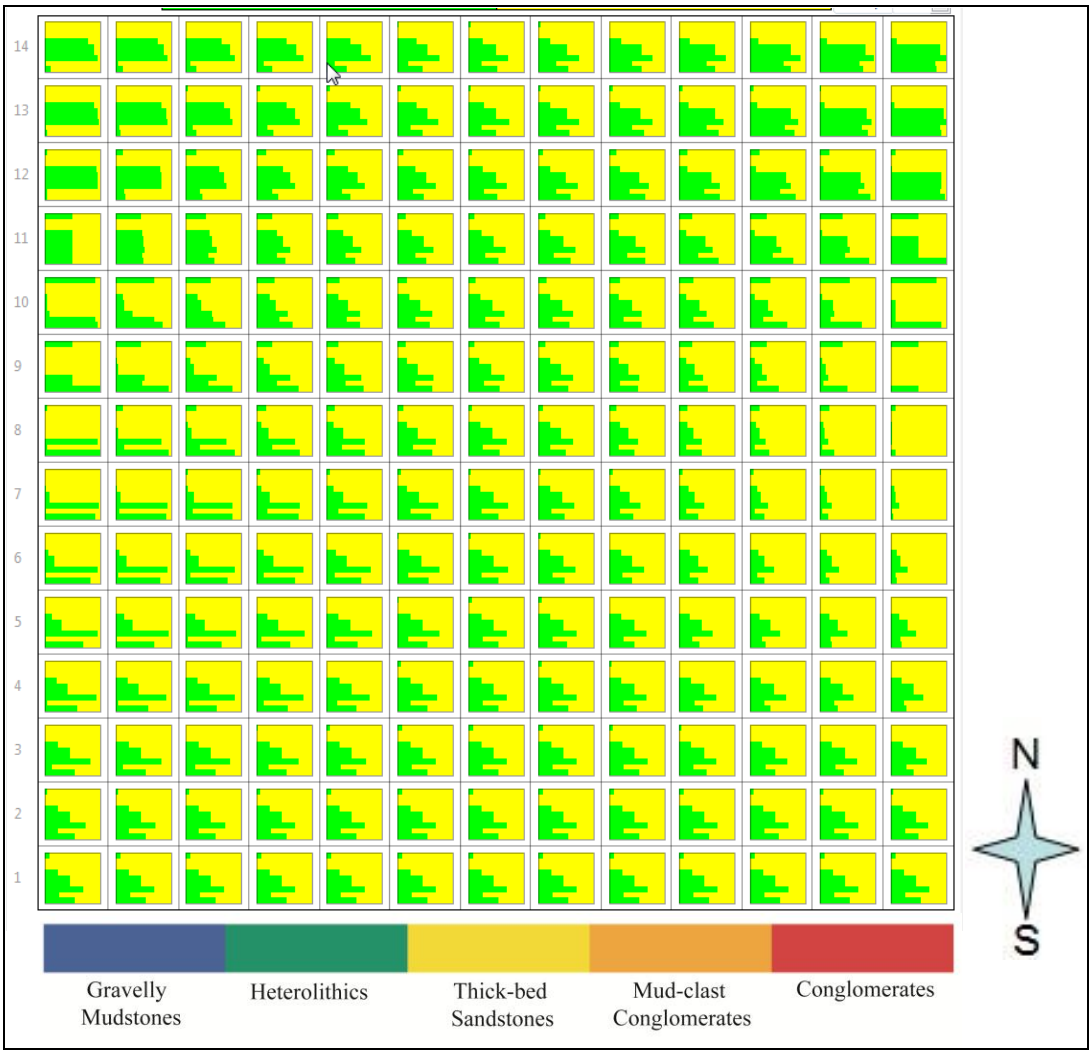

Figure 3.38 Matrix proportion curve for the unit C2.1-up with a grid of 5X5 for X and Y and computing by the VPC created. In this unit the infill of the VPC is made with the thick-bedded sandstones because is the dominant composition and it is not used the smooth tool. There are only two lithofacies, sandstones and heterolithics. It can be observed major percentage of sand composition on the East of the matrix. If one checks Figure 3.13, wells AA-05 and AA-08 have big percentage of sandstones facies and they are situated in the SE region of the outcrop. Also, well log AA-12bis is composed mainly by sandstones and in the Matrix or Proportion, it can be seen that tendency on the West (layers 7 and 8).

Method	Fitting model	Range X	Range Y	Range Z	Azimuth
SIS	Non-stationary	500	100	0.5	-64

Table 3.4 Stochastic method used in unit C2.1-up (the one chosen after comparing several runs with different methodology and parameters values) and the correspondent values of the parameter that describe the variogram. X, Y and Z in meters. The azimuth chosen is related with the orientation of the anisotropy and we used an average value parallel to the current directions (290°, i.e., WNW-ESE) cf., Chapter 2.

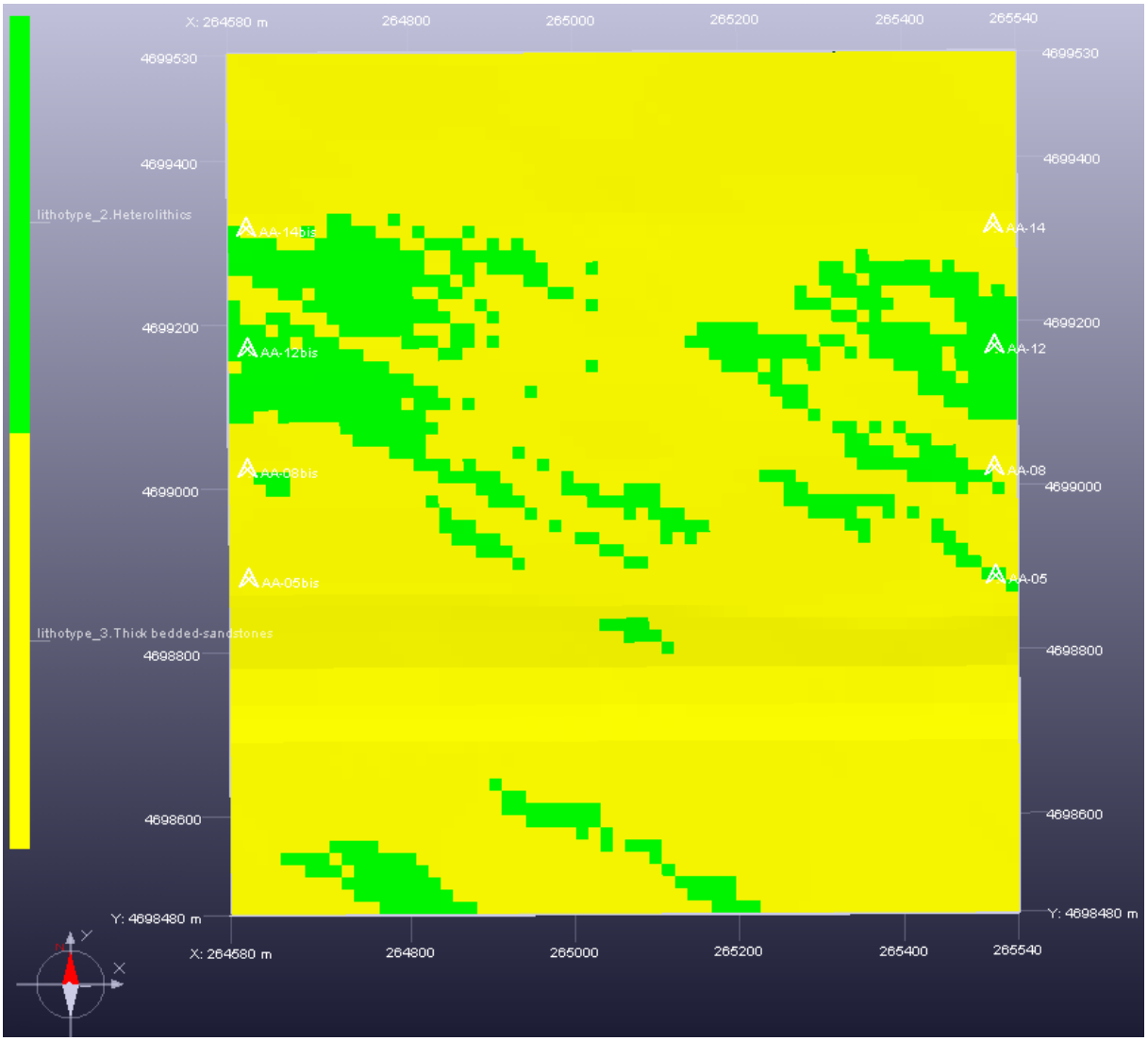

Figure 3.39 Top view of the facies distribution in unit C2.1-up. The orientation of the anisotropy is marked by the heterolithic layering (green). The dominant facies is thick-bedded sandstones as one expected after checking the outcrop characterization.

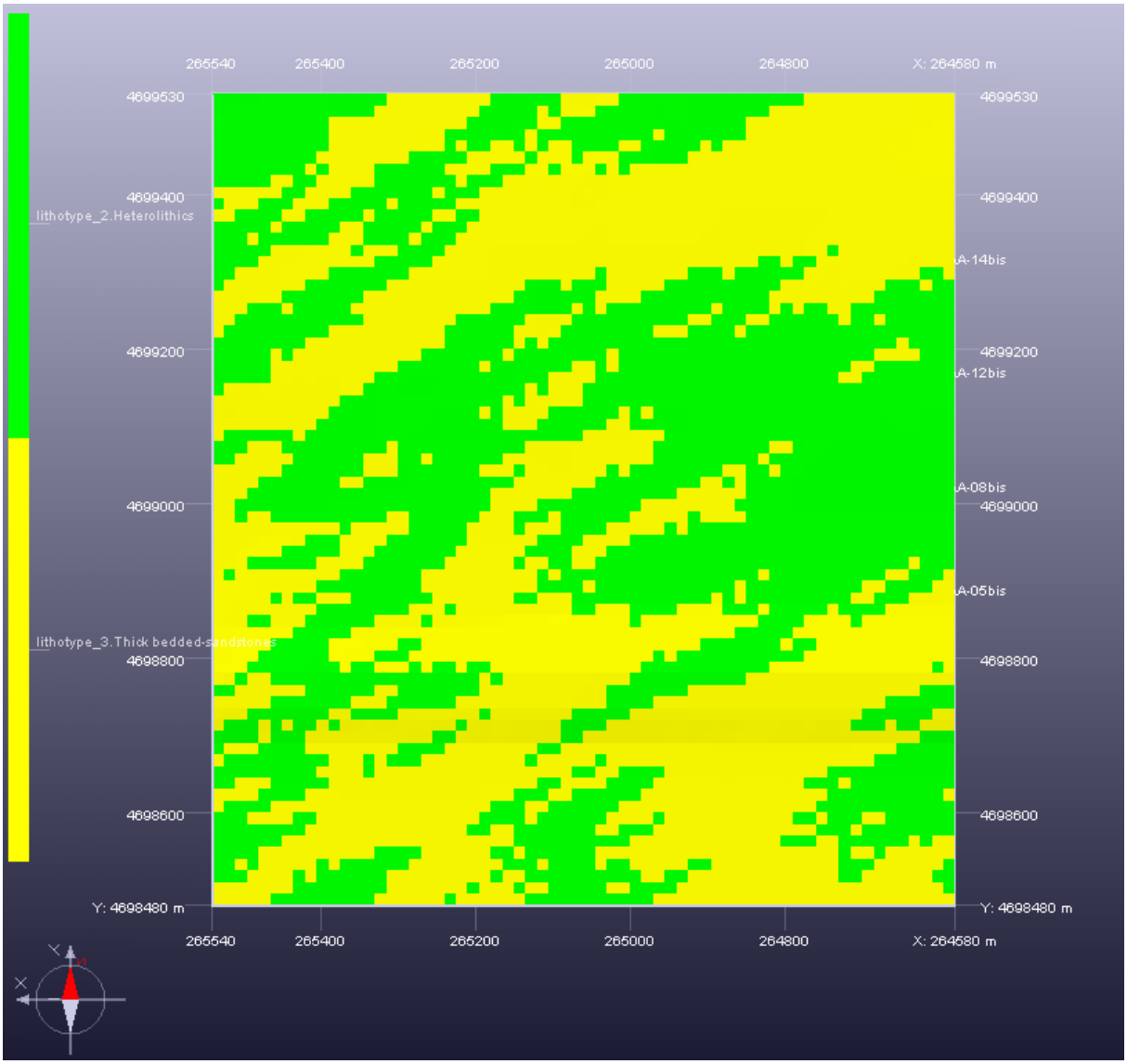

Figure 3.40 Bottom view of the facies distribution in unit C2.1-up on Ainsa-1 Quarry outcrop. It is shown as well the anisotropy with its parallel orientation to current direction but it should take into account, that this is a mirror image of Figure 3.39. There is more presence of heterolithic material on the base of this unit than on top and this is related with the depositional boundary between the middle package and upper package in C2.1 channel form.

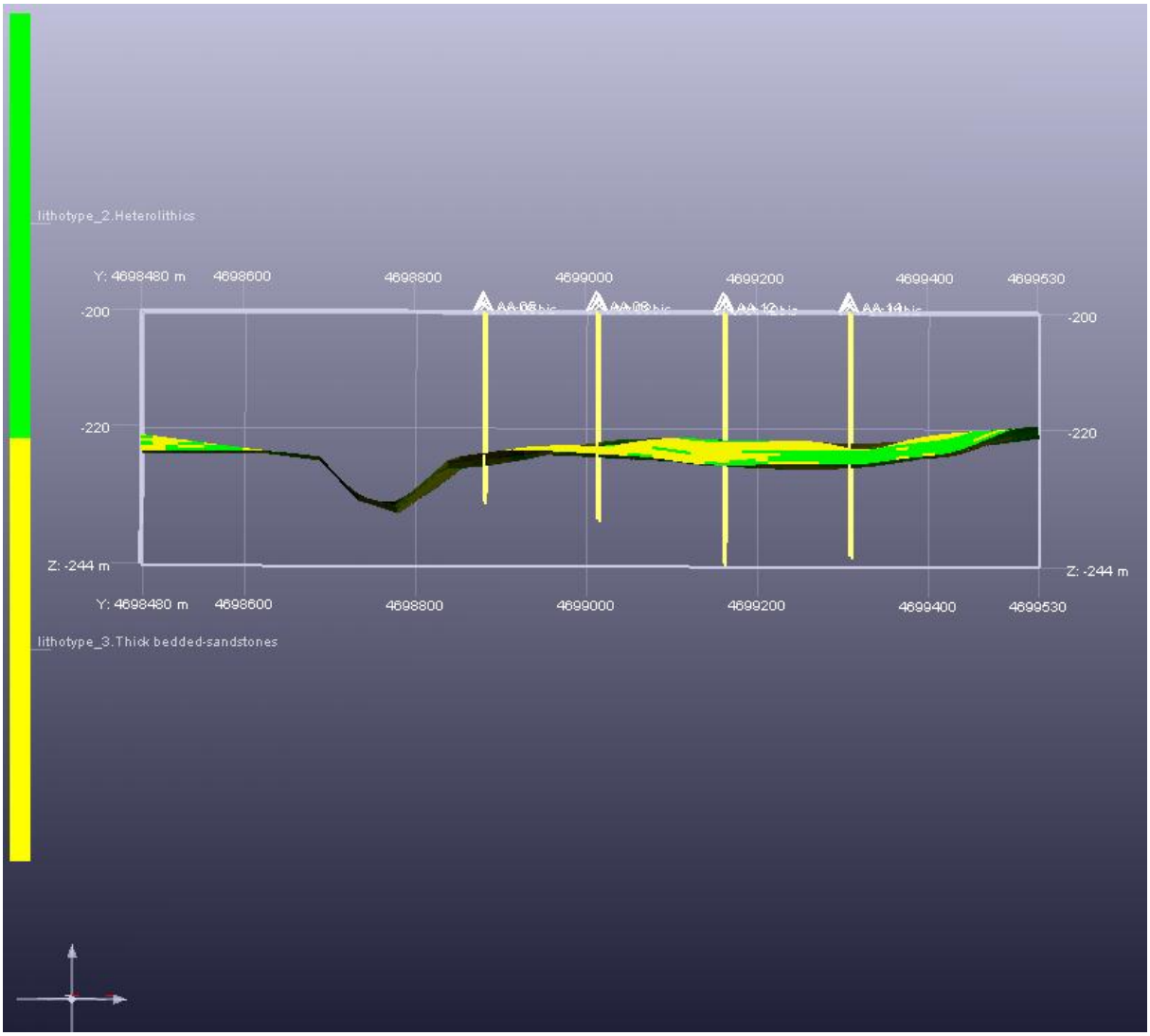

Figure 3.41 Front view of the facies distribution in unit C2.1-up on Ainsa-1 Quarry outcrop. The convex-up top bottom is draped with a base of H facies, as it is shown in Figure 3.40. Above, there are a beds of TkS that increase southwards.

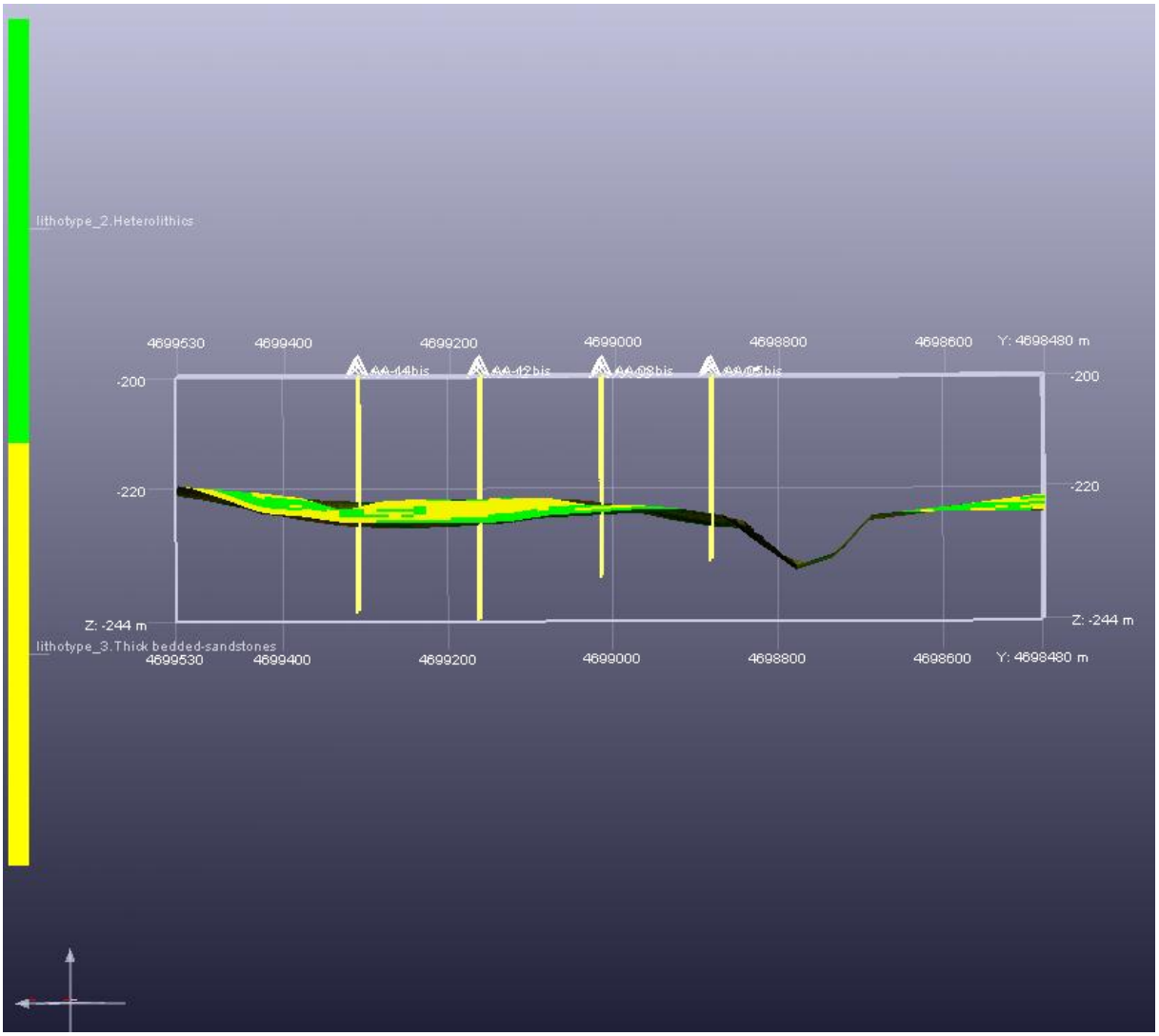

Figure 3.42 Bottom view of the facies distribution in unit C2.1-up on Ainsa-1 Quarry outcrop. Sandstone has more presence in the middle part of this unit, as we explained in Figure 3.38, the Matrix of Proportion. The H facies as basal filled continue at the back part, as well.

UNIT C2.1-MP-LP

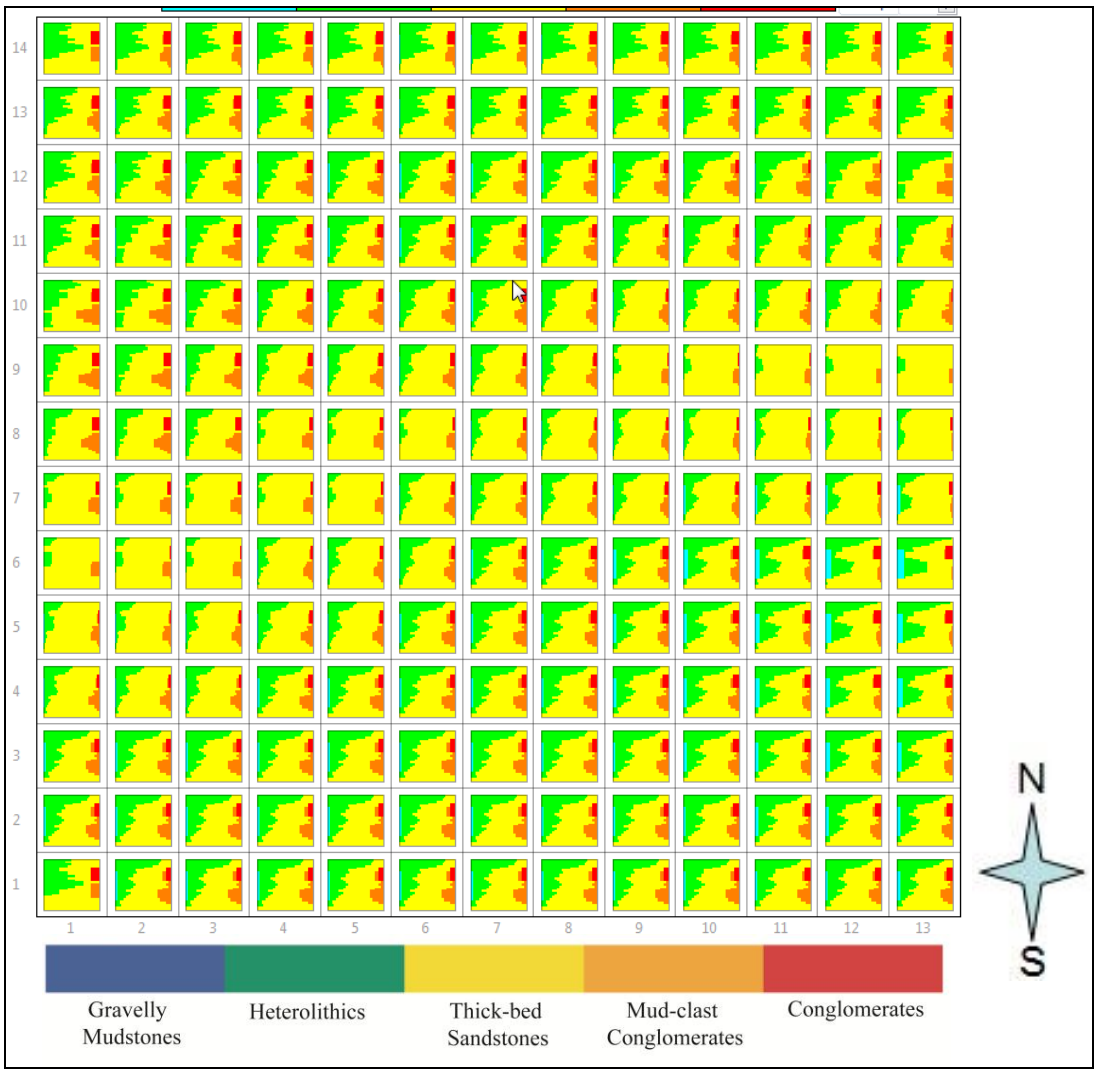

Figure 3.43 Matrix proportion curve for the unit C2.1-mp-lp with a grid of 5X5 for X and Y and computing with areas. In this unit the infill of the VPC is made with the TkS facies because is the dominant composition and it is used the smooth tool to avoid sharp boundaries. From the property map, one can observe to areas with TkS as dominant facies, on the East and West and these two areas can be part of a channel. For this reason, we created two areas, one the interpreted channel with the VPC of AA-05, AA-08, AA-05bis and AA-08bis and the other with the rest of the VPC. Figure 3.44 shows the property map used to create these two areas.

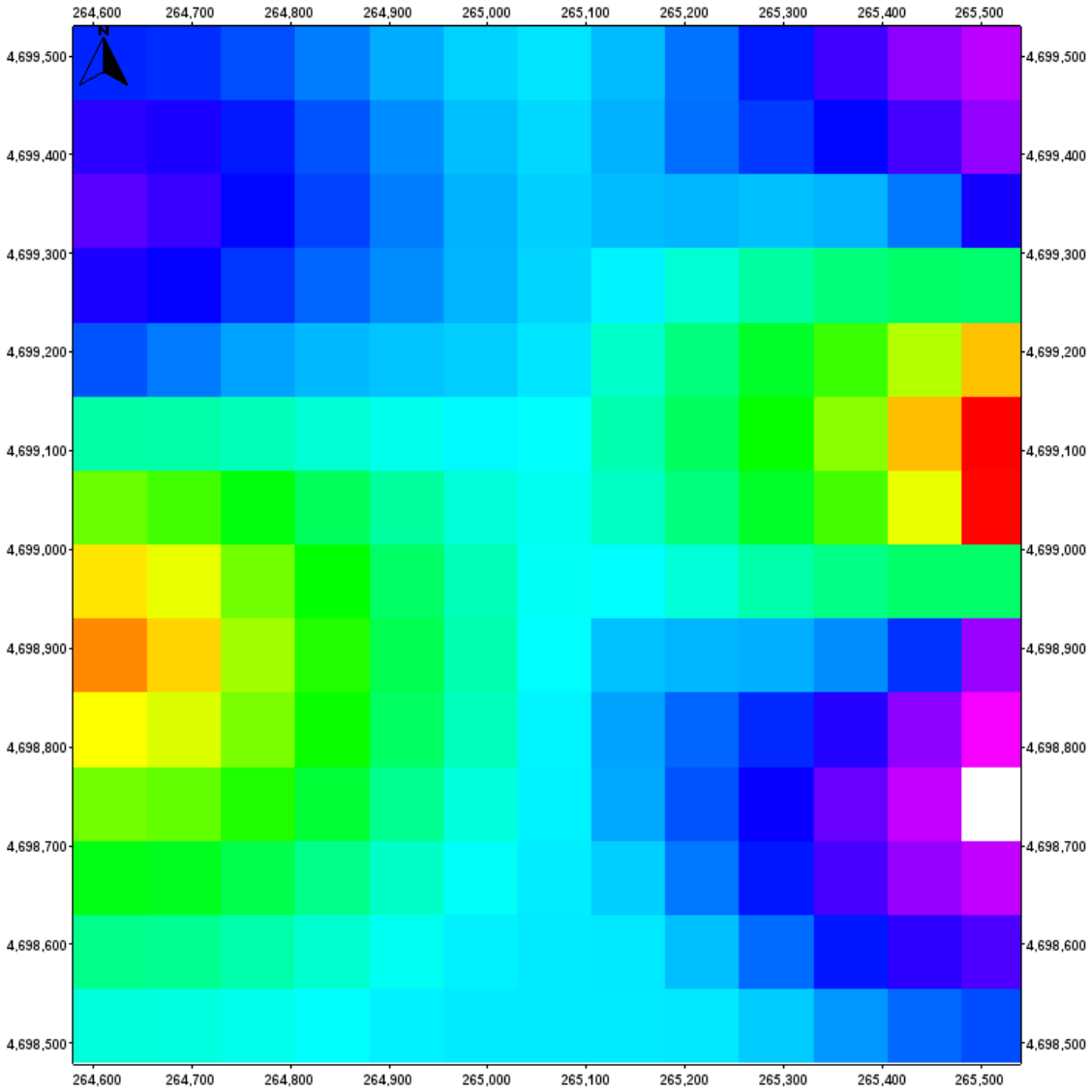

Figure 3.44 Property map used to create the Matrix proportion of the unit C2.1-mp-lp, showing the thickness of the TkS facies, where red colors represent high thickness whereas blue ones represent low ones

Method	Fitting model	Range X	Range Y	Range Z	Azimuth
SIS	Non-stationary	500	100	0.5	-64

Table 3.5 Stochastic method used in unit C2.1-mp-lp (the one chosen after comparing several runs with different methodology and parameters values) and the correspondent values of the parameter that describe the variogram. X, Y and Z in meters. The azimuth chosen is related with the orientation of the anisotropy and we used an average value parallel to the current directions (290°, i.e., WNW-ESE) cf., Chapter 2.

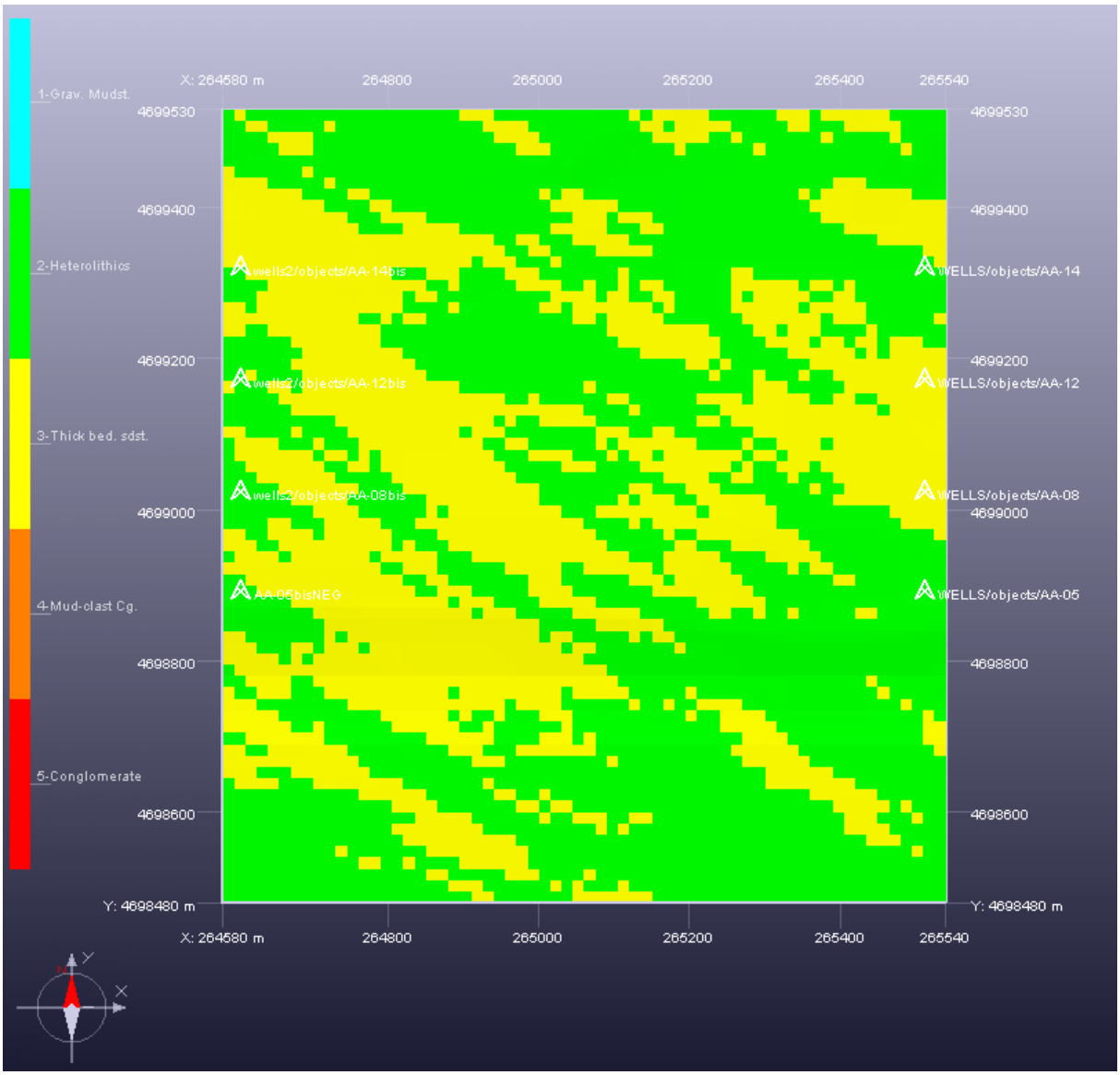

Figure 3.45 Top view of the facies distribution in unit C2.1-mp-lp. The layering of the facies marks the orientation of the anisotropy. The dominant facies, in the whole unit, is TkS as one expected after checking the outcrop characterization. In this unit a bed of H facies covers the sandstones.

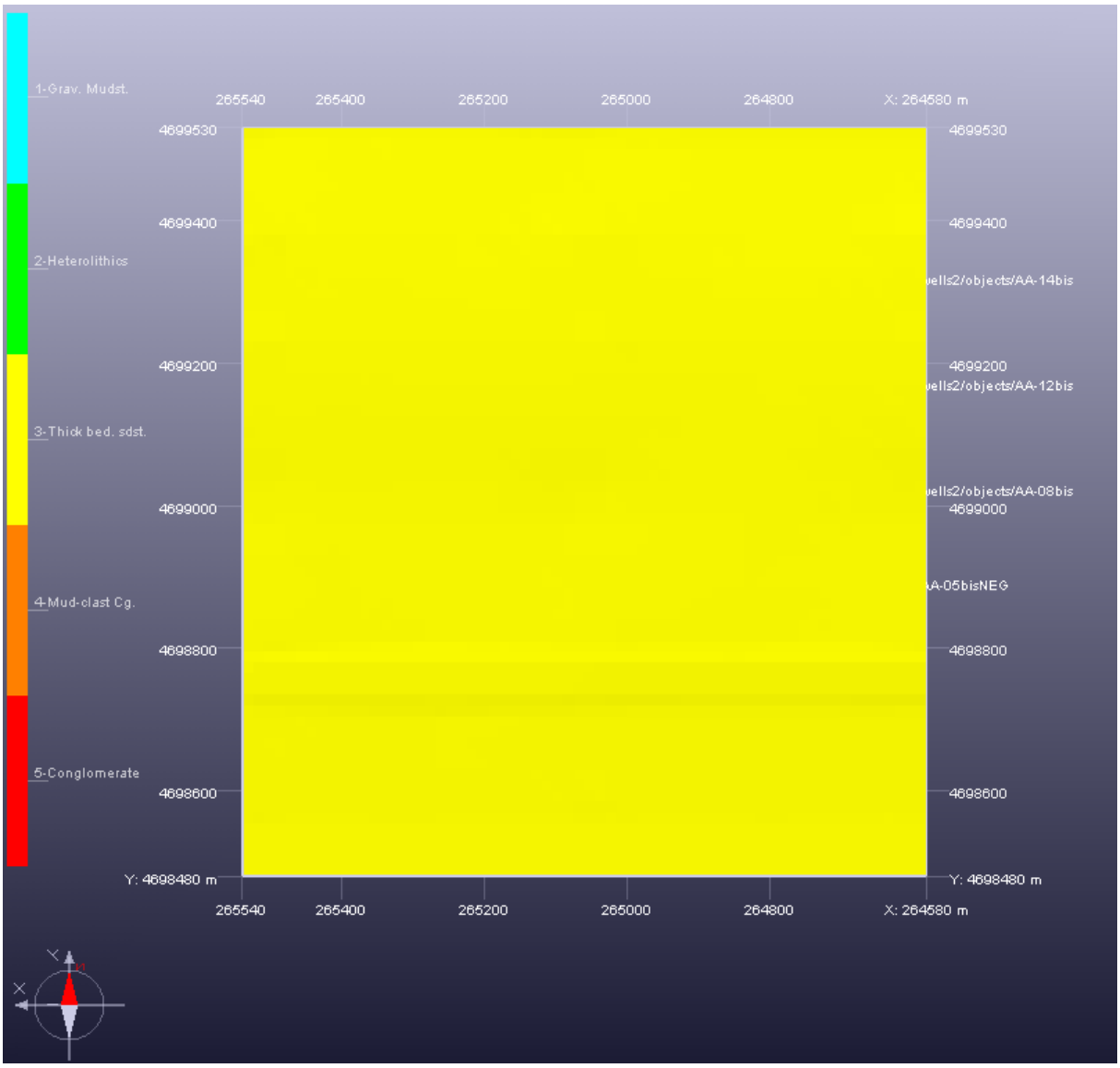

Figure 3.46 Bottom view of the facies distribution in unit C2.1-mp-lp on Ainsa-1 Quarry outcrop. There are only TkS and this is related with the fact that the VPC infill is made with this facies and the layering of the unit is parallel to top.

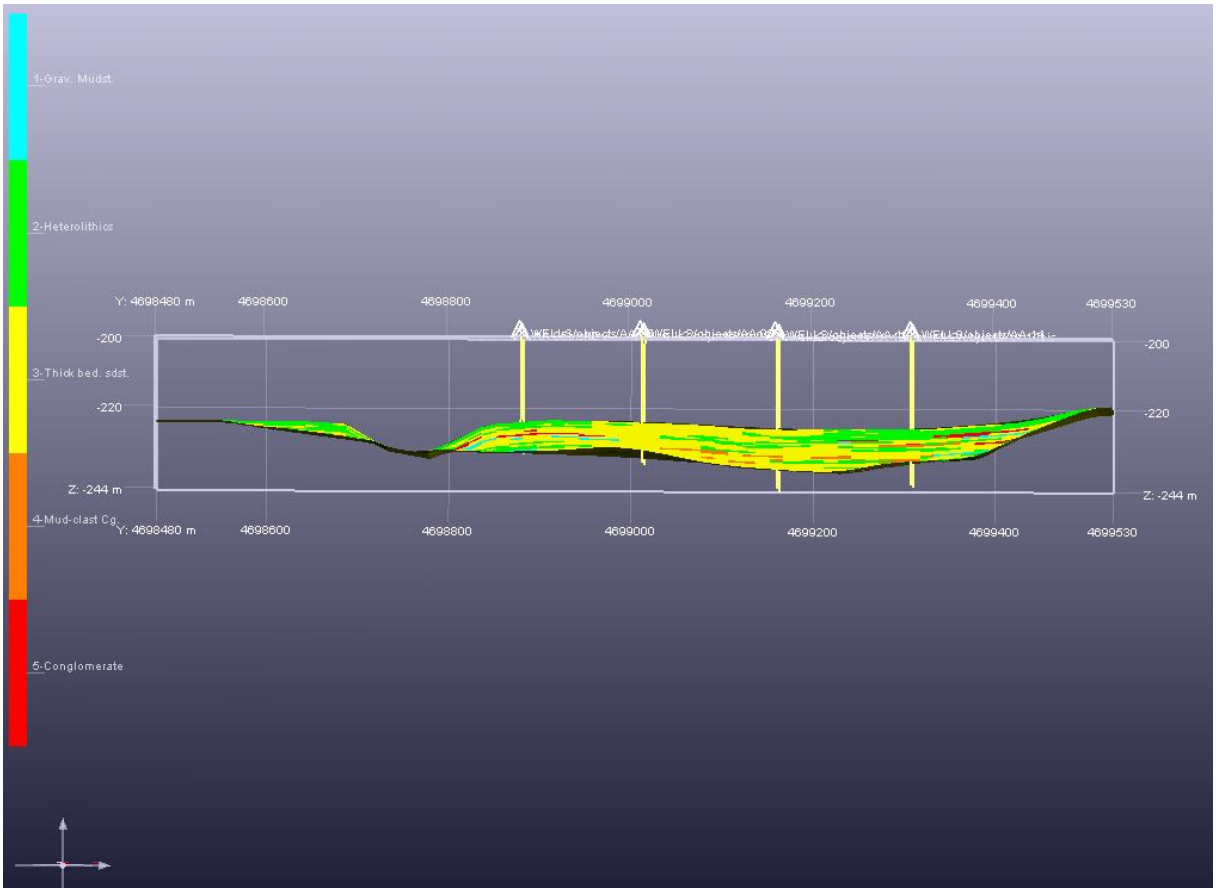

Figure 3.47 Front view of the facies distribution in unit C2.1-mp-lp on Ainsa-1 Quarry outcrop. The division between the middle package and the lower package is situated at the base of a h facies bed, which in this simulation we can follow almost across the entire channel form set. The dominant facies is TkS and McC and C appear as well and these layers are important features that should be preserved and for that reason it is particularly important to check during the modeling process

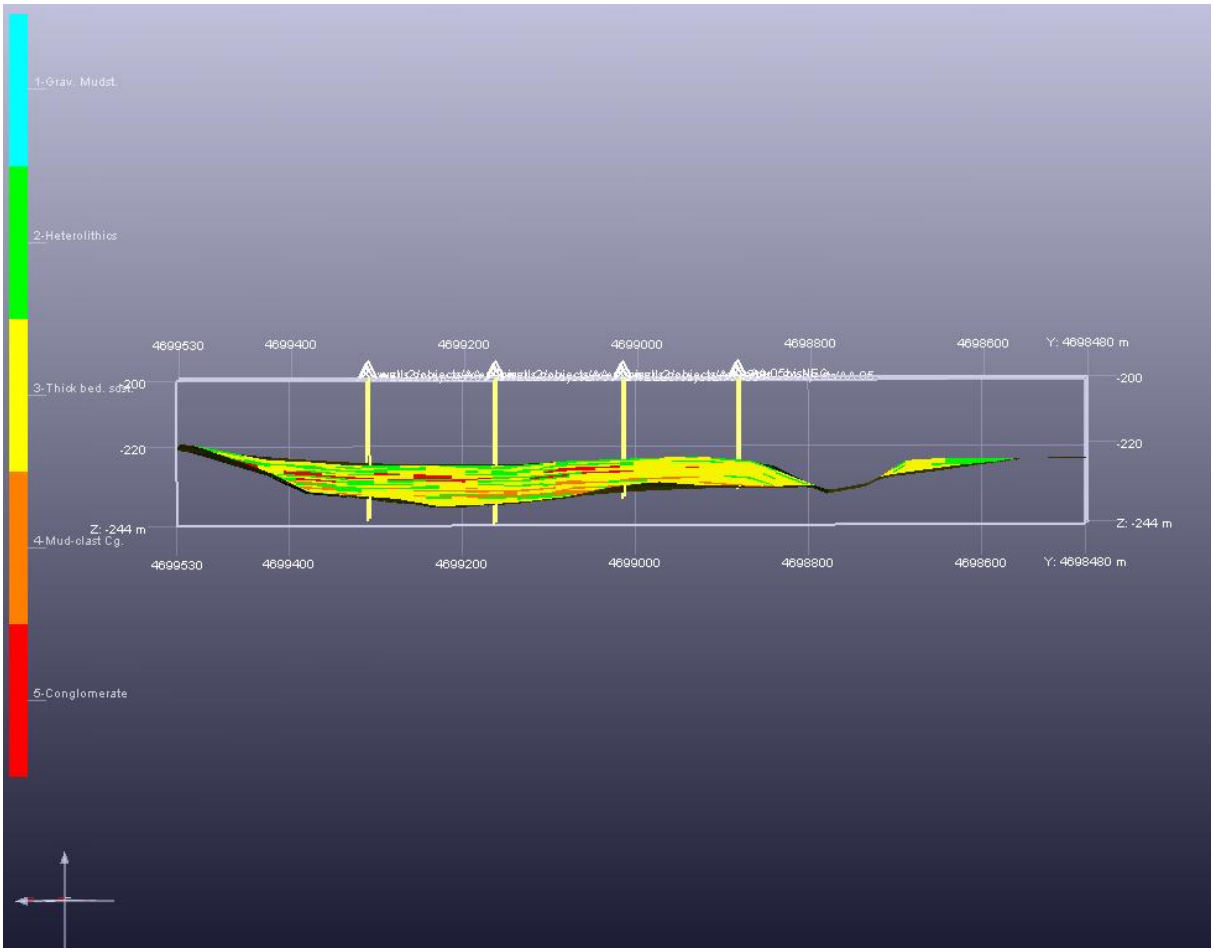

Figure 3.48 Back view of the facies distribution in unit C2.1-mp-lp on Ainsa-1 Quarry outcrop. The differences with the front view are the percentage of H facies and the presence of McC and C almost across the entire main body of the unit.

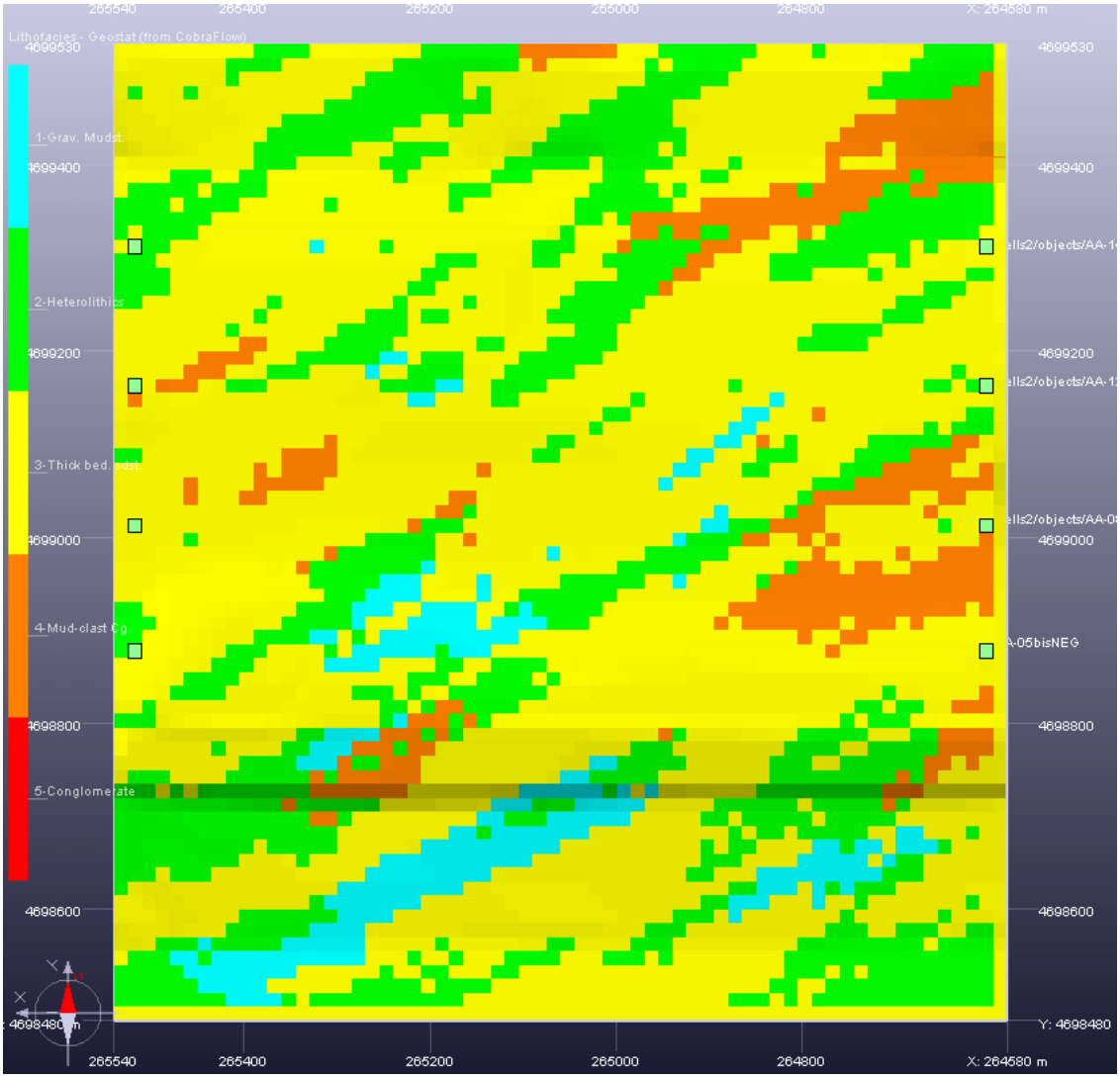

Figure 3.49 Cross-section of the facies distribution in unit C2.1-mp-lp. The cross section on. k = 12 show the distribution of the different facies following the anisotropy defined (Table 3.5). It can be observed some small percentage of gravelly mudstones facies as well, proximal to the bottom of this unit.

UNIT C1

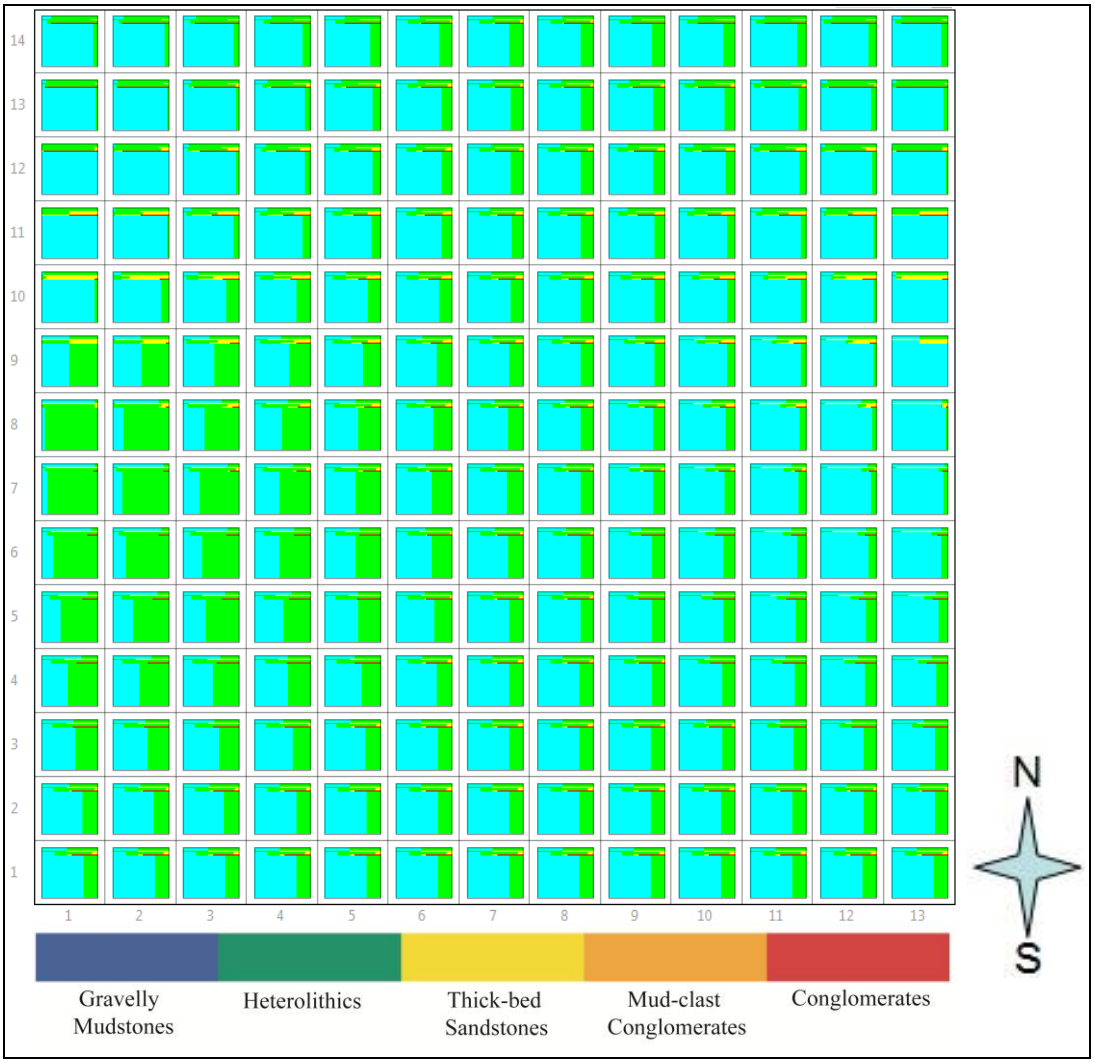

Figure 3.50 Matrix proportion curve for the unit C1with a grid of 5X5 for X and Y and computing by the VPC created. In this unit the infill of the VPC is made with the facies gravelly mudstone because is the dominant composition and it is not used the smooth tool. It can be observed major percentage of heterolithic facies in the SW of the outcrop. This is related with the vpC of the discretized wells AA-05bis and AA-08bis.

Method	Fitting model	Range X	Range Y	Range Z	Azimuth
Plurigaussian	Non-stationary	500	100	0.5	-70

Table 3.6 Stochastic method used in unit C1 (the one chosen after comparing several runs with different methodology and parameters values) and the correspondent values of the parameter that describe the variogram. X, Y and Z in meters. The azimuth chosen is related with the orientation of the anisotropy and we used an average value parallel to the current directions (290°, i.e., WNW-ESE) cf., Chapter 2.

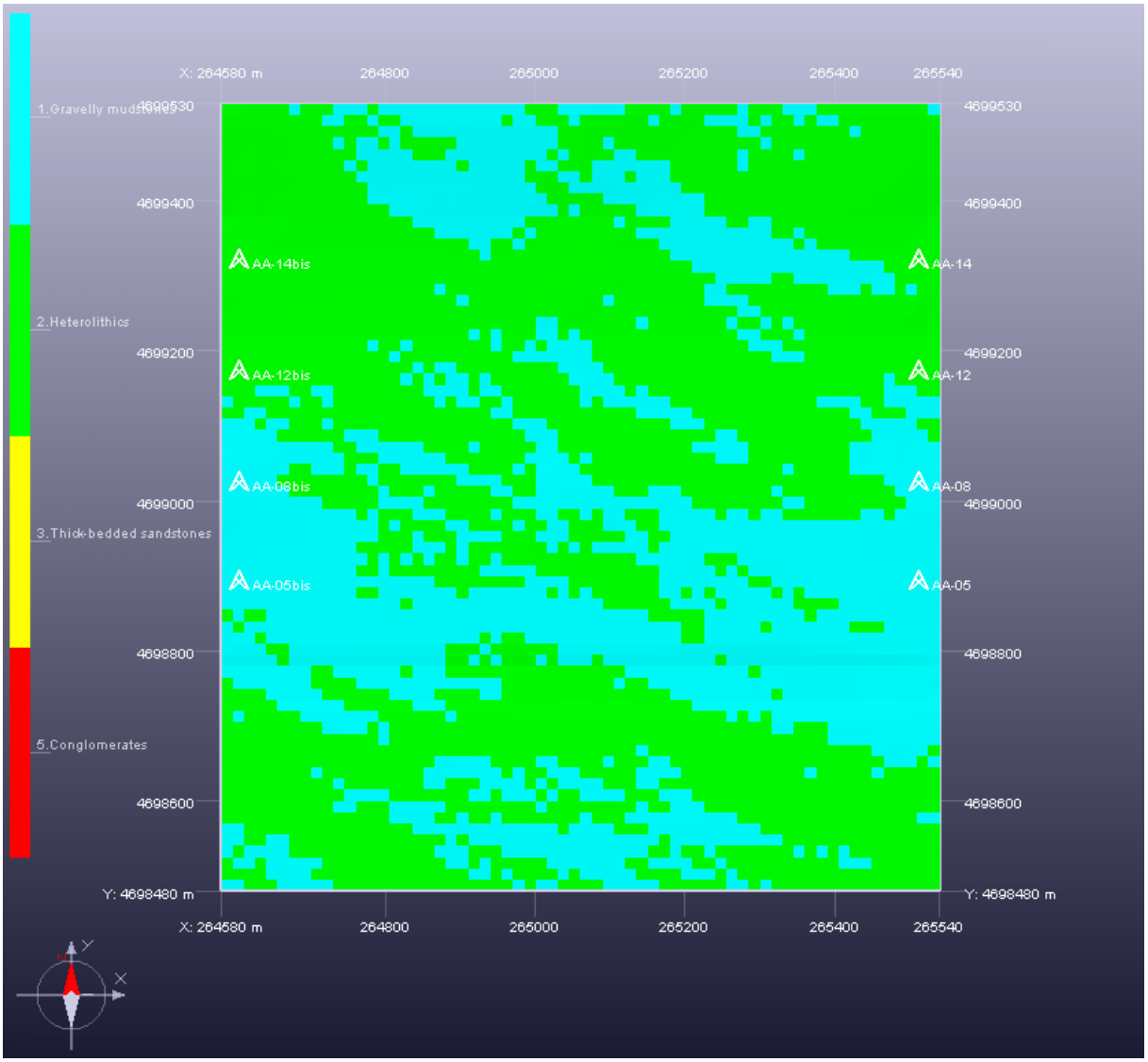

Figure 3.51 Top view of the facies distribution in unit C1 and for this reason the top of the Ainsa-1 Quarry outcrop. The orientation of the anisotropy is followed by the facies gravelly mudstones (blue ones) and heterolithics (green ones), which are the dominant facies.

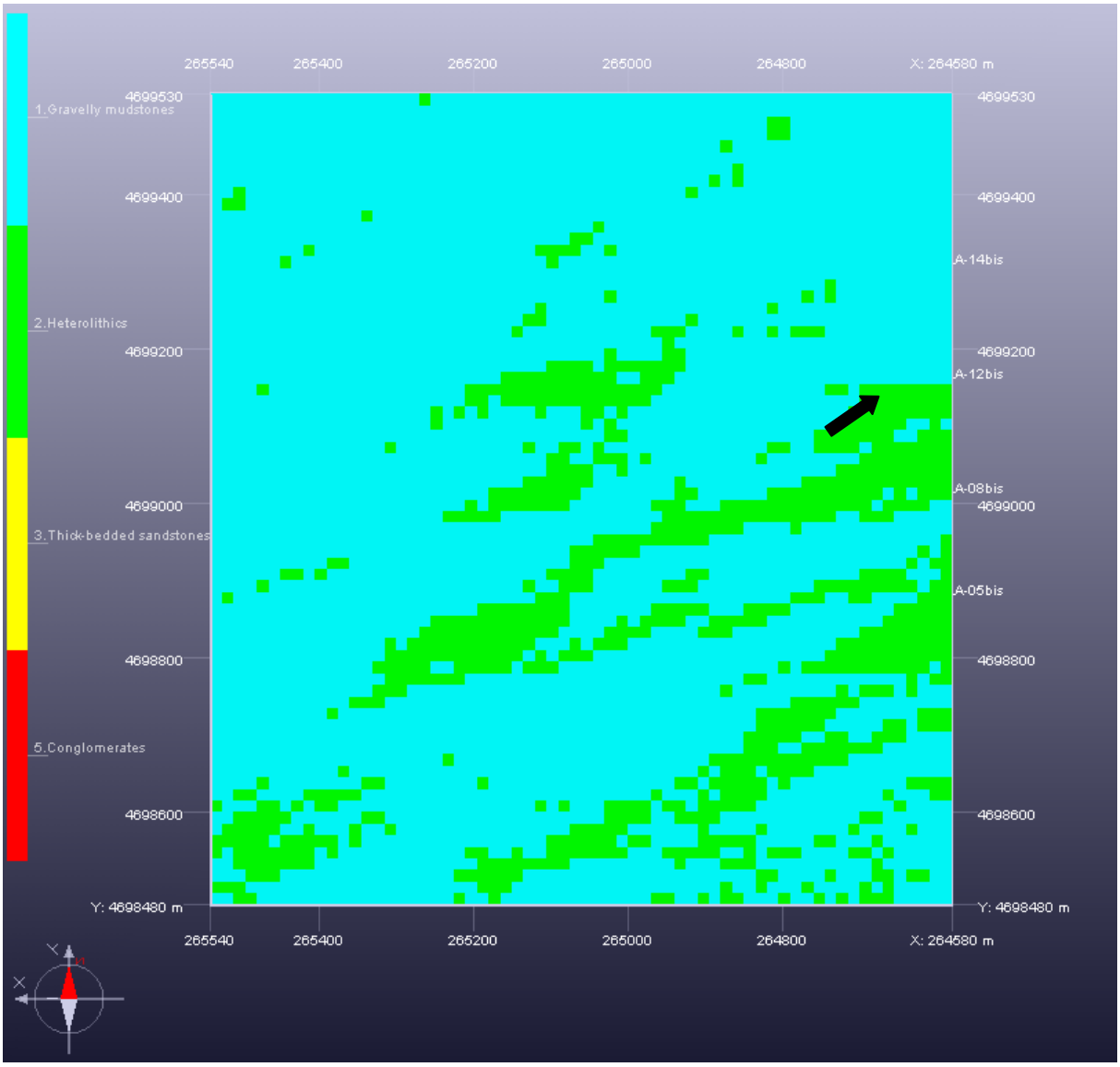

Figure 3.52 Bottom view of the facies distribution in unit C1 and for this reason the bottom of the Ainsa-1 Quarry outcrop. The dominant facies is gravelly mudstones as one expected after checking the outcrop characterization. The presence of heterolithics is greater on the SW and W of the outcrop. Note the abrupt change of facies between wells AA-12bis and AA-08bis (black arrow), due to an artefact of simulation. This artefact is related: (1) to the high difference in facies proportion between the two wells (AA-08bis: 71% of gravelly mudstones and AA-12bis: 8%) and (2) by the small interwell distance. It will be corrected in the next version of the software.

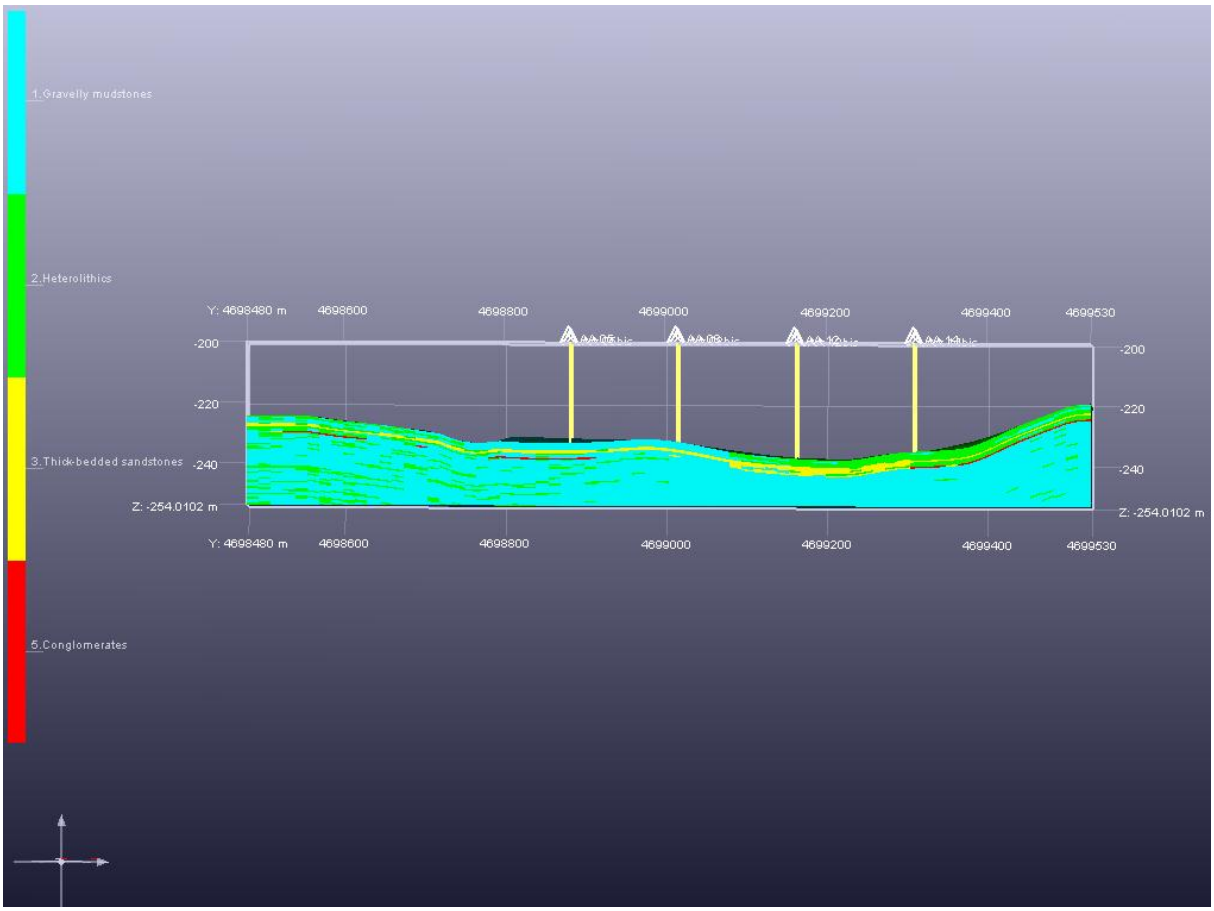

Figure 3.53 Front view of the facies distribution in unit C1. On the front view the heterolithics facies look well simulated and displayed. Moreover, in this unit we can observe some presence of conglomerates and the most noticeable aspect in here, it is the presence of a thick-bedded sandstones layer, crossing almost all the outcrop parallel to the main horizontal direction as well as in the perpendicular direction. For possible future works this layer could be part of the reservoir joining both zones (the main reservoir and the small one) creating a possible flow path.

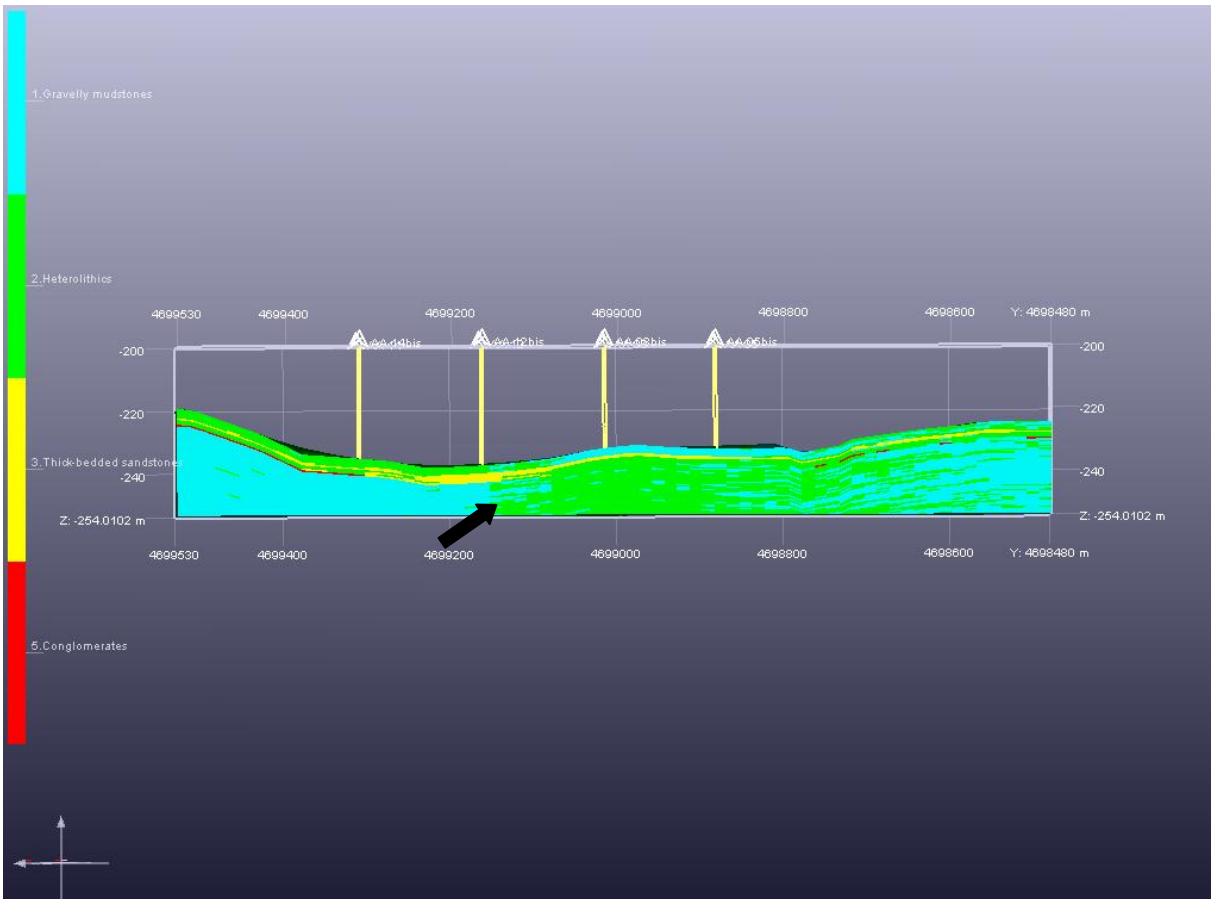

Figure 3.54 Back view of the facies distribution in unit C1. The sandstone layers continue backwards as we can check from this picture, which means that has a great continuity. Also, there is a presence of conglomerates as well, on the north and south of the outcrop. Arrow marks the abrupt facies change discussed in Figure 3.52.

FINAL FACIES MODEL (GoCad view)

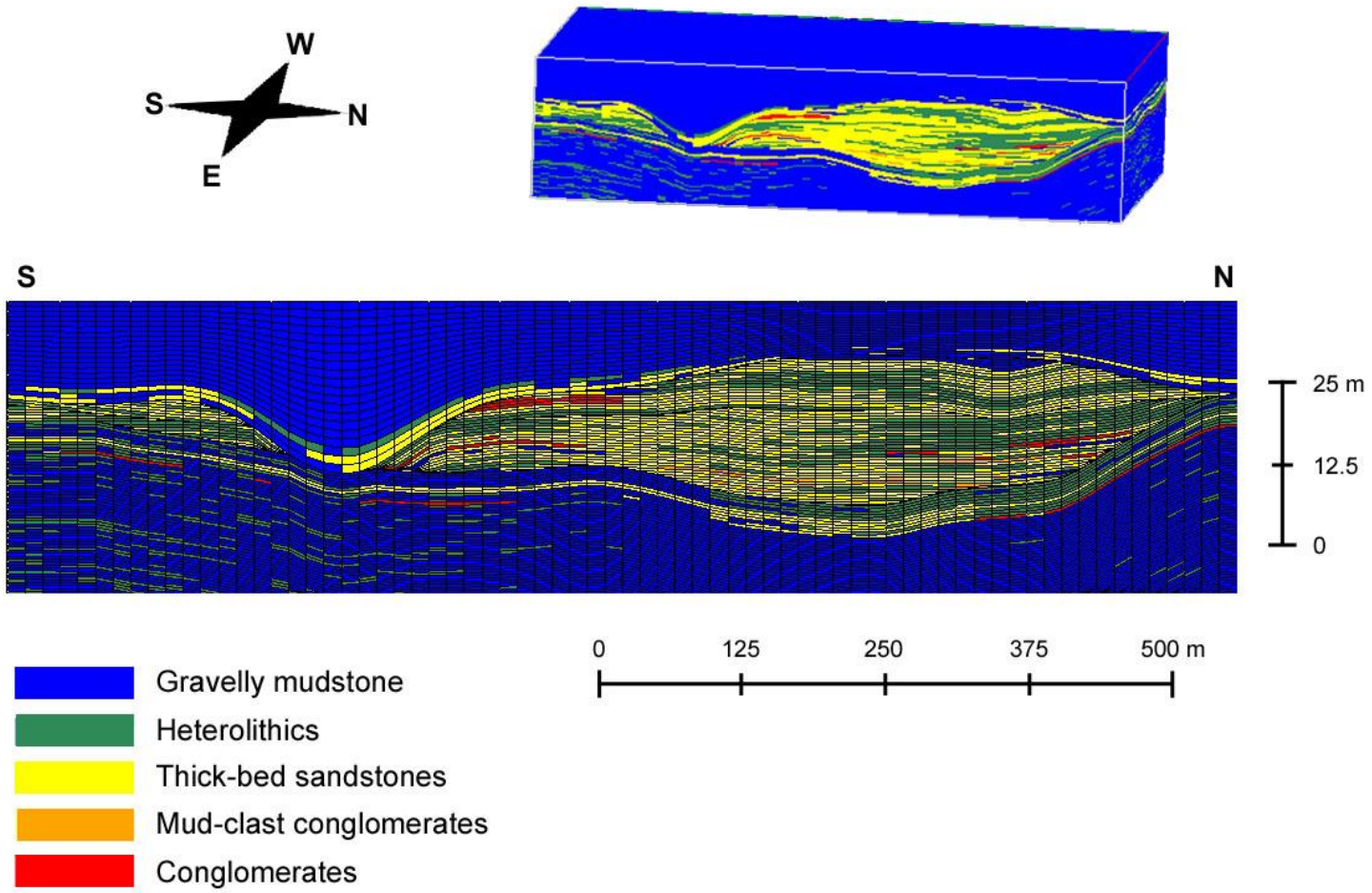

Figure 3.55 Three-dimensional facies simulation showing the architecture and facies distribution of the Ainsa-1 Quarry outcrop (GoCad software) from an pixel-based methods simulation. Vertical exaggeration is 5x. Each color corresponds to one facies, as it is shown in the legend. It is displaying the vertical section crossing the 3D model through the well logs set up in the front, so it can be compared with the correlation panel achieved from the outcrop field studies, (Figure 2.4A) to be aware about the weaknesses of the model.

It is obvious that the generated model cannot resemble completely the reality. Based on the purpose of the modeling and its forward application, some characteristics can be defined as the criteria of correctness of the model. Since this facies model is supposed to be used for fluid flow simulations, some important features should be preserved in the facies model:

1. Pinch out geometries, which are truncated to surfaces Base C2, Top C2.1 and Base C3.
2. Levee depositional sediments (i.e. heterolithics and gravelly mudstone) at both ends of the model.
3. Distribution and proportion of the heterolithics facies such as conglomerates and mud clast conglomerates in the reservoir area (units C2.2, C2.1).

These criteria have to be preserved during the modeling operation and are crucial to provide some guidelines for the manipulator. Also, the migrated channels during the depositional time can be observed from the top view. The periodic stacks of sandstone (central channel deposits) and heterolithics (channel margin facies) in channel form set C2 can be indicative of migrating the channel through time.

For these reasons, from the final model (Figure 3.55) we can test out that:

1. The model is well defined in terms of orientation, structure and architecture, i.e., vertical layering for each unit: proportional for C3, follow Base for C2.2 and C2.1up, follow top for C2.1mp-lp and C1.
2. The simulations of every unit have the minor problem of the “blocky” vertical layering (mostly for H lithofacies in units C2 and C1) and the lateral continuity, but in general terms the geometry is well accurate and the facies proportions obtained are well constrained, cf., histograms for each facies in each unit.
3. Globally, except for unit C3, comparing all the simulation made for each unit, we chose matrix of proportion of 5X5 because the lateral continuity of facies distribution seems to be better than for Matrix of 10X10.
4. It is observed a minor problem in the unit C2.1mp+lp, regarding to the facies distribution at the border of the channel but this is related with the same problem than in PETREL at the border of the channel because of the choice of "Follow Top" in the modeling grid step.

5. In this study we adopt the connectivity definition given by Pardo-Iguzquiza and Dowd (2003), so connectivity is defined as the percentage of pairs of connected cells for a particular facies, direction and separation. This means that in here we measured both vertical and horizontal connectivity, mostly in the reservoir zone.

Chapter 4 Fluid flow simulation

4.1 Petrophysical parameters

As discussed before, the Ainsa-1 channel sediments include five geological facies as follows: gravelly mudstone, heterolithics, thick-bedded sandstone, conglomerates and mud clast conglomerates. Eight synthetic wells across the outcrop were selected and their facies distribution along the well was considered.

The fluid flow simulation required the assignation of several rock properties. Because the outcrop is not at reservoir conditions, typical reservoir values for these kinds of materials were used (properties taken from subsurface reservoirs in the same depositional environment) and diverse scenarios were assumed for the petrophysical values.

Petrophysical properties can be assigned to lithofacies after simulation using a simple average value attribution or a more refined law based on spatial trends deduced from wells (Lerat et al., 2007). In this case, average, isotropic and uniform values were assigned to lithofacies for the sake of simplicity. On one hand, the values of density, volume of clay, porosity, permeability (Kx, Ky, Kz), P-impedance and P-velocity employed for each of the facies, are listed in the Appendix 1, together with graphical representations of these properties. Table 4.1 summarizes the porosity and permeability values applied for each of the facies observed in the synthetic logs.

The permeability chosen for thick-bedded sandstones and gravelly mudstones lithofacies falls into the same order of magnitude used by Falivene et al., (2007) paper, whereas for Heterolithics, Conglomerates and Mud-clast Conglomerate lithofacies, we decided to increase by one or two order of magnitude respectively, for the first simulation and keep decreasing them in the next runs to be able to check the real influence of heterolithics in the fluid flow inside a reservoir.

Moreover, we gave a noticeable permeability to these facies rather than 1mD (Falivene et al., 2007) because they are quite different; conglomerates and mud-clast conglomerates

correspond to a sandy matrix with pebbles of sandstone (conglomerates) or mudstones (mudstone-clast conglomerates) i.e. a fair to bad reservoir, whereas gravelly mudstones correspond to a muddy matrix (non reservoir).

	Facies	Ø (porosity)	K_x (mD)			K_y (mD)			K_z/K_x
1	**Gravelly mudstones**	0.000	0	0	0	0	0	0	0
2	**Heterolithics**	0.050	40	40	40	40	40	40	0.001
3	**Thick-bedded sandstones**	0.300	2000	2000	2000	2000	2000	2000	0.1
4	**Mud-clast conglomerates**	0.150	500	50	5	500	50	5	0.1
5	**Conglomerates**	0.250	2000	2000	2000	2000	2000	2000	0.1

Table 4.1 Petrophysical parameters corresponding to each facies observed in Ainsa outcrop section and for each run.

Table 4.1 clarifies that gravelly mudstones and heterolithics are non-reservoir facies because of their low porosity and permeability values, even zero for mudstones, whereas thick-bedded sandstones and conglomerates have larger values of porosity and horizontal and vertical permeability. Mud-clast conglomerates are considered a reservoir material with bad quality (low permeability).

From these values the pretrophysical model was built in GoCad software only for the reservoir zone, for C2 channel form set; In other words, we created an active grid block (ACTNUM equal to 1 in C2 and zero in C1 and C3) including the units which could be good reservoir by looking at reservoir facies percentage in each area. In Figure 4.1 it can be observed that there are two main isolated areas in the reservoir: a small zone situated on the south of the model and a big one occupying almost the centre of the model. Moreover, underneath these zones, there is a non-reservoir layer followed by a thin layer of thick-bedded sandstones. Because of computing time restriction, in this study we only focused in the main big reservoir area.

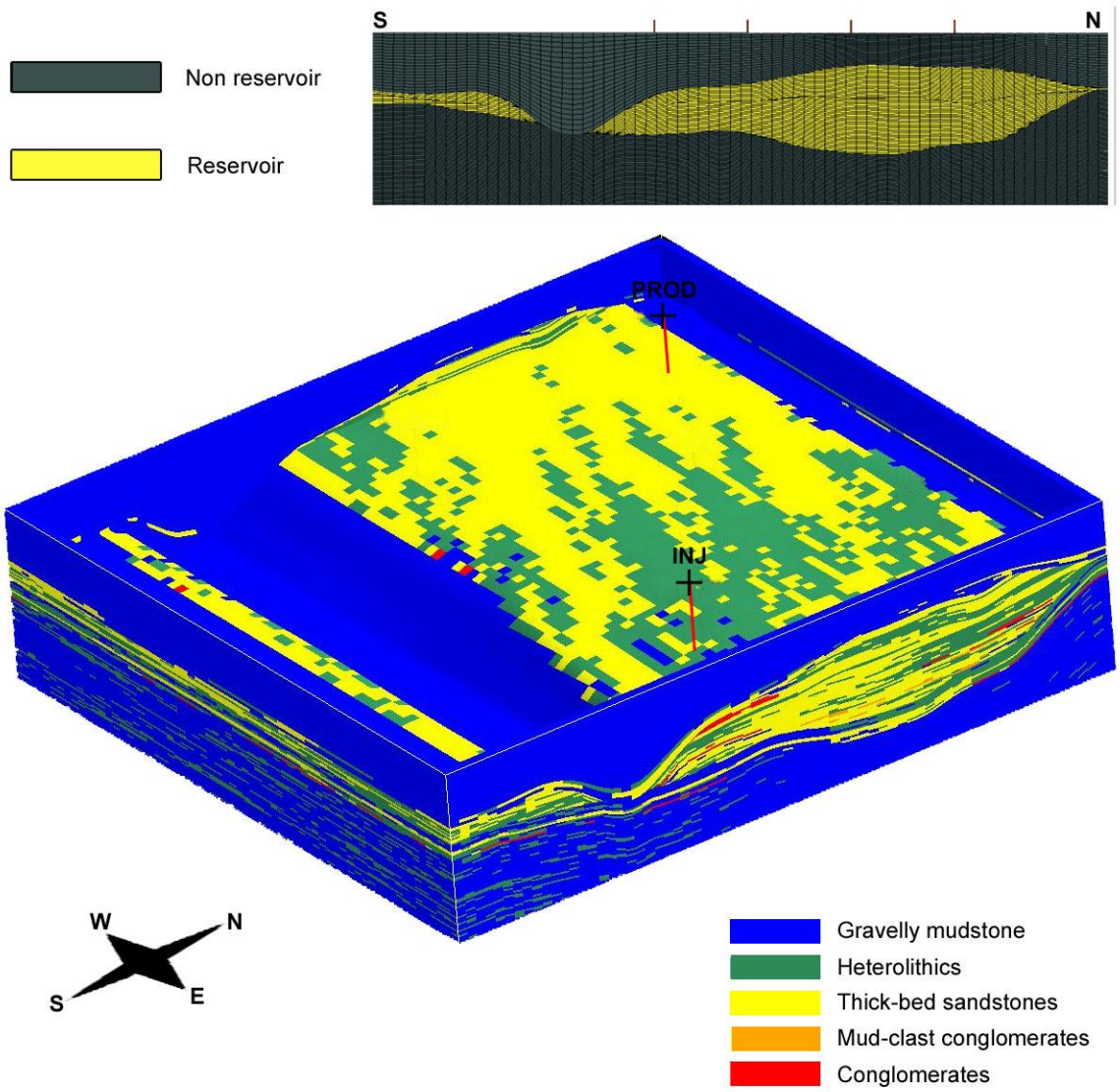

Figure 4.1 View of the reservoir zone with the different facies, which includes C2.2, C2.1-up and C2.1-mp-lp units. The injector and producer wells used for the different fluid flow simulations are displayed.

The petrophysical models for porosity and permeability are shown in Figure 4.2, Figure 4.3 and Figure 4.4.

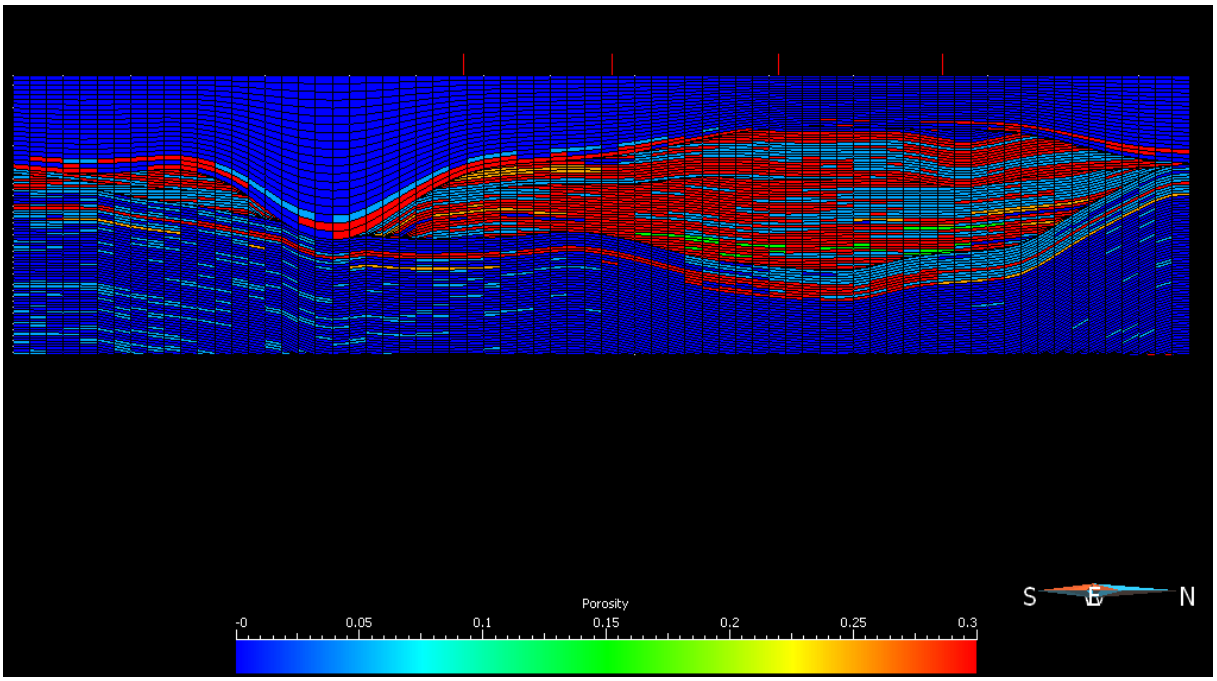

Figure 4.2 3D porosity model for Ainsa-1 Quarry outcrop.

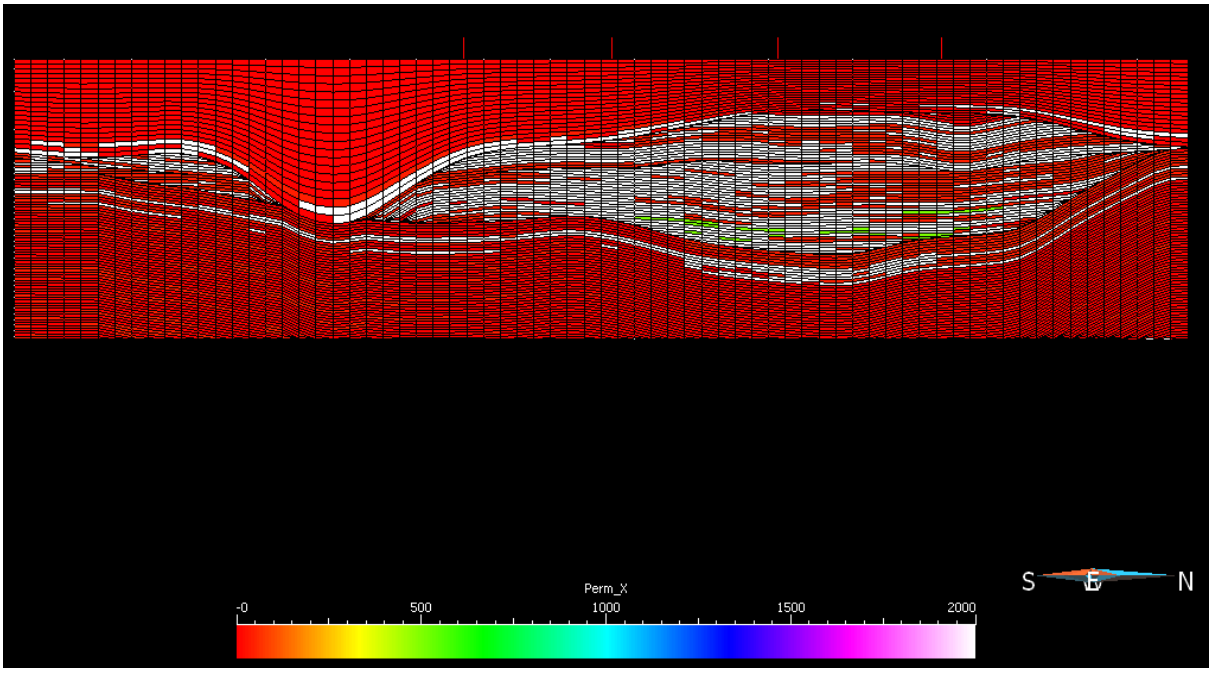

Figure 4.3 3D X and Y permeability model for Ainsa-1 Quarry outcrop.

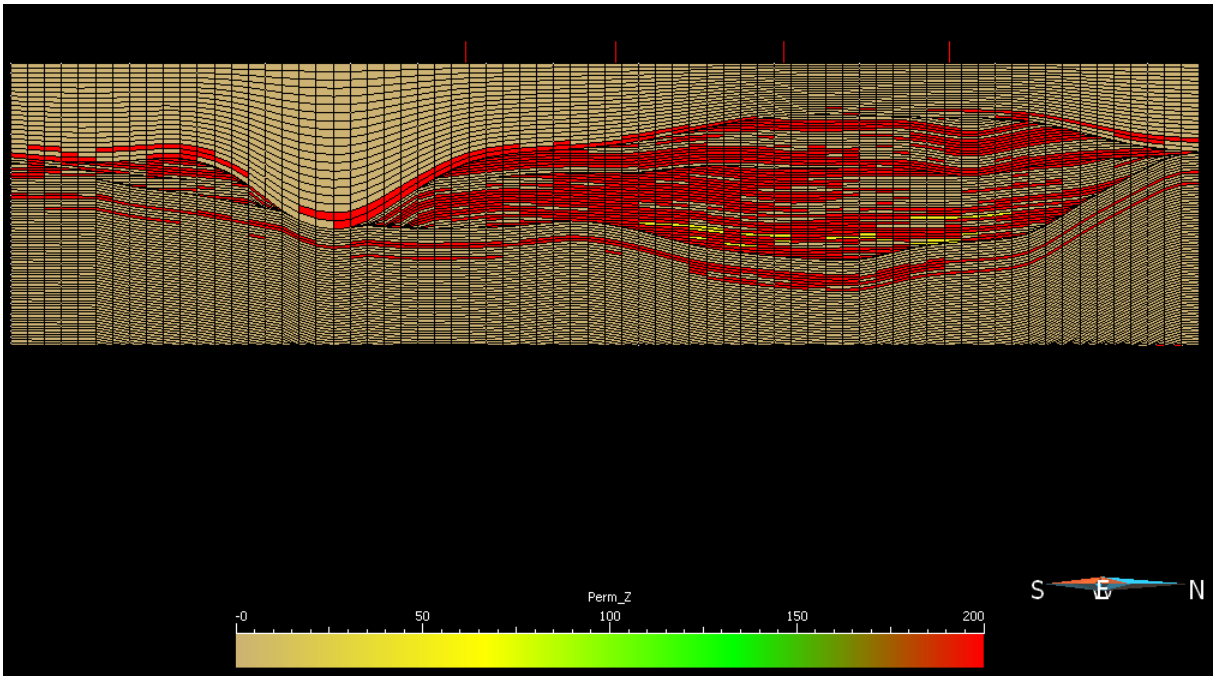

Figure 4.4 3D Z-permeability model for Ainsa-1 Quarry outcrop.

4.2 Fluid flow simulation workflow

The general workflow to construct reservoir model is illustrated in Figure 4.5. This section corresponds to the upscaling and fluid flow simulation components of this workflow, nevertheless, applying upscaling was not required on either set of models, because the fluid-flow simulator could directly handle the geological grid in terms of number of cells (649650).

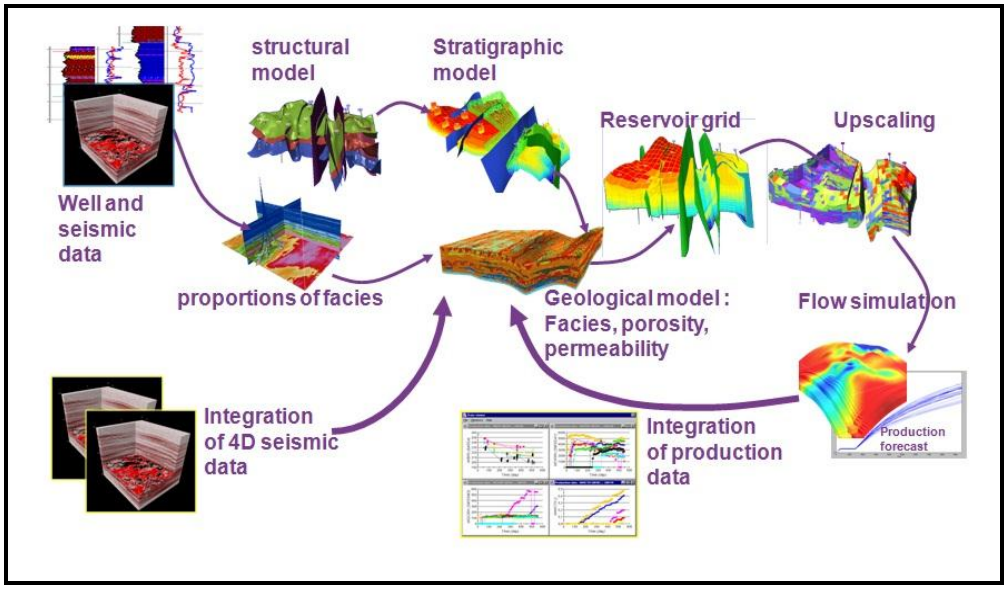

Figure 4.5 Usual reservoir characterization workflow showing the different inputs to construct a geological model. Based on this geological model, a reservoir grid can be defined allowing fluid flow simulation and production data integration into the final model, gaining understanding on the reservoir behavior.

For flow simulation we have to take into account:

1. Structure parameters.
2. Rock parameters.
3. Fluid parameters.
4. Production parameters, related with the reservoir production system.

Structure parameters:

In terms of geostatistical parameters, it is important to check the quality of the grid referring to cell thickness, structure and spatial variability model, the facies model, the facies connectivity, etc. In Table 3.1, one can check the structure model of the Ainsa-1 Quarry outcrop, divided by units and their layering. Table 4.2 shows the total number of cells of the grid and for each unit, which is directly related to the simulation time.

It is also required to define our trap properties, which in this case, has a reference depth situated at -2220 m and a base depth at -2255 m. The initial pressure at the reference depth is 253.52 bar, the reservoir temperature is 50°C (no thermal effects) and the initial oil-water contact (OWC) is situated at -2255 m depth.

Units	Number of cells	Zones
C2.2	98560	Reservoir 250880
C2.1-up	40320	
C2.1-mp-lp	112000	
C1	309120	Non reservoir 398720
C3	89600	
All facies	649650	All grid

Table 4.2 Number of cells in Ainsa-1 structural model.

Rock parameters:

About the petrophysical parameters, as it is explained before, the permeability in horizontal dimension is isotropic and it remains the same for all the facies except for the Mud-clast Conglomerate lithofacies that varies from 500 mD to 5 mD in the different simulations. The porosity remains the same for all the facies in each simulation. Moreover, for the rock compressibility we used a constant value of 0.0000330 bar^{-1}.

Fluid parameters:

The next step is introducing a PVT model (Figure 4.6), which in this case consists of two phases (Oil and water), set a single relative permeability model for all the facies and no capillary pressure. The relative permeability model is given by a tabulation (Figure 4.7). The residual oil saturation was zero for all facies and the irreducible water saturation was approximately 0.29. Oil density is 0.833 g/cc and water density is 1.08 g/cc at surface conditions, simulating a highly favorable displacement. Temperature at surface conditions is 15.5 °C.

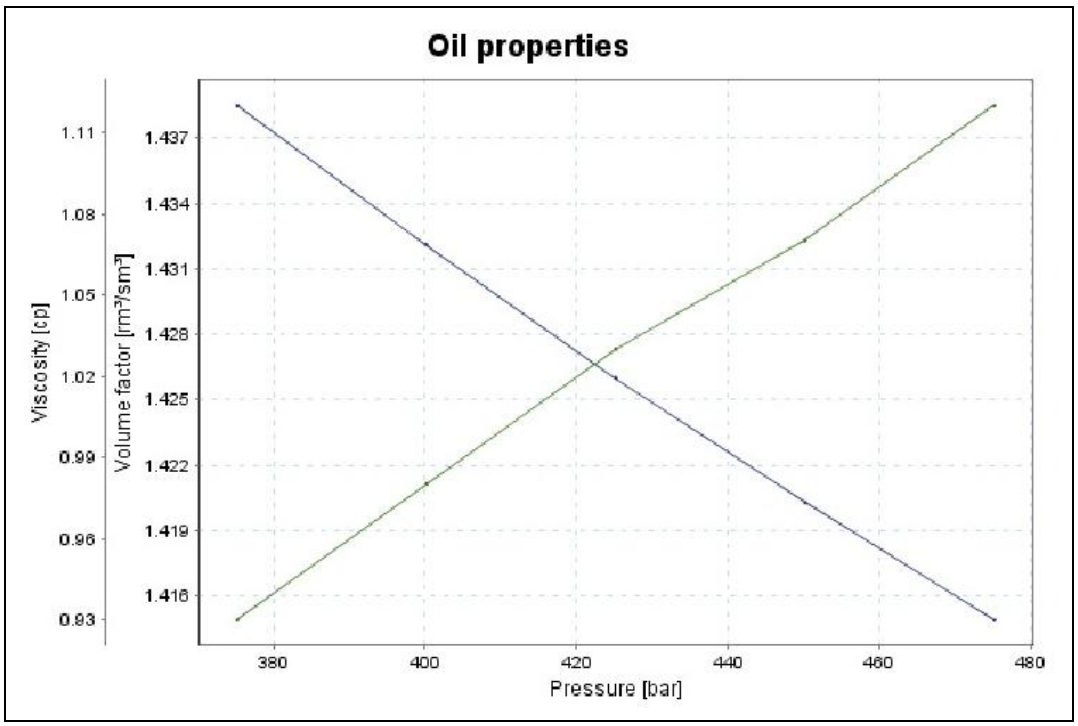

Figure 4.6 Oil viscosity and volume factor vs. pressure in PVT model.

a)

End Point	Value
Sat.	
SWI	0.296290
SORW	0
Pc	[bar]
Kr	
KRWM	1
KROWM	1
Kr Params	
N W Imb.	3.289604
N OW Imb.	5.606234

b)

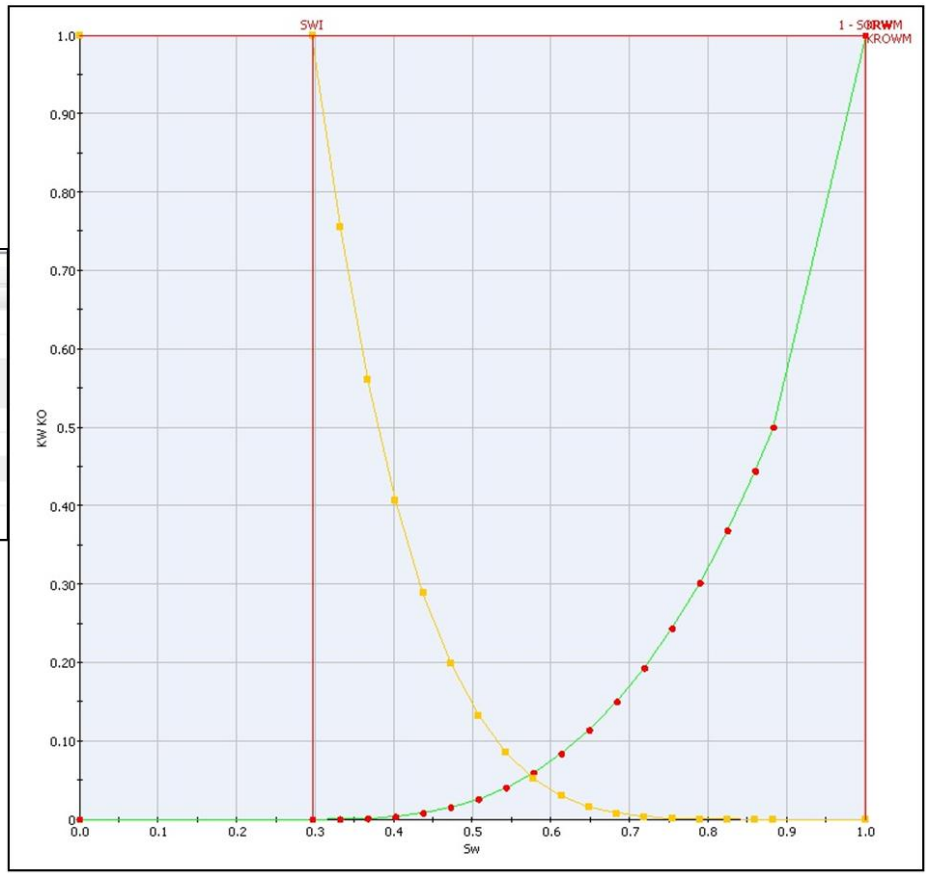

Figure 4.7 Kr-Pc model. We designed a single model for all the facies. Figure a) end values of water and oil saturation and relative permeability. Figure b) Kr vs. Sw.

Production parameters:

The two-phase fluid flow simulation was achieved using a quarter five-spots injection production, using PumaFlow from the underdevelopment software, OpenFlow Suite 2012. The producer and injector wells are located in opposite corners of the Ainsa-1 model, as it can be seen in Figure 4.8. The bottom perforation for both is -2300 m depth and the BHP for injector well is 400 bar and for producer is 15 bar. The water/oil rates and their behaviors, vary from one simulation to another, this will be described in the section 4.3. However, in all the cases the rates are maintained constant and the pressure can vary, this means that the flow through the wells is controlled by the rate.

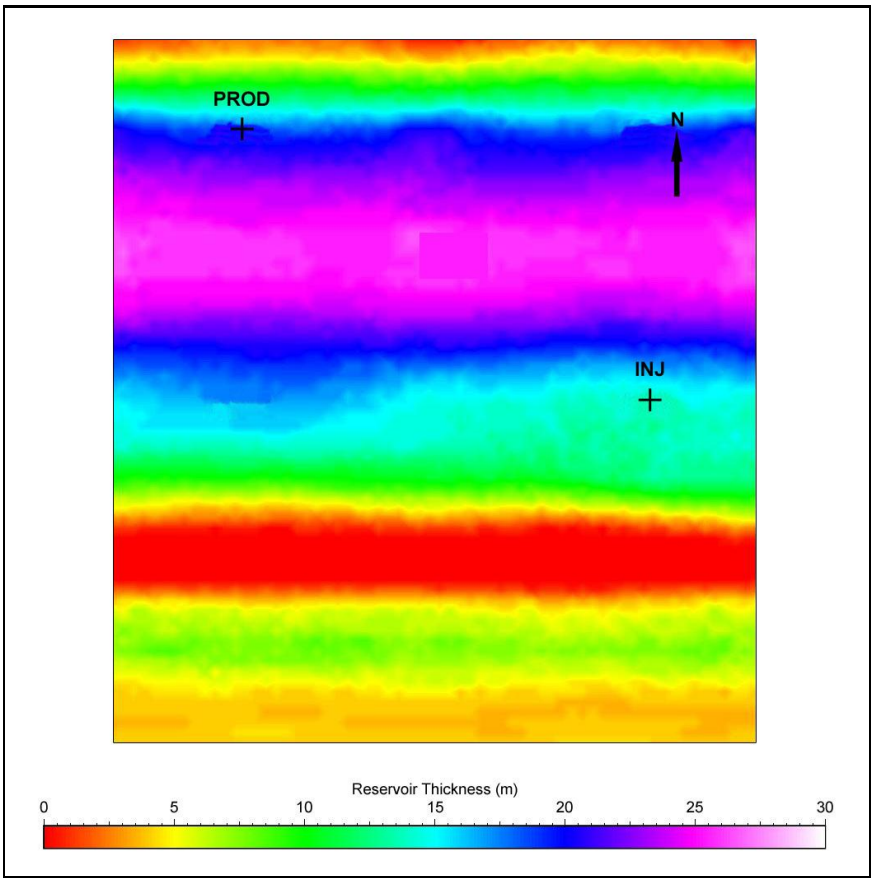

Figure 4.8 Reservoir thickness map showing the production wells location. They are situated one in front of the other in diagonal corners, in zones where the thickness tends the decrease.

Finally, the PumaFlow simulations were run to predict two-phase flow results for the outcrop and facies models. These simulations were conducted on the finely gridded outcrop characterization and on the finely gridded facies models obtained from the Plurigaussian and SIS simulations.

The simulations were run at least until water breakthrough at the production well because the simulation run time was relatively high given the number of cells, and the primary focus was on checking the flow paths inside the reservoir due to heterogeneities. Fluid-flow variables investigated checked were oil production rate, water injection rate, producer and injector bottom-hole pressures, watercut at the producer, water saturation distribution. Moreover, in some of the simulation, we reproduced a natural depletion before the water injection, during a period of six months.

Because of computing time restrictions, only 15 realizations were simulated, from which we chose four to show in this study because there were the most relevant ones, in terms of changing in petrophysical parameters, simulation times and rates.

4.3 Fluid flow simulation results

In the next pages, we display the results of the fluid flow simulations. Each simulation contains:

1. Table showing the parameters introduced to do the run, oil and water rate, BHP, period simulated and natural depletion if is simulated.
2. Table with petrophysical properties' used.
3. Pictures which show the water saturation distribution:
    - Front view.
    - Back view.
    - Top view.
    - Bottom view.
    - Cross-section, if necessary.
4. Water in place at surface conditions versus oil in place at surface conditions.
5. BHP for injector and producer.

At the end of this section it can be seen a comparison of the three flows simulations by displaying the top views (Figure 4.33). From this perspective it is easier recognize the flow paths that the water injected follows through the reservoir, until it reaches the producer well.

4.3.1 First simulation

Well	BHP (bar)	Water rate (m3/day)	Oil rate (m3/day)	Natural depletion	Simulation time
Injector	400	400	/	Open after 6 months	10 years
Producer	15	/	500	Yes during first 6 months	10 years

Table 4.3 Production parameters values used in this first fluid flow simulation for Ainsa-1 reservoir model.

	Facies	Ø (porosity)	K_x (mD)	K_y (mD)	K_z
1	Gravelly mudstones	0.000	0	0	0
2	Heterolithics	0.050	40	40	0.004
3	Thick-bedded sandstones	0.300	2000	2000	200
4	Mud-clast conglomerates	0.150	**500**	**500**	50
5	Conglomerates	0.250	2000	2000	200

Table 4.4 Petrophysical properties values used in this simulation.

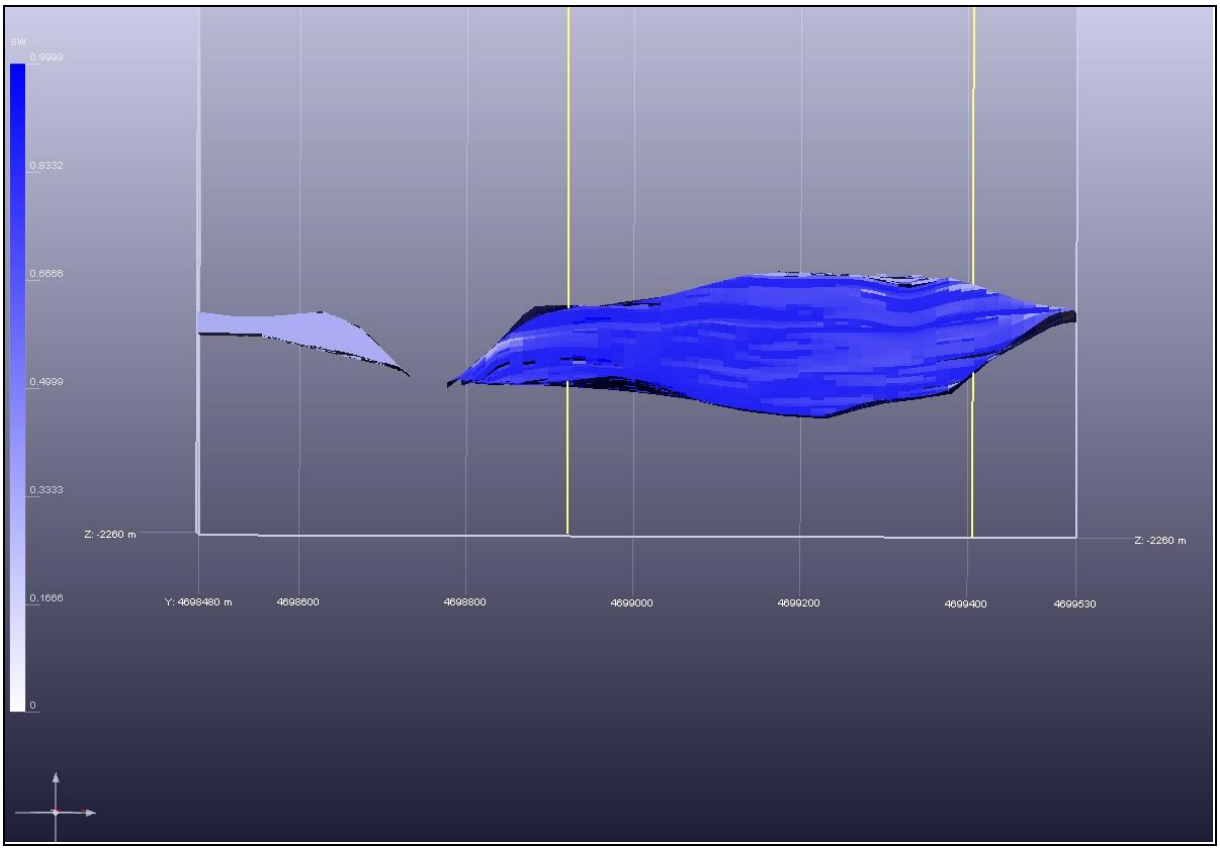

Figure 4.9 Front view of the water saturation in the main body of the reservoir at the end of the simulation period and the situation of the injector and producer wells. Layers with stronger blue colors means higher water saturation and they correspond with facies with high permeability and porosity. The whiter parts correspond with the zones where there are heterolithic facies. In this case, it seems there is no difference in behaviors between TkS and McC and C facies. The small volume reservoir is not connected due to the C3 erosive unit on top, which created a break on the unit C2 and for that reason it does not receive any water injection.

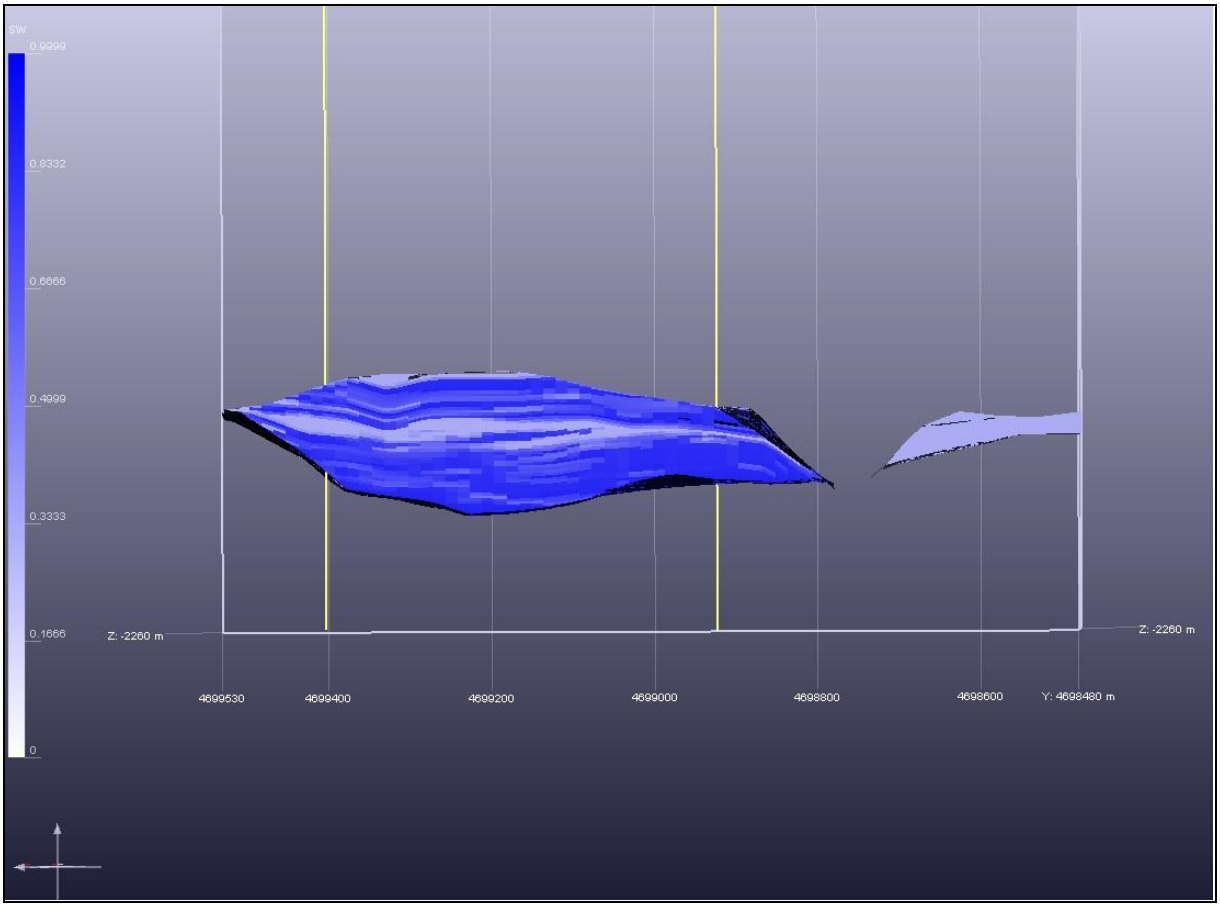

Figure 4.10 Back view of the water saturation in the main body of the reservoir at the end of the simulation period and the situation of the injector and producer wells. The whiter parts correspond with the zones where there are heterolithic facies. In this case, there is more presence of H facies in the back part than on the front.

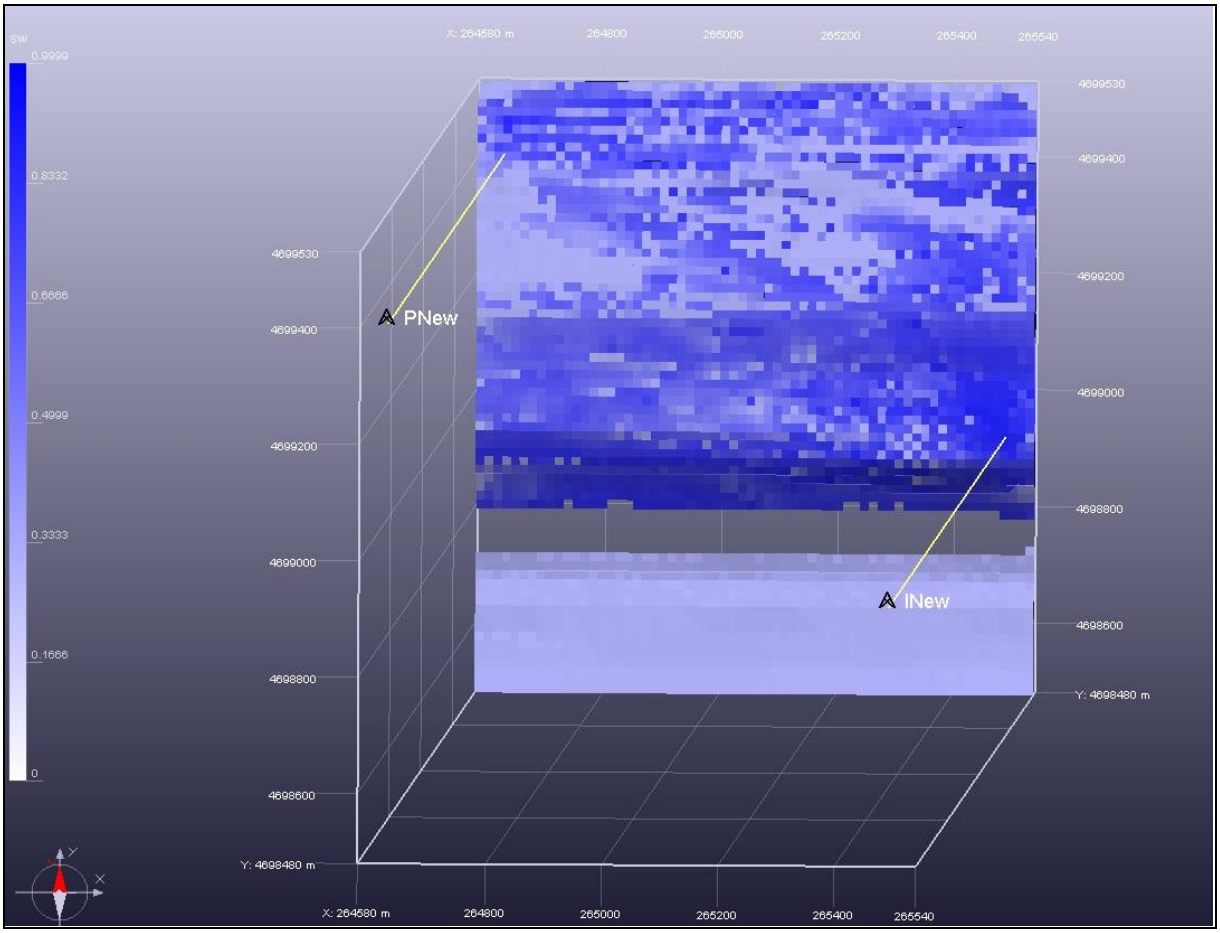

Figure 4.11 Top view of the reservoir for the first simulation showing the situation of the wells and the water saturation after the time applied in this run. The water reaches the producer well, most of the reservoir is charged by this water and most of the oil is drained after 10 years production thanks to the natural depletion first and the water injection after (second recovery). There is an accumulation of water near the injector well in comparison with other zones of the reservoir and this is a normal and expected behavior even if in that zone we can find a big range of heterogeneities, almost in the vertical direction. Facies gravelly mudstones, McC, heterolithics, conglomerates and of course, TkS appear in this area of the outcrop. It is shown some path flows mostly related with the channels directions, with the sandstones and good-reservoir facies. In Figure 4.33 is displayed a comparison of these path flows patterns from the top map views of the three simulations.

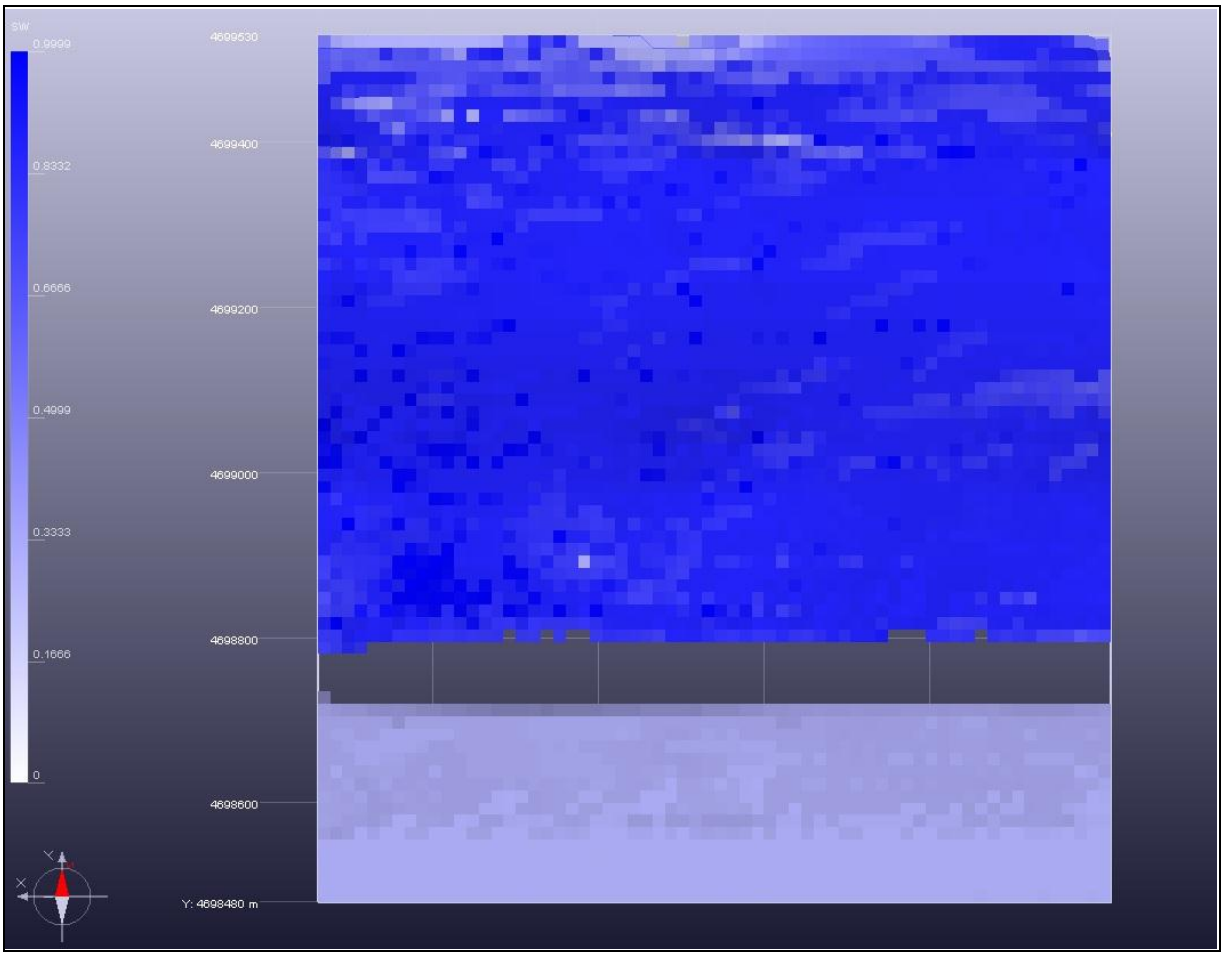

Figure 4.12 Bottom view of the first simulation facies distribution in the reservoir. As one expected, most of the base of the reservoir presents strong blue colors, which means that all the porosity in the facies is filled by water from the injection. This is because during the facies modeling step we designed (following the outcrop) the bottom of C2.1-mp-lp with only thick-bedded sandstones, which have high porosity and permeability and thus, it is a good reservoir facies.

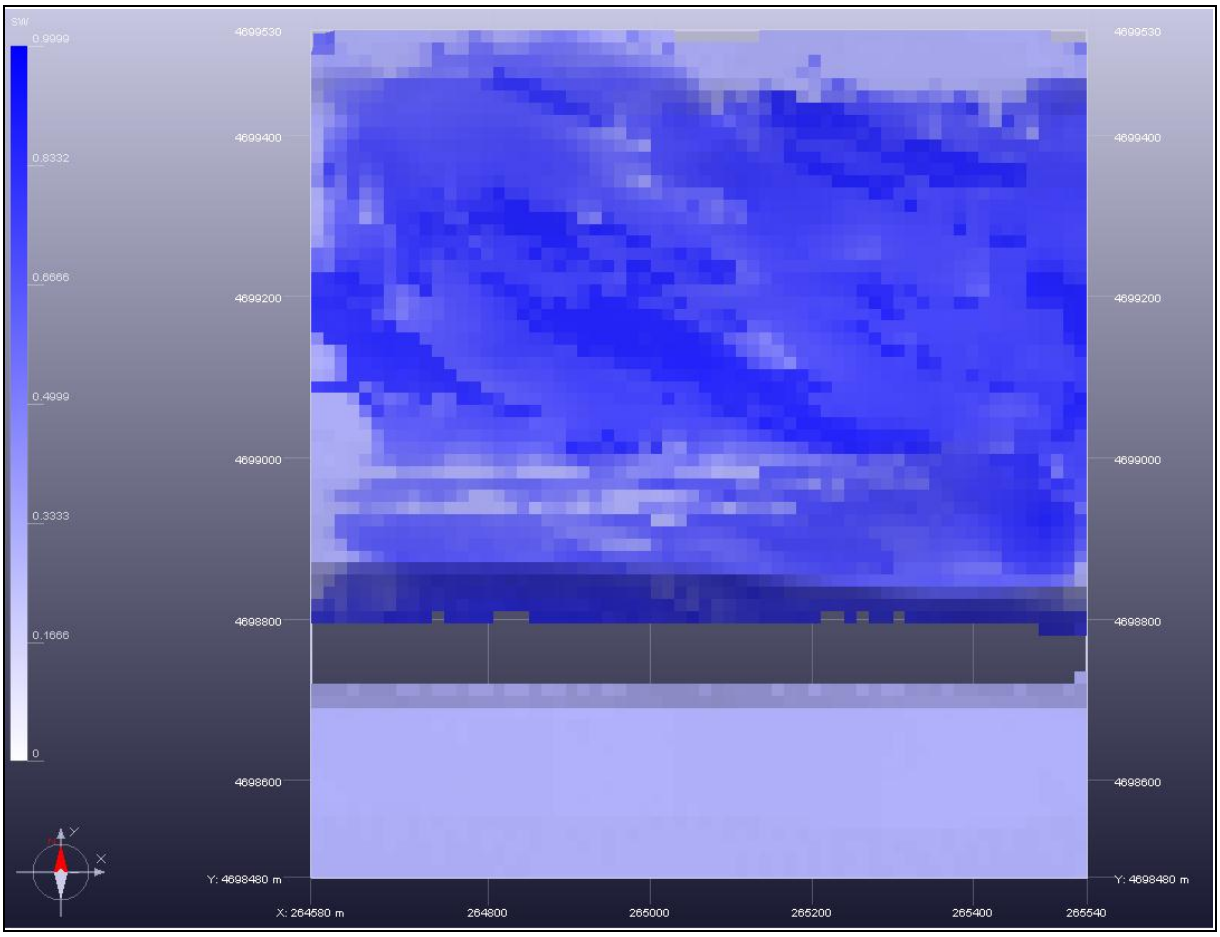

Figure 4.13 Cross-section and top view in K117 showing the paths flow related with good reservoir facies for stronger blue colors. The white colors that perform a "strange form" perpendicular to the main horizontal direction of the outcrop, correspond with the "blocky" heterolithics facies. There is one situated in Y=4699000 and X=264580 and crosses almost all the reservoir and another one situated at the end of the outcrop that crosses all the outcrop. These two flow paths, although they are related with the petrophysical properties of the facies, they are formed by the accumulation of heterolithic facies due to the "problem" of the grid geometry in this unit.

Figure 4.14 Graphic of the oil-water production at surface conditions. Brown line corresponds to oil production and it can be observed some anomalies at the beginning of the simulation. After 8 years of production trying to maintain a rate of 280 m^3/day, after the failed attempt of producing 400 m^3/day the production drops and quite rapidly after the breakthrough. The water (blue line) reaches the producer well after 7.5 years production.

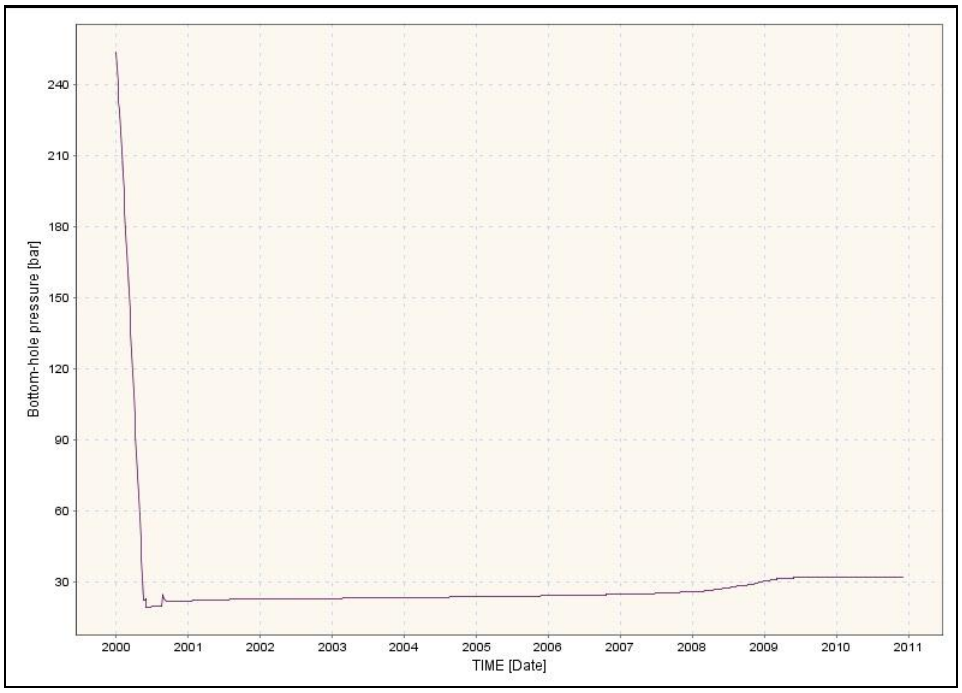

Figure 4.15 Bottom hole pressure on the water injector well. It presents an anomaly at the beginning of the simulation, the pressure drops until less than 30 bars and this is not realistic. It can be related with a problem of trying to maintain the water rate during all the simulation time, but also it could be related with a numerical diffusion of time steps during the running of the simulations.

Figure 4.16 Bottom hole pressure on the oil producer well. It presents the same anomaly that the injector BHP at the beginning of the simulation and until the end, the pressure drops until less than 30 bars and this is not realistic. It can be related with a problem of trying to maintain the water rate during all the simulation time, but also it could be related with a numerical diffusion of time steps during the running of the simulations.

4.3.2 Second simulation

Well	BHP (bar)	Water rate (m3/day)	Oil rate (m3/day)	Natural depletion	Simulation time
Injector	400	400	/	Open after 6 months	8 years
Producer	15	/	500	Yes during first 6 months	8 years

Table 4.5 Production parameters values used in this first fluid flow simulation for Ainsa-1 reservoir model.

	Facies	Ø (porosity)	K_x(mD)	K_y (mD)	K_z
1	Gravelly mudstones	0.000	0	0	0
2	Heterolithics	0.050	40	40	0.004
3	Thick-bedded sandstones	0.300	2000	2000	200
4	Mud-clast conglomerates	0.150	**50**	**50**	50
5	Conglomerates	0.250	2000	2000	200

Table 4.6 Petrophysical properties values used in this simulation.

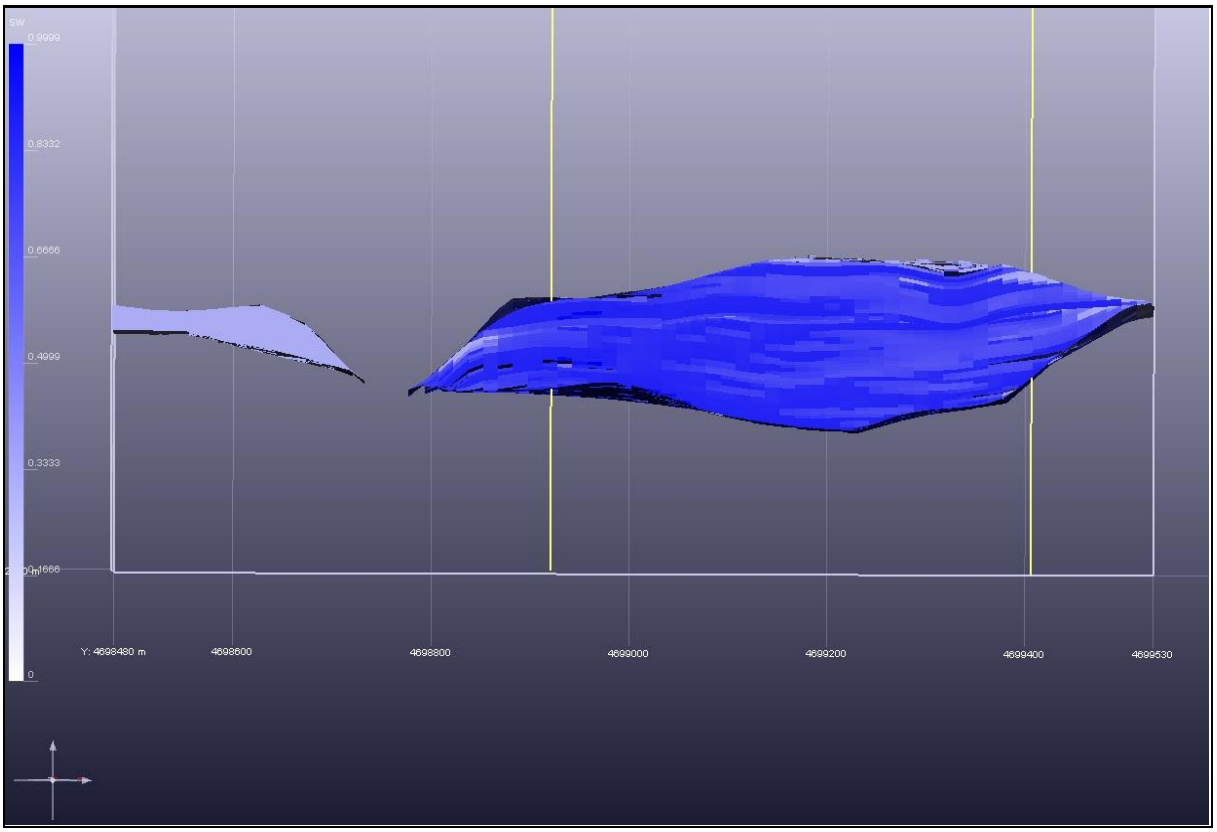

Figure 4.17 Front view of the water saturation in the main body of the reservoir at the end of the simulation period and the situation of the injector and producer wells. In this case, second simulation, there are no big differences with respect the other simulation. However, it can be distinguish more the McC layers along the horizontal direction of the reservoir. As in the previous simulation it can be observed clearly the heterolithic facies, whiter zones and "the black holes" are the gravelly mudstones lithofacies, which represent non-reservoir facies.

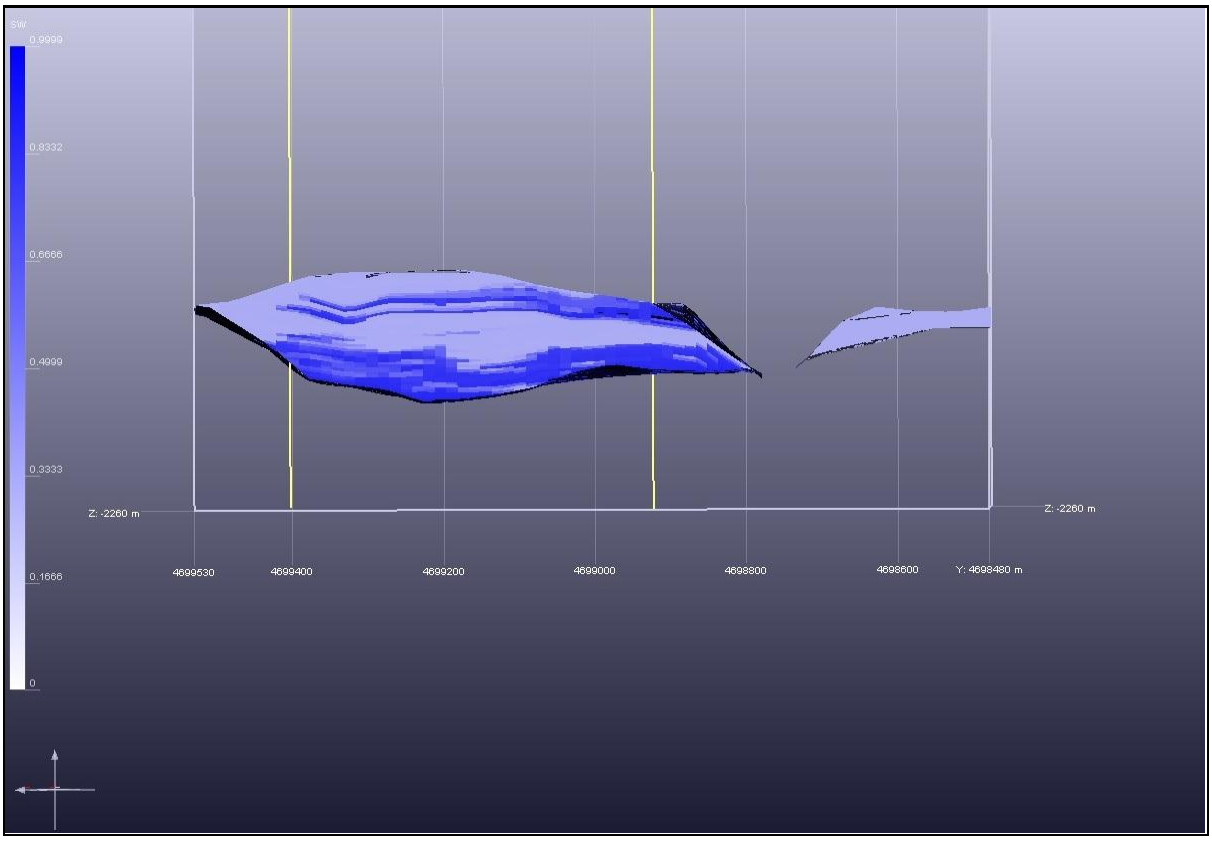

Figure 4.18 Back view of the water saturation in the main body of the reservoir at the end of the simulation period and the situation of the injector and producer wells. Comparing with the previous simulation it is possible to observe big differences, because on the first simulation apart from the heterolithic beds, the rest of the back part was filled from bottom to top by the water injection. However in here, it is shown four distinct areas: (1) the bottom part completely saturated by water, (2) the middle of the channel form set C2.1 undersaturated, (3) the upper part almost completely filled by water and (4) the unit C2.2 which remains undersaturated. This is related with the petrophysical properties of each facies, more or less permeability and porosity, although in here one should take into account that in this simulation for the same water rate than the previous one, the simulation time is less and for this reason the water does not reach those areas on the back of the reservoir.

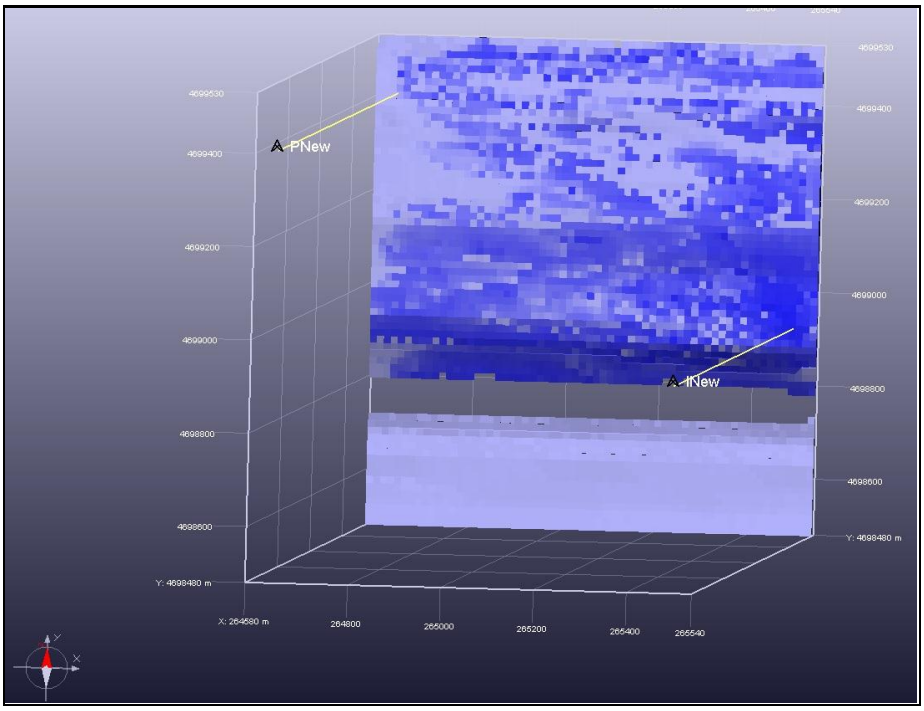

Figure 4.19 Top view of the reservoir for the second simulation showing the situation of the wells and the water saturation after the time applied in this run. There are no big differences on top of the reservoir between the first simulation and this one. There is less water saturation near the producer well than in the other case and along the entire reservoir as well and this is related with the simulation time for same water rate.

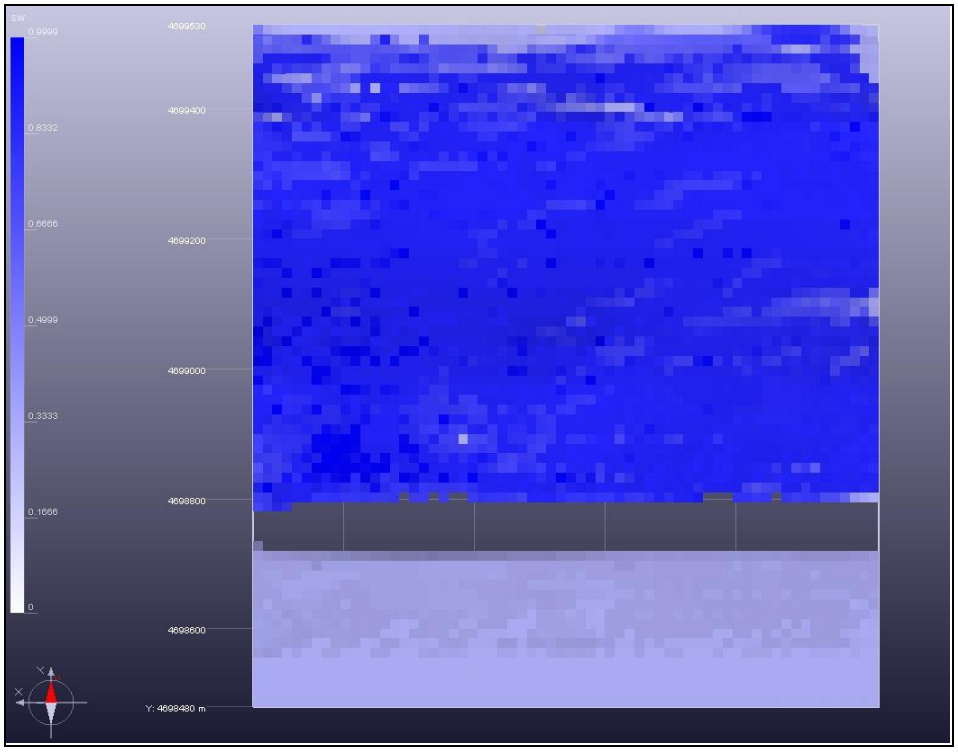

Figure 4.20 Bottom view of the second simulation facies distribution in the reservoir. In the bottom part of the reservoir, there is no difference and this is caused by the TkS infilled during discretization step, as it is explained before in Figure 4.12.

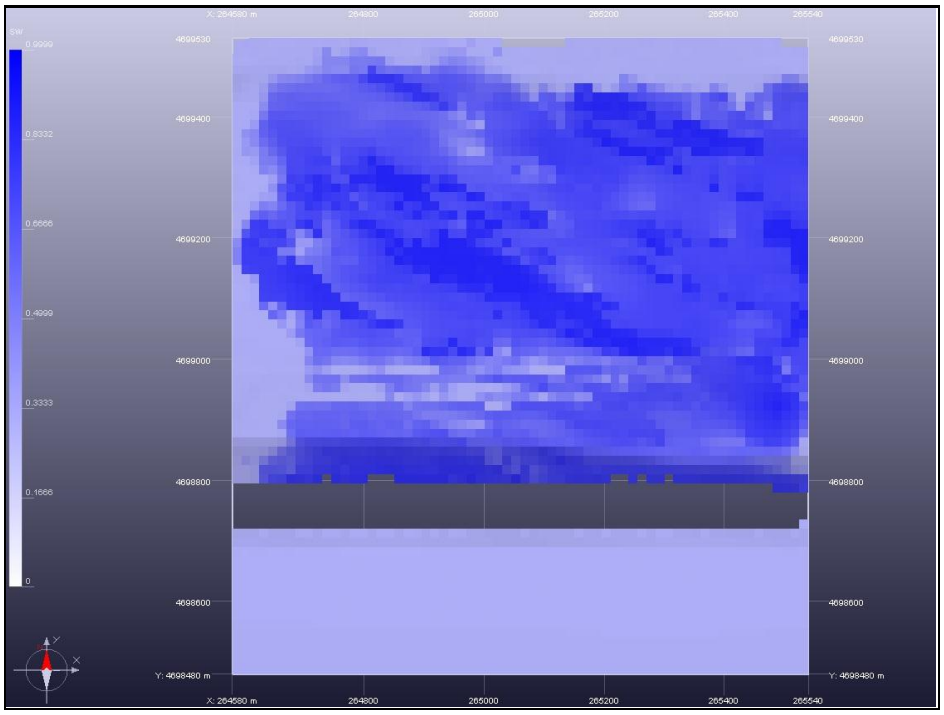

Figure 4.21 Cross-section and top view in K117 showing the paths flow related with good reservoir facies As it explained before, the water injected does not reach the same areas than in the previous simulation and for this reason the zones with low saturation are more intensified. It is possible to observe perfectly the problem of the "blocky" heterolithic facies, mostly on the north of the reservoir, where the boundary between the good reservoir facies and non reservoir facies follow almost at straight line, perpendicular to the main horizontal direction.

Figure 4.22 Graphic of the oil-water production at surface conditions. Green line corresponds to oil production and brown line to water production. it can be observed same anomalies behavior then the previous run. Moreover, after 8 years the production drops quite rapidly after the breakthrough. The water reaches the producer well after 7.5 years production.

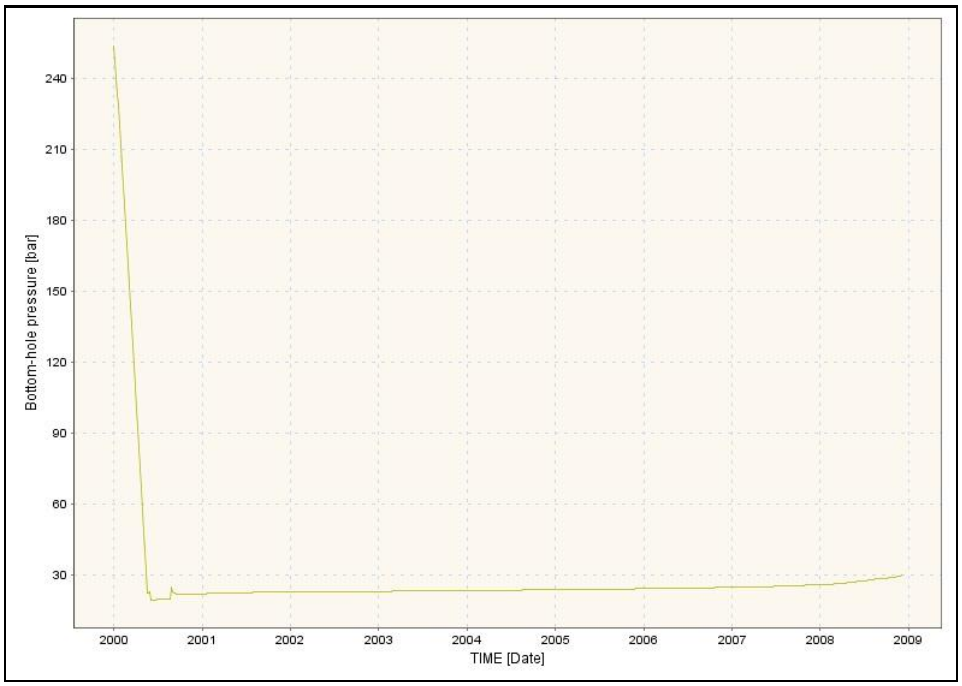

Figure 4.23 Bottom hole pressure on the water injector well. It presents the same anomaly in BHP at the beginning of the simulation and also it tries to increase the pressure at the end-time, like in the previous run.

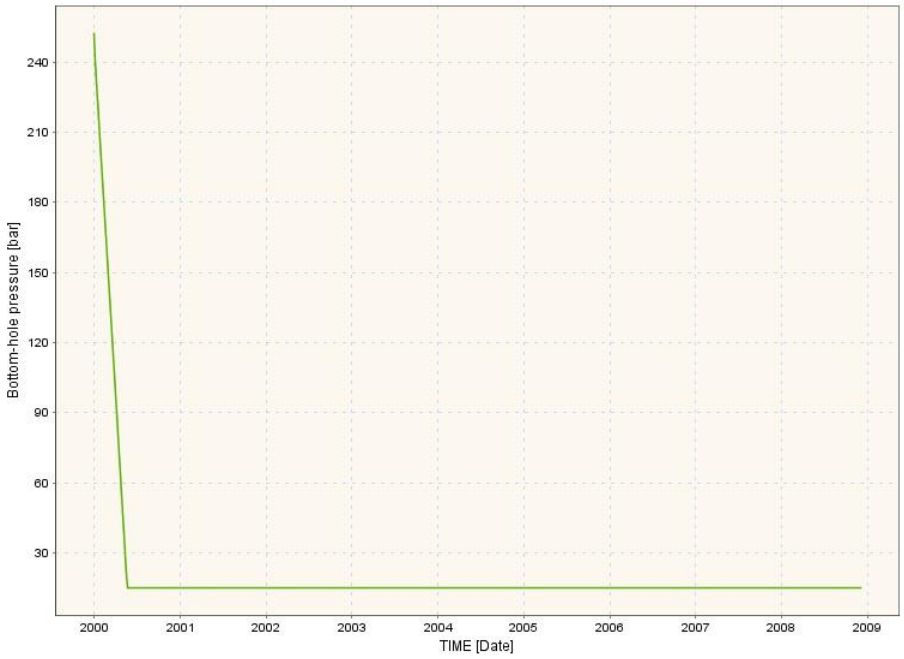

Figure 4.24 Bottom hole pressure on the oil producer well. It presents the same anomaly than the previous producer well in the first simulation, the BHP drops until 15 bars and remains the same during all the simulation time.

4.3.3 Third simulation

Well	BHP (bar)	Water rate (m3/day)	Oil rate (m3/day)	Natural depletion	Simulation time
Injector	400	400	/	Open	8 years
Producer	15	/	400	No	8 years

Table 4.7 Production parameters values used in this first fluid flow simulation for Ainsa-1 reservoir model.

	Facies	Ø (porosity)	K_x(mD)	K_y (mD)	K_z
1	Gravelly mudstones	0.000	0	0	0
2	Heterolithics	0.050	40	40	0.004
3	Thick-bedded sandstones	0.300	2000	2000	200
4	Mud-clast conglomerates	0.150	5	5	0.5
5	Conglomerates	0.250	2000	2000	200

Table 4.8 Petrophysical properties values used in this simulation.

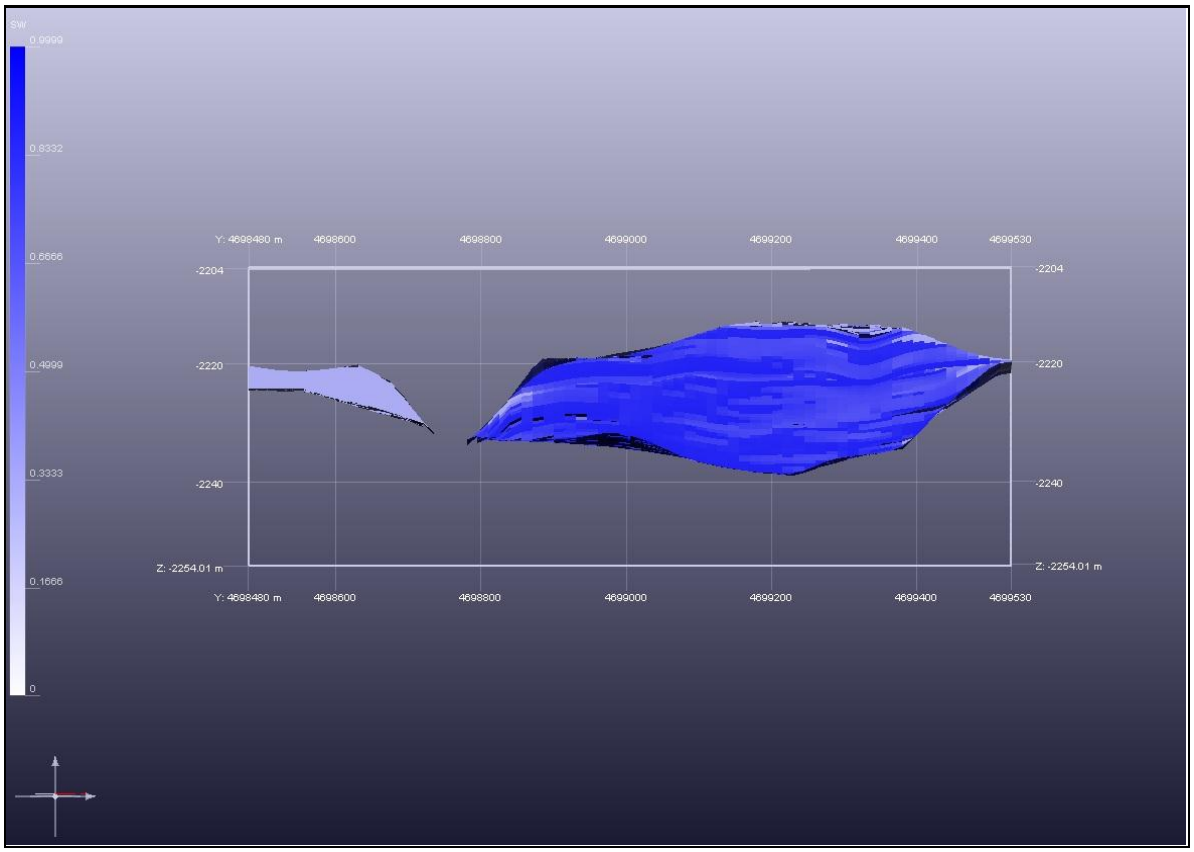

Figure 4.25 Front view of the water saturation in the main body of the reservoir at the end of the simulation period and the situation of the injector and producer wells. On the third simulation, it is reduced the horizontal permeability and vertical permeability of the McC lithofacies in two order of magnitude regarding the first simulation. This decrease is observed on the front of the reservoir model by the black holes or layers that are situated near the bottom of the model. On the south these black areas are bigger because the McC lithofacies are closed to Gravelly mudstone lithofacies (non-reservoir). The rest of the model has no big differences in terms of water saturations and path flows.

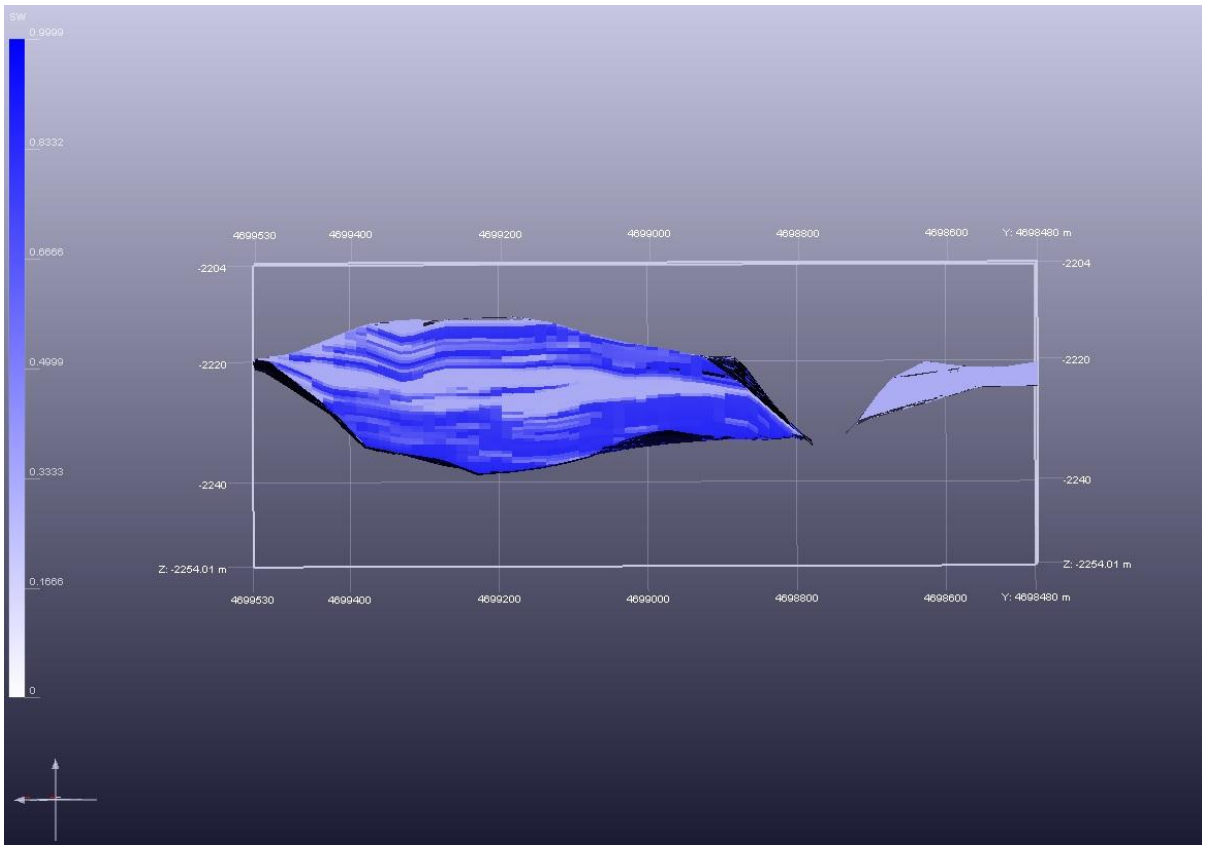

Figure 4.26 Back view of the water saturation in the main body of the reservoir at the end of the simulation period and the situation of the injector and producer wells.
Comparing with the previous simulations it is possible to observe big differences. In here, the water rate remains the same than the others runs and the simulation time is the same than the second simulation, however the water injection starts at the beginning of the simulation, there is no natural depletion. This produces an increase of the water saturation on the back part of the reservoir with respect to the second simulation. Moreover, it is shown the really clear the paths followed by the water from the injector to the producer well and they correspond, as it is mentioned before with high quality sands.

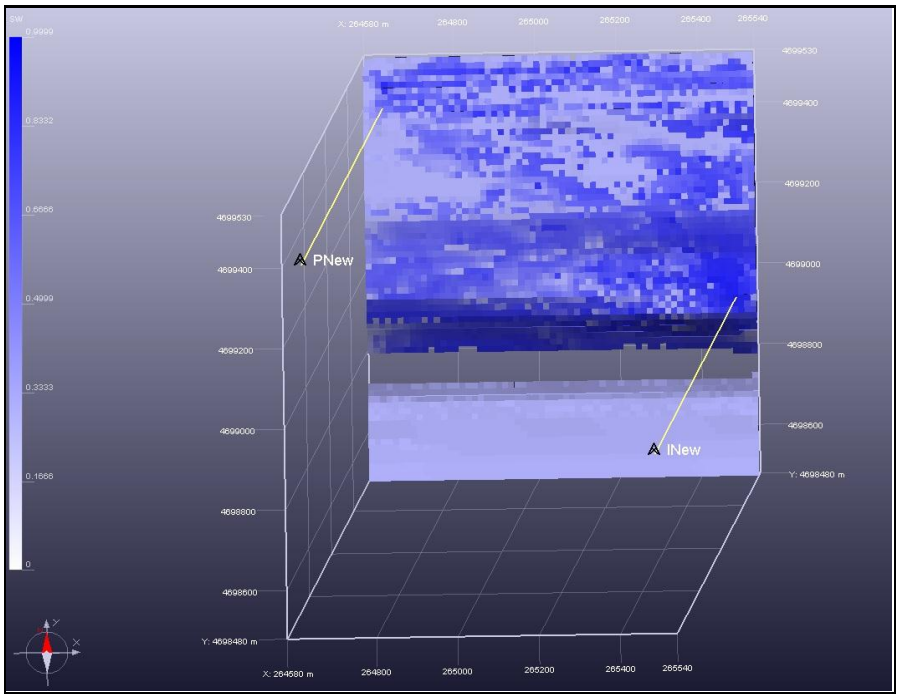

Figure 4.27 Top view of the reservoir for the third simulation showing the situation of the wells and the water saturation after the time applied in this run. This simulation looks the same on top than the top of the first simulation (Figure 4.11) and this can be related with the fact that the water injection starts from day 1, which means an increase of volume of water (in total) drainage the reservoir.

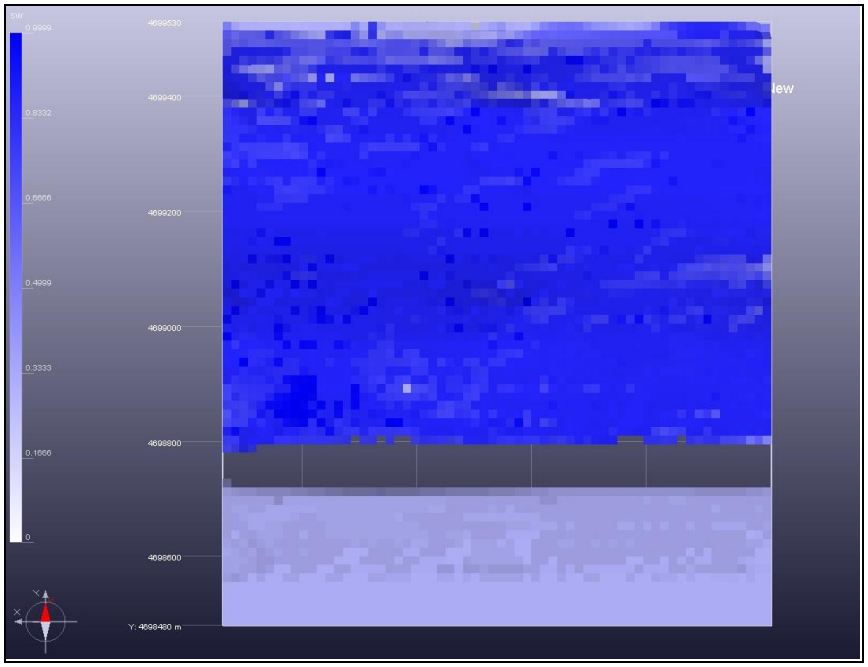

Figure 4.28 Bottom view of the second simulation facies distribution in the reservoir. As it was noticed before, the bottom part of the reservoir is completely water saturated, first of all, because this is the first zone for being filled and secondly because it is formed by thick-bedded sandstones which, have great porosity and permeability.

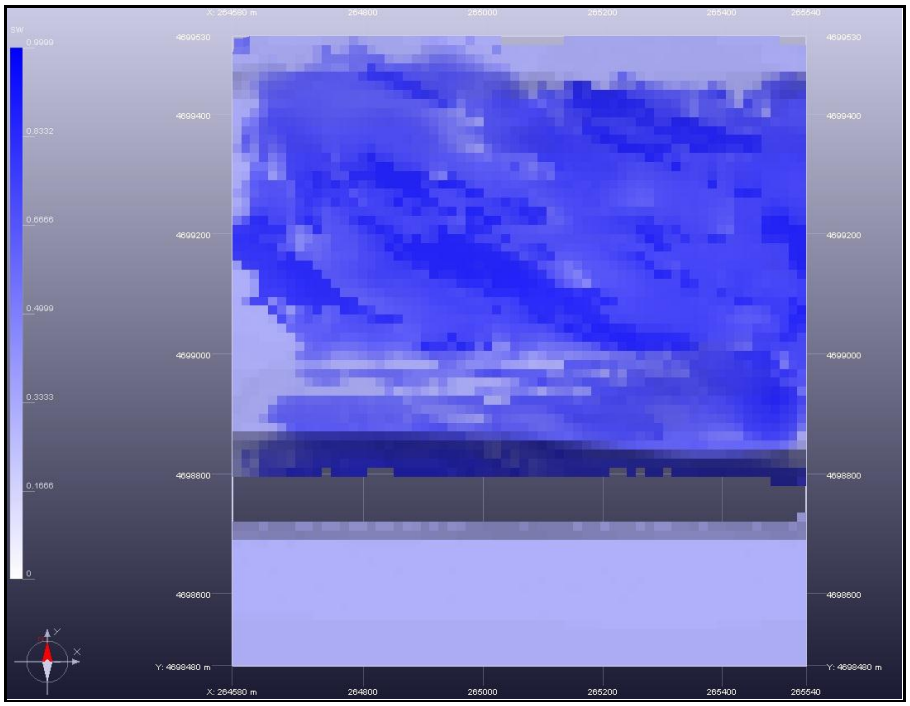

Figure 4.29 Cross-section and top view in K117 showing the paths flow related with good reservoir facies. As it happens for the top view, this cross-section has the same features of path flows than the first simulation (Figure 4.13), which means that in first simulation the reservoir was overestimated in terms of oil production, because in seven years and six months (the time for natural depletion in second simulation) the water reaches the producer well (breakthrough) and quickly it arrives until the point of watercut. This can be seen as well in the oil/water rate plot.

Figure 4.30 Graphic of the oil-water production at surface conditions. Green line corresponds to the water production and brown line to oil production. It can be observed an anomalies behavior an early time, which means, as it was considered a priori that this anomaly is caused probably by the intention of keeping a large water rate during all simulation time. Other possibility could be a numerical error of the software but what it is clear is that this anomaly is not related with the production mechanism in terms of natural depletion or water injection.

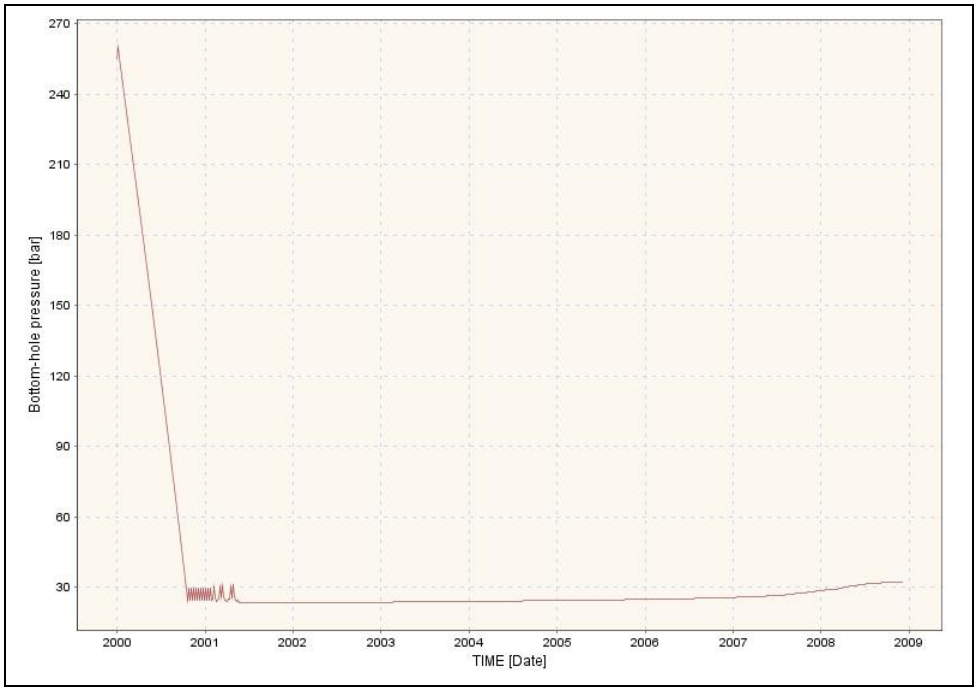

Figure 4.31 Bottom hole pressure on the water injector well. It presents a bigger anomaly in BHP at the beginning of the simulation than the rest of the simulations, it tries to increase the pressure several times but it fails and the pressure remains behind 30bars during all the simulation.

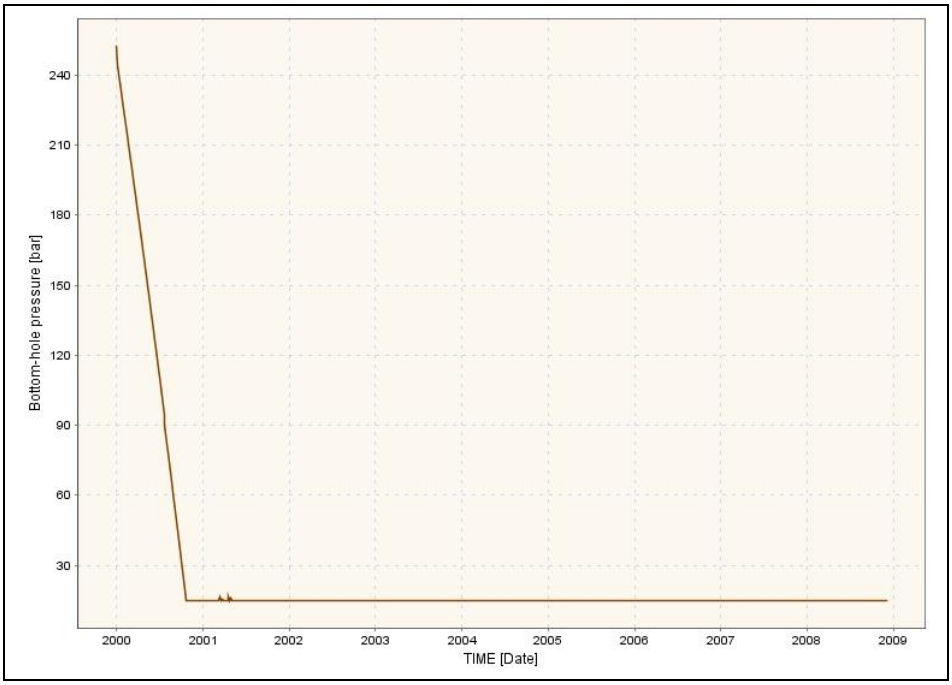

Figure 4.32 Bottom hole pressure on the oil producer well. It presents the same anomaly than the previous producer well in the others simulations with the difference that, as in the case of the injector BHP it looks like the software during the run tries to reaches again the designed BHP (different peaks) but fails as well, remaining in a value of 15 bars approximately.

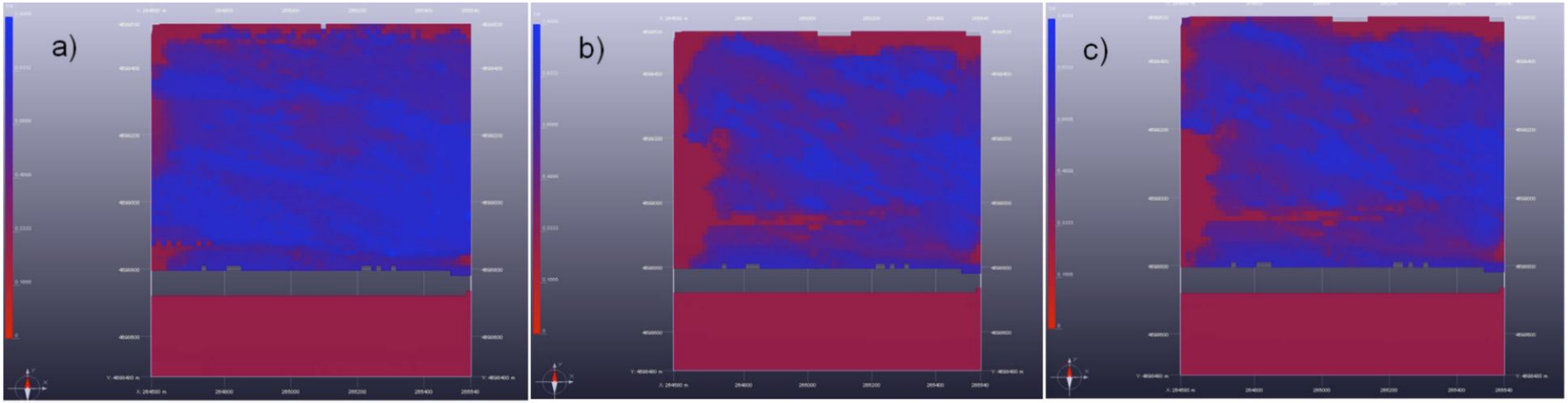

Figure 4.33 Flow paths of the three fluid flow simulations, after 8 years simulation for cross-sections K 98. Blue color corresponds to water saturation zones. Figure a) corresponds to first simulation and thus a Kv of 50 and Kh of 500 mD for McC, with natural depletion the first six months. It can be seen that most of the reservoir domain is almost completely filled by the water injected from the injector situated on the lower right corner. Moreover, it is shown paths with stronger blue color corresponding with the high quality sands defined by the channels (paleocurrents) and mark areas with good efficiency of the recovery process. Figure b) shows the flow paths for second simulation when Kv is 5mD and Kh is 50mD for the McC lithofacies. This simulation starts with natural depletion the first six months as well. It can be observed less water saturation comparing with figure a) and a series of low water saturation paths (reddish colors within the main blue color domain) that correspond with the H lithofacies and possible McC facies as well. The water reached the producer well but the reservoir is not completely filled by water as in the other case. Figure c) corresponds with the third simulation with a decreasing of Kv until 0.5mD and Kh of 5 mD. The water injection is applied from the beginning of the simulation and because of that it can be seen that the reservoir contains more injected water than in case b). However, there are larger zones with low water saturations as one expected from the reduction of permeability, which results in increasing of the heterogeneities in the reservoir volume and more differences among the facies.

Chapter 5 Discussion

5.1 Facies modeling

The result of the stochastic approach is an integrated geological model that honors the hard data (well data) in terms of structural and stratigraphical and lithofacies interpretation.

However, the results show that there are differences between the responses measured from the outcrop and the facies distribution obtained after simulation. These differences are related to

- The number of synthetic wells (8 wells) used to control the facies simulation

- The parameters used in the geostatistical approach

- The stratigraphic model resulting from the geological interpretation of the outcrop.

For this reason, to obtain reliable facies distributions with stochastic methods, the following steps should be accomplished (Falivene et al., 2007):

1. Depending on the geological context, one should consider stationarity or trends in proportions, geometrical characteristics of facies elements in terms of statistical properties, such as proportions, variograms, standard deviation, etc.

2. For reproducing the facies distribution by stochastic modeling, the grid size should be adapted to the vertical and lateral sizes of the heterogeneities.

3. Take into account the relationship between the soft data used for the modeling algorithms and the geometrical parameters describing the facies distribution, i.e. the resultant sizes of the facies patterns are correlated with the variogram ranges or with the slope of the variogram in the SIS methods.

4. Finally, the hard data conditioning the simulation (synthetic well-log data in this case) should remain inchanged by the modeling approach.

In this study the facies modeling was achieved following two kinds of pixel-based methods (described in chapter 2): (1) Plurigaussian simulation and (2) Sequential indicator simulation, after evaluating the scale of the problem, the depositional setting, the objective and mostly the limited data available. Due to the limited dataset and the complexity of the heterogeneities visible on the outcrop, the two methods were combined to reproduce the depositional model. Moreover, this approach has been applied successfully in other studies dealing with such deep-water deposits.

In both cases, plurigaussian (for units C1 and C2.2) and SIS (for units C3, C2.1-up and C2.1-mp-lp), in order to account for anisotropy (flow direction 290°, on the outcrop), we introduced for the variography constant values of sill and nugget (1 and 0.1, respectively), but we changed the ranges. Moreover, the variograms were computed for the vertical direction because the number of wells is too low to interpret with confidence horizontal variograms (not enough geological sampling in the horizontal domain).

As we explained before, the variability of the model is dependent on the values attributed for the range values in major horizontal X = 500m, minor horizontal Y = 100m and vertical directions Z = 0.5m (vertical values should be at least the height of the cells), for all the facies. These values were chosen after checking several simulations because they reproduced the best spatial continuity on the facies distribution, as observed on the outcrop.

Some of the variograms exhibited oscillations (channel-form set C.2), which correspond to wavelengths of associated periodicity. In this case, it can be related with the continuity of the lithofacies and the lengths of lithofacies patterns. However, these two tendencies are quite closed (0.8 and 1.1), thus we assumed as one tendency.

Apart from the variogram criteria, we decided to choose a 3D matrix of proportion to introduce lateral trends in the relative vertical distribution of facies of the geological units. Furthermore, in most of the units, except for unit C3, the simulation was made with a matrix of proportion of 5X5, which allows a better lateral continuity of facies distribution than Matrix of 10X10.

On other hand, another kind of criteria was defined in this case to check the accuracy of the final model and these characteristics are explained on the chapter 2 of this study, but as a summary are: (1) Pinch out geometries, (2) levee depositional sediments, (3) distribution and proportion of heterolithic facies and (4) distribution of mud-clast conglomerates and conglomerates in the channel form set C2.

These criteria were preserved during the modeling operations and in compilation with structural parameters, we could check that:

- The geological model of the Ainsa Quarry outcrop is well defined in terms of (1) orientation with the major direction oriented towards WSW-NSN and the minor direction towards SSE-NNW, (2) structure and architecture. It is easy to observe that the boundary surfaces that divide the model in different units follow the same shapes than in the outcrop, starting with the base of the C3 (the most noticeable and easiest to observe due to the erosive nature), to a smaller scale as the convex-up top on the top part of the middle package of C2.1-mp-lp.

- The main problem related with the structural parameters that can be seen in this model is in the unit C2.1mp+lp. The facies distribution at the border of this zone seems quite blocky and onlapping the unit C1. This is because the C2.1 mp-lp layer geometry was designed following the Top and as we explained before the grid layering style has large impact on the later facies modeling. An alternative option would have been an isoproportional gridding.

- In general terms, the simulation of the facies distribution seems slightly "blocky", mostly in the vertical direction for Heterolithic facies and with lateral continuity lower than in the outcrop. This can be related with the matrix of proportion used, which gives the lateral trend and also due to the lack of horizontal variograms. However, these differences between the facies model and the outcrop are small if we take into account the aim of this study.

- With regard to the connectivity, we adopted the definition given by Pardo-Iguzquiza and Dowd (2003), meaning that we measured both vertical and horizontal connectivity, mostly in the reservoir zone, because the potential heterogeneities can play an important role in terms of barriers or baffle zones. From the different simulations we could check that in most of the cases the sand connectivity in horizontal and in vertical direction is greater than for the outcrop. Also, it is possible to observe sand-paths parallel to the anisotropy direction. This can be related with the lack of horizontal variograms that can result in the simulation of too narrow or not well connected heterolithics beds.

- Finally, this model is only constrained by the hard data from the wells logs which means that using a seismic constraint, for example for computing the matrix of proportions, would optimize the modeling of the facies distribution and some problems as the lateral continuity would decrease.

5.2 Fluid flow simulation

For the fluid flow simulation we created a petrophysical property model from the facies model. To each facies is assigned a constant value of porosity and permeability (Table 4.1). Only for Mud-clast conglomerates we changed the permeability from run to run, based on the studies of Falivene et al. 2007. For each simulation, we tried to maintain a constant value of water rate and oil rate from a given bottom hole pressure. The simulation consisted of single-phase fluid flow through the reservoir volume created from the Ainsa-1 quarry outcrop.

Geological heterogeneity is recognized as a major control on reservoir production and it includes variations in grain-size, porosity, mineralogy, lithologic texture, rock mechanical properties, structure and diagenetic processes (Eaton, 2006). All these factors cause variations in hydraulic conductivity, storage, and porosity, and thus control flow and transport through these rocks. The type of geological heterogeneity that was taken into account in this study basing on the scale of the problem it was related with the petrophysical properties of the facies and large scale structure, as layering, bedding, etc.

For testing the influence of large scale heterogeneities in the reservoir, first of all, we checked the simulation-model properties. This means that we observed zones where the simulation model preserves high-permeability geologic features such as channels (paleocurrents) and we assumed that probably the flow would follow these paths, verifying the high-quality sands and would be affected by shales, mostly on vertical dimension.

It is commonly observed that vertical permeability is lower than horizontal permeability and this happens due to vertical flow crosses strata (the presence of a thin shale layer can reduce Kv dramatically while having only minor effect on horizontal permeability). This relation is a direct result of the flows in the fine-scale reservoir description (Stern, 2005).

After this test, we run the different simulations, which were defined for being affected mainly by permeability heterogeneities without confounding effects. Thanks to this, they give an intuitive visualization of flow patterns, which can be probably similar to the flow paths in oil-recovery processes.

First of all, we could check that in our model when the injection starts the reservoir is charging radially from the injector until the water reaches the producer well (BTT). Therefore, it looks that most of the oil is drained, vertically and horizontally, and this confirms that the

well pattern-geometry chosen (quarter five-spots injection production) is a good choice for this reservoir.

Secondly, large scale flow paths, reservoir volume swept by the waterflood are related with the continuity of the heterogeneities in both vertical and horizontal dimension along the reservoir volume. However, the overall flow distribution is quite similar on the three simulations, because the percentage of McC is not big enough inside the reservoir. But when one checks that at fine scale, when the model is observed locally the next variations can be observed:

1. Fluid-flow simulations demonstrate that relatively long-range heterogeneities features, such as vertical and horizontal interbedded contrasts, may have significant effects on flow behavior.

2. The extent of flow path decreases with increasing range of heterogeneity. In other words, with an increase of non-reservoir facies (from 500 mD to 5mD for Kv in McC) the time that injected water needs to reach the producer well increases and, thus the volume of reservoir filled by water is less.

3. Water saturation maps (Figure 4.13, Figure 4.21 and Figure 4.29) indicate differences in the degree of flow path within the reservoir as a function of petrophysical heterogeneity. These models are obtained after 8 years of flow simulation.

4. The differences in saturation distributions are attributed mostly to the range of permeability values among the facies models.

5. As, we expected from the modeling (constant values of porosity and permeability) there is no presence of fingering tendency on the front of the path flow, being fingering referred as preferential channeling of fluids (Pranter, M.J. et al. 2006).

6. On the water saturation pictures appear some zones with really low saturation values and this is related with low petrophysical properties; they are not artifacts.

The oil production rate exhibits, usually, an anomaly at an early time and this anomaly is also reflected on the bottom-hole pressure and the ratio of injection/production rate. Moreover, this anomaly occurs as well in the injector well and it is shown in the BHP, also.

This anomaly was interpreted at first as a consequence of natural depletion, which causes a pressure drop until the "bubble point" (PT state which generates gas) and for this reason the oil production could drop until almost zero. However, after simulating the fluid-flow with

water injection since the beginning, the anomaly continues to appear on the graphics. Therefore, it was considered as a consequence of the excessive water injection (to keep constant rate the well should be under high pressures) that affects the mechanics in the simulator which constrains the bottom-hole pressure. Injection/production flow-rate profiles show that the three models have no good injectivity due to the pressure anomaly.

The watercut, in the models, increases rapidly after breakthrough and this can be correlated with the length and the range of permeability values of the different facies, which influence this flow behavior.

Finally, the lateral variation observed at the Quarry outcrop during flow simulation is mostly perpendicular but also parallel to the paleocurrent directions. The possibility to observe the parallel variations is closely linked to the creation of the other four synthetic wells on the back of the outcrop. This gives a better constraint of the facies distribution creating an "illusion" of 3D modeling.

This suggests one important conclusion of the modeling and flow-simulation study: the crosscutting relationships of heterolithics inside a reservoir (analogue outcrop) should be captured in the modeling process as 3D data. However, nowadays, most facies modeling based on outcrops are restricted to 2D due to the shortage of 3D data, but this may change with new technologies (LIDAR and GPR), which give access to 3D information.

Chapter 6 Summary and conclusions

This study presents a specific workflow developed to build a geological model, which could reproduce in detail the heterogeneities distribution inside the analogue outcrop chosen (Ainsa-1 quarry outcrop). Through, this study we have arrived to next conclusions:

1. The good accuracy of a facies model distribution depends on stochastic algorithms and the structural model created (network cells and surfaces boundaries which give the geometry)

2. In general terms, the geology model built for this study is well accurate with realistic simulation of geometric and stratigraphic model oriented with the major direction towards WSW-NSN. The only problem is the wrong impact that the reference surface creates at the border of this zone in the unit C2.1-mp-lp.

3. This facies model, presented in this study, honors the hard data from the well logs but the final design looks slightly blocky and with no large lateral continuity. This can be related with matrix of proportion used in every unit. This could be improved with a seismic constraint to be introduced for the construction of a new matrix.

4. Sand connectivity follows channel flows and it is overestimated in this model on the horizontal dimension. This is related with the small dataset (only 8 vertical synthetic wells) that cannot simulate reliable horizontal variograms.

5. Vertical permeability is lower than horizontal permeability, because the presence of non-reservoir layers can reduce mostly Kv with minor effect on Kh. This can be observed at smaller scale on the heterolithic lithofacies, which has a permeability ratio of 0.001 because it is a facies forms by packages of layered mudstones and sandstones beds up to 10 cm.

6. The reservoir is charging with water from the injector radially, confirming the well-pattern choice for this reservoir (quarter five-spots injector-producer).

7. Overall flow distribution is quite similar on the three runs but looking a smaller scale, it can be observed some patterns on the flow behavior produced by heterogeneities:

- Long range heterogeneities features have significant effects on the flow behavior.

- Decreasing of flow extension with increasing the range of heterogeneity on the model. Water saturation is related with the petrophysical parameters of the facies, mostly with the permeability.

- The water cut increases fast after breakthrough due to the constant permeability values among the facies.

- There is an anomaly on the pressure behavior at early times, usually and it is correlated with an excessive water injection that affects the BHP.

- There are perpendicular and parallel lateral variations during the flow simulation related with the paleocurrents directions.

Following the results of this study the further studies can be suggested:

• Improve facies model and structural model, decreasing the size of the cells at the first step of modeling design, for later upscaling.

• Using seismic constraint to build a more detailed geological model to improve the uncertainties in heterogeneity distribution, mostly perpendicular to the major horizontal direction of the outcrop.

• Use different well patterns injector/producer, increasing the number of wells or using the peripheral water injection pattern, to check the flow responses and the relation with the heterogeneities.

• Join the two parts of the reservoir volume by creating a possible flow path, thanks to the thick-bedded sandstone on the unit C1, which has a large lateral continuity.

• Use other petrophysical properties to better constraint the heterogeneities in the reservoir model, as the volume of shales.

Allow the petrophysical properties as porosity and permeability to vary within facies to have the opportunity to check short-scale heterogeneities within the reservoir model

Appendix 1- Selected petrophysical properties for the different facies of the Ainsa-1 quarry outcrop

	Facies	Vp (m/s)	RHOB (g/cm3)	Ip (g/cm3 m/s)	Facies phi	Vshales	Kx (mD)	Ky (mD)	Kz/Kx
1	Gravelly mudstones	2345	2,281	5350	**0,000**	**0,658**	0	0	
2	Heterolithics	2244	2,161	4850	**0,050**	**0,414**	40	40	0,001
3	Thick-bedded sandstone	2200	2,073	4560	**0,300**	**0,050**	2000	2000	0,1
4	Mudstone-clast conglomerates	2465	2,312	5700	**0,150**	**0,064**	500	500	0,1
5	Conglomerates	2405	2,287	5500	**0,250**	**0,136**	2000	2000	0,1

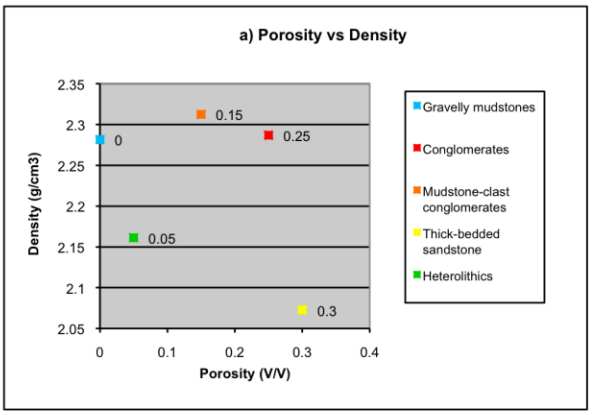

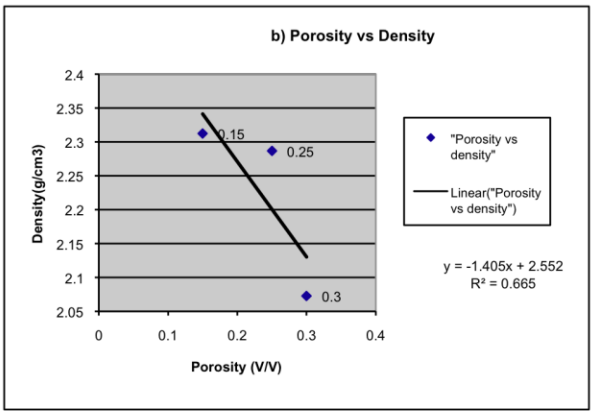

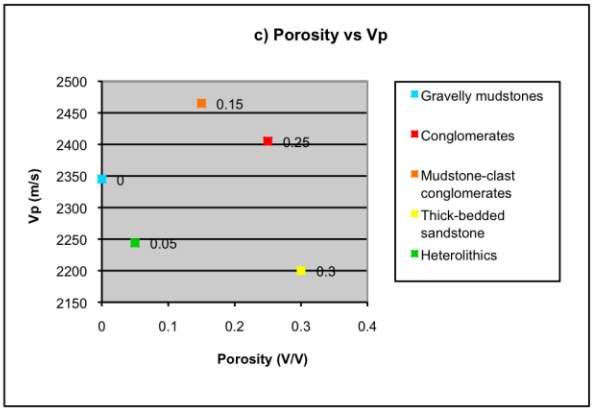

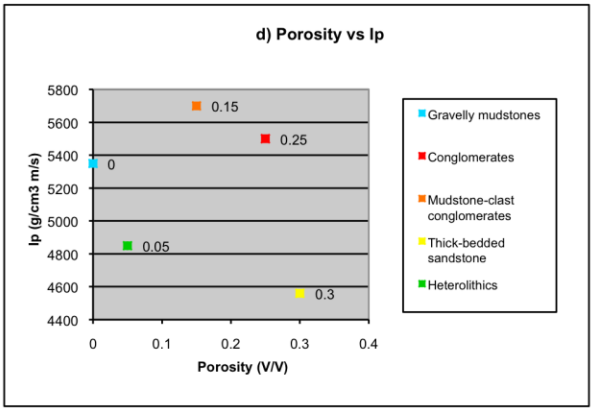

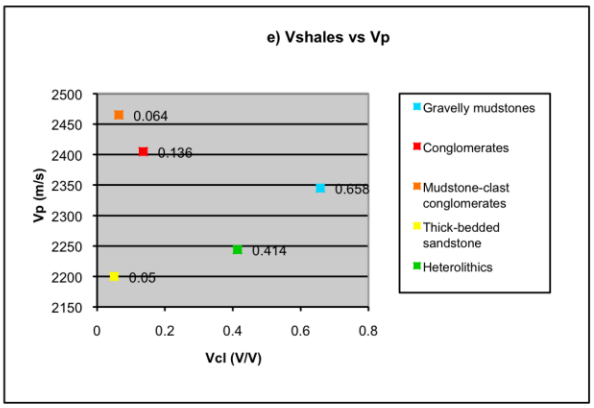

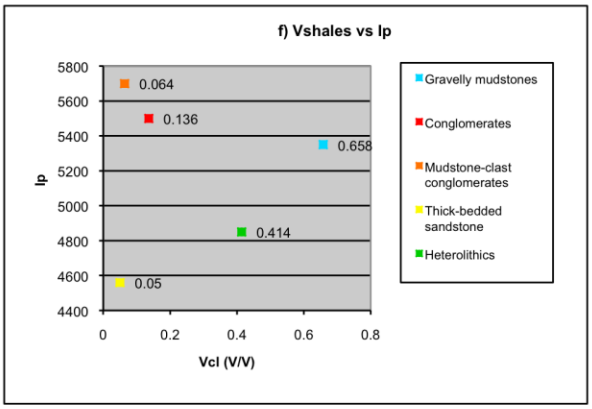

Acknowledgements

De Amsterdam a Paris, pasando por el país de los trolls, los vikingos y por supuesto el petróleo, Noruega, mas concretamente en Bergen. Este es el resumen de mi periplo "masteriense" el cual termina aquí, entregando esta tesis, la cual puede ser un buen ejemplo y refleja lo aprendido en estos dos años, en todos los sentidos. Durante este tiempo he conocido a muchos personajes, me he apoyado en mucha gente y me he dejado guiar por muchos otros;

A todos ellos quiero agradecerles este trabajo, que como siempre, los que me conocen bien lo saben, termino de escribir corriendo y atropelladamente. Por tanto, estos agradecimientos serán breves que no carentes de sentido ni sentimiento:

First of all, I would like to thank the members of the IFP Energies nouvelles, that they contributed on this study, mostly for my supervisor Olivier Lerat, for his good guidance, advice and patience during the entire project, Brigitte Doligez for her patience, as well, and for helping me with my doubts about Geostatistics and Christophe Preux for his help during the fluid-flow simulation step and François Rouge for giving me this opportunity.

Moreover, I need to thank my supervisor from UiB (Bergen) Ritske Huismans, for being always available to give me good advises during these six months by mail or by phone. Also, I would like to thank all the members from the Universitet i Bergen and the Vrije Universiteit Amsterdam that helped me to arrange this internship period.

To all of them GRACIAS.

I want to thank to my master-fellows for all the good and, also bad moments, for the laughter and the madness shared in Amsterdam and in Bergen, during the field trips or in the lab, following courses or hanging out. It was a pleasure to share these two years with you, guys.

To all the great people that I met during this period of time, you gave me the strength to keep on going, you helped to relax, to have fun, to laugh louder right Fede? And of course, to FOCUS. For all these things and many more I would like to thank, Fede, Claudia or

Valentina, Stefano, Alba and many others, more than just roommates, more than friends, my support and my family. GRACIAS.

Por supuesto, no puedo dejar de mencionar a mis princesitas de barrio, las de toda la vida, las de siempre y antes, las que lo han visto todo y lo que queda, por ejemplo una boda: Noelia felicidades! A todas ellas, por los momentos compartidos en los madriles o en los diferentes destinos, por el jamoncitos y otras cositas enviadas para hacer mas llevadera la morriña. GRACIAS.

A mis pequeñas locas de la colina Ruth y Diana, POR TODO, por noches en vela, por las catarsis sufridas, por los skypes de horas, por los cumpleaños sorpresas, por la sangria. Creo que no tengo mas que añadir. GRACIAS.

A mi familia, en especial a mis padres, por todo el apoyo recibido, por creer mas en mi, por los mimos y por las broncas, por los viajes de asentamiento en destino, de nuevo por todo y porque si GRACIAS.

Y por supuesto, el ultimo parrafo, eso ya lo sabe el, es para Gonzo, GRACIAS, pero de las de verdad, sin el esta tesis no habria visto la luz, ya puedes respirar! Pero sobre todo, por ser parte de mi, por conocerme mejor que yo, porque al fin se ve la luz al final.

References

- Arbués, P. et al. 2010. The Ainsa quarry outcrop revisited via orientation models built from LIDAR data. 72nd EAGE Conference & Exhibition incorporating SPE EUROPEC 2010 Barcelona, Spain, 14 - 17 June 2010.
- Arbués, P. et al. 2007. Context and architecture of the Ainsa-1-Quarry channel complex, Spain, in T. H. Nilsen, R. D. Shew, G. S. Steffens, and J. R. J. Studlick, eds., Atlas of deep-water outcrops: AAPG Studies in Geology 56, CD-ROM, 20 p.
- Arbués, P. et al. 2010. Improved field trips by use of Virtual Outcrops and complementary techniques: the UB approach. EAGE Workshop: GeoSkill 2010 29 September - 1 October 2010, Pau, France.
- Bakke, K. et al. 2008. Compound seismic modeling of the Ainsa II turbidite system, Spain: Application to deep-water channel systems offshore Angola. Marine and Petroleum Geology 25 (2008), pp. 1058–1073.
- Clark, J.D. et al. 2008. Deepwater channel bypass and deepwater channel bypass and backfilling processes from the Eocene Ainsa Basin, South-Central Pyrenees, Spain. Adapted from oral presentation at AAPG Annual Convention, San Antonio, Texas, April 20-23. Search and Discovery Article #50094.
- Das Gupta, K. and Pickering, K.T. 2008. Petrography and temporal changes in petrofacies of deep-marine Ainsa–Jaca basin sandstone systems, Early and Middle Eocene, Spanish Pyrenees. Sedimentology (2008) 55, pp. 1083–1114.
- Eaton, T.T. 2006. On the importance of geological heterogeneity for flow simulation. Sedimentary Geology, Vol. 184, Issues 3-4 (February 2006), pp. 187-201.
- Falivene, O. et al. 2006. Best practice stochastic facies modeling from a channel-fill turbidite sandstone analog (the Quarry outcrop, Eocene Ainsa basin, northeast Spain). AAPG Bulletin, Vol. 90, No. 7 (July 2006), pp. 1003–1029.

- Falivene, O. et al. 2006. Hierarchical geocellular facies modeling of a turbidite reservoir analogue from the Eocene of the Ainsa basin, NE Spain. Marine and Petroleum Geology 23 (2006), pp. 679–701.
- Falivene, O. et al. 2007. Statistical grid-based facies reconstruction and modeling for sedimentary bodies. Alluvial-palustrine and turbiditic examples. Geological Acta, Vol.5, No 3, 2007, pp. 199-230.
- Falivene, O. et al. 2007. Synthetic seismic models from outcrop-derived reservoir-scale three-dimensional facies models: The Eocene Ainsa turbidite system (southern Pyrenees). AAPG Bulletin, Vol. 94, No. 3 (March 2010), pp. 317–343.
- Fernández, O. et al. 2004. Three-dimensional reconstruction of geological surfaces: An example of growth strata and turbidite systems from the Ainsa basin (Pyrenees, Spain). AAPG Bulletin, Vol. 88, No. 8 (August 2004), pp. 1049–1068.
- Heard, T.G. and Pickering K.T. 2008. Trace fossils as diagnostic indicators of deep-marine environments, Middle Eocene Ainsa-Jaca basin, Spanish Pyrenees. Sedimentology (2008) 55, pp. 809–844.
- Heimsund, B. O. 2005. Mathematical and numerical methods for reservoir fluid flow simulation. Doctoral thesis, Mathematics department, University of Bergen, March 2005.
- Hoffman, M. et al. 2009. Tectono-stratigraphic analysis of a deep-water growth basin, Ainsa Basin, Northern Spain. Adapted from oral presentation at AAPG Annual Convention, Denver Colorado, June 7-10, 2009. Search and Discovery Article #30102 (2009).
- Jennings, J.W. et al. 2000. Geostatistical analysis of permeability data and modeling of fluid-flow effects in carbonate outcrops. SPE Reservoir Evaluation & Engineering Vol. 3 No. 4, pp. 292-303.
- Lerat, O. et al. 2007. Construction of a stochastic geological model constrained by high-resolution 3D seismic data - Application to the Girassol Field, offshore Angola. SPE Annual Technical Conference and Exhibition, Anaheim, California, November 2007, pp. 11-14.
- Martinsen, O.J. and Thurmond, J.B. 2008. Understanding Deep-Water Architecture from process interpretation at outcrop: An (ancient to modern) perspective. Adapted from oral

presentation at AAPG Annual Convention, San Antonio, Texas, April 20-23, 2008. Search and Discovery Article #50122 (2008).

- Melick, J. et al. 2004. The Lutetian Ainsa Sequence: an example of a small turbidite system deposited in a tectonically controlled basin. Search and Discovery Article #50007 (2004).
- NACSN 1983. North American Commission on Stratigraphic Nomenclature, North American stratigraphic code: AAPG Bulletin, Vol. 67, pp. 841-875.
- Pardo-Igúzquiza, E., and Dowd P.A. 2003. CONNEC3D: A computer program for connectivity analysis of 3D random set models. Computers and Geosciences, Vol. 29, pp. 775–785.
- Pickering, K.T. and Bayliss, N.J. 2009. Deconvolving tectono-climatic signals in deep-marine siliciclastics, Eocene Ainsa basin, Spanish Pyrenees: Seesaw tectonics versus eustasy. Geological Society of America, Geology 2009, 37, pp. 203-206.
- Pickering, K.T. and Corregidor, J. 2000. 3D reservoir-scale study of Eocene confined submarine fans, South-Central Spanish Pyrenees. Deep-Water Reservoirs of the World: 20th Annual research conference, Vol. 15, pp. 776-781.
- Pranter, M.J. et al. 2006. Reservoir-scale characterization and multiphase fluid-flow modeling of lateral petrophysical heterogeneity within dolomite facies of the Madison Formation, Sheep Canyon and Lysite Mountain, Wyoming, USA. EAGE/Geological Society of London, Petroleum Geosciences, Vol. 12, pp. 29–40.
- Scheevel, J.R. 2001. Principal component analysis applied to 3D seismic data for reservoir property estimation. SPE Reservoir Evaluation & Engineering, Vol. 4, No. 1, pp. 64-72.
- Schwab, A.M. et al. 2006. Seismic expression of channel outcrops: Offset stacked versus amalgamated channel systems. Marine and Petroleum Geology 24 (2007), pp. 504–514.
- Stern, D. 2005. Practical aspects of scaleup of simulation models. SPE Journal of Petroleum Technology, Vol. 57, No. 9, pp. 74-81.
- Sullivan, M.D. et al. 2004. An integrated approach to characterization and modeling of deep-water reservoirs, Diana field, western Gulf of Mexico. Integration of outcrop and modern analogs in reservoir modeling: AAPG Memoir 80, pp. 215–234.

- Zadeh, M.K. 2011. Quantitative interpretation of multi-dimensional seismic models turbidite channels from the Ainsa-1 Quarry analogue (Spain). Master thesis, IFPEN.